OPTIMAL SIZING OF HYBRID MICROGRIDS WITH CONSIDERATION OF GLOBAL WARMING EFFECTS: A MARS AND GRG APPROACH

A THESIS SUBMITTED TO
THE GRADUATE SCHOOL OF NATURAL AND APPLIED SCIENCES
OF
MIDDLE EAST TECHNICAL UNIVERSITY

BY

YAVUZ YILMAZ

IN PARTIAL FULFILLMENT OF THE REQUIREMENTS
FOR
THE DEGREE OF MASTER OF SCIENCE
IN
MECHANICAL ENGINEERING

APRIL 2024

Approval of the thesis:

OPTIMAL SIZING OF HYBRID MICROGRIDS WITH CONSIDERATION OF GLOBAL WARMING EFFECTS: A MARS AND GRG APPROACH

submitted by **YAVUZ YILMAZ** in partial fulfillment of the requirements for the degree of **Master of Science in Mechanical Engineering Department, Middle East Technical University** by,

Prof. Dr. Naci Emre Altun
Dean, Graduate School of **Natural and Applied Sciences** _____

Prof. Dr. M. A. Sahir Arıkan
Head of Department, **Mechanical Engineering** _____

Assoc. Prof. Dr. Onur Taylan
Supervisor, **Mechanical Engineering, METU** _____

Prof. Dr. Gerhard-Wilhelm Weber
Co-supervisor, **Faculty of Engineering Management, PUT** _____

Examining Committee Members:

Prof. Dr. Derek Baker
Mechanical Engineering, METU _____

Assoc. Prof. Dr. Onur Taylan
Mechanical Engineering, METU _____

Assist. Prof. Dr. Altuğ Özçelikkale
Mechanical Engineering, METU _____

Assist. Prof. Dr. Tuğçe Yüksel Bediz
Mechatronics Engineering, Sabancı Univerity _____

Assist. Prof. Dr. Ahmet Alperen Günay
Mechanical Engineering, İD Bilkent University _____

Date:26.04.2024

I hereby declare that all information in this document has been obtained and presented in accordance with academic rules and ethical conduct. I also declare that, as required by these rules and conduct, I have fully cited and referenced all material and results that are not original to this work.

Name, Surname: Yavuz Yılmaz

Signature :

ABSTRACT

OPTIMAL SIZING OF HYBRID MICROGRIDS WITH CONSIDERATION OF GLOBAL WARMING EFFECTS: A MARS AND GRG APPROACH

Yılmaz, Yavuz
M.S., Department of Mechanical Engineering
Supervisor: Assoc. Prof. Dr. Onur Taylan
Co-Supervisor: Prof. Dr. Gerhard-Wilhelm Weber

April 2024, 103 pages

This study from the METU North Cyprus Campus projects load and power demands spanning from 2026 to 2050, integrating regional global warming forecasts from the IPCC's Sixth Assessment Report into the design of an optimal microgrid system. Using the Multivariate Adaptive Regression Splines (MARS) method, hourly load, wind speed, and solar irradiance are forecasted, facilitating accurate estimations of the potential electricity generation from solar PV and wind turbines. Different combinations of these renewable sources, augmented with battery storage, are optimized through the Generalized Reduced Gradient (GRG) method. The overarching aim is to minimize the Weighted Average Cost of Energy (waCOE) while upholding a specific renewable energy fraction (Fres) of 60% where possible. Statistical insights from the analysis reveal a rising trend in electricity demand due to global warming, escalating from 6,367 MWh in 2026 to 6,605 MWh by 2050. Wind power is expected to decrease by approximately 21.9% under global warming scenarios, while solar power exhibits a slight increase, hinting at the varying impacts of climate change on these energy sources. The optimization of hybrid microgrid configurations (WT+PV+BESS)

across scenarios showcases their critical role in achieving energy security and economic efficiency. Notably, in the face of global warming, these configurations effectively manage waCOE, with a significant reduction to 0.188 Euros/kWh for 2039 and maintaining a low 0.236 Euros/kWh for 2050. The network tariff is 0.175 Euros/kWh for all scenarios. This indicates that comprehensive, integrated renewable systems are imperative for future energy solutions, adapting to environmental changes while ensuring sustainable and cost-effective energy supplies.

Keywords: global warming, load forecasting, microgrids, renewable energy sources, renewable power forecasting, sustainable energy systems.

ÖZ

KÜRESEL ISINMA ETKİLERİNİN DİKKATE ALINDIĞI HİBRİT MİKRO ŞEBEKELERİN OPTİMAL BOYUTLANDIRILMASI: BİR MARS VE GRG YAKLAŞIMI

Yılmaz, Yavuz
Yüksek Lisans, Makina Mühendisliği Bölümü
Tez Yöneticisi: Doç. Dr. Onur Taylan
Ortak Tez Yöneticisi: Prof. Dr. Gerhard-Wilhelm Weber

Nisan 2024 , 103 sayfa

ODTÜ Kuzey Kıbrıs Kampüsü'nde yapılan bu çalışma, 2026'dan 2050'ye kadar olan yük ve güç taleplerini, IPCC'nin Altıncı Değerlendirme Raporu'ndan bölgesel küresel ısınma tahminlerini, en uygun mikroşebeke sistem tasarımına entegre ederek projelendirmektedir. Çok Değişkenli Adaptif Regresyon Eğrileri (MARS) metodu kullanılarak saatlik yük, rüzgar hızı ve güneş ışınımı tahmin edilmekte, bu da güneş panelleri ve rüzgar türbinlerinden potansiyel elektrik üretiminin doğru bir şekilde hesaplanmasını kolaylaştırmaktadır. Bu yenilenebilir kaynakların farklı kombinasyonları, pil depolama ile birlikte, Genelleştirilmiş Azaltılmış Gradyan (GRG) metodu aracılığıyla optimize edilmektedir. Genel amaç, yenilenebilir enerji oranını (Fres) mümkün oldukça %60'ta tutarken, Ortalama Ağırlıklı Enerji Maliyetini (waCOE) en aza indirmektir. Analizden elde edilen istatistiksel içgörüler, küresel ısınmadan dolayı artan bir elektrik talebi eğilimi ortaya koymakta, 2026'da 6,367 MWh'den 2050'de 6,605 MWh'ye yükselmektedir. Küresel ısınma senaryoları altında rüzgar enerjisinin yaklaşık %21.9 oranında azalması beklenirken, güneş enerjisi hafif bir artış göstererek,

iklim değişikliğinin bu enerji kaynakları üzerindeki farklı etkilerine işaret etmektedir. Hibrit mikroşebeke konfigürasyonunun (WT+PV+BESS) diğer senaryolar karşısındaki güvenliği ve ekonomik verimlilik elde etmedeki kritik rolünü sergilemektedir. Özellikle küresel ısınmanın yaşandığı durumda, bu konfigürasyonlar waCOE'yi etkili bir şekilde yönetmekte ve 2039 için 0,188 Euro/kWh'ye önemli bir düşüş sağlamakta ve 2050 için düşük 0,236 Euro/kWh seviyesini korumaktadır. Tüm senaryolar için şebeke tarifesi 0,175 Euro/kWh'dir. Bu, çevresel değişikliklere uyum sağlarken sürdürülebilir ve maliyet etkin enerji tedariklerini garanti altına alan kapsamlı, entegre yenilenebilir sistemlerin gelecekteki enerji çözümleri için zorunlu olduğunu göstermektedir.

Anahtar Kelimeler: Küresel ısınma, talep tahmini, mikroşebekeler, yenilenebilir enerji kaynakları, yenilenebilir güç tahmini, sürdürülebilir enerji sistemleri.

To my family

ACKNOWLEDGMENTS

First and foremost, I would like to thank my supervisor, Assoc. Prof. Onur Taylan and Prof. Gerhard-Wilhelm Weber, for their invaluable guidance, encouragement, and expertise throughout the research process. Their unwavering support and mentorship have been instrumental in shaping this work.

My heartfelt thanks go to my family Gülüzar Yılmaz, Prof. Dr. Murteza Yılmaz and Oğuz Yılmaz for their unwavering support and encouragement throughout my academic journey. Their love and belief in me have been a constant source of motivation.

I also, specifically would like to thank Prof. Dr. Oktar Aşoğlu, Prof. Dr. Barış Bakır, Prof. Dr. Banu Atalar, and Dr. Vildan Kayku.

TABLE OF CONTENTS

LIST OF TABLES

TABLES

LIST OF FIGURES

FIGURES

CHAPTER 1

INTRODUCTION

1.1 Background and Motivation

The urgent global issue of climate change is mainly caused by the rising concentration of greenhouse gases in the Earth's atmosphere. These gases, such as methane (CH_4), carbon dioxide (CO_2) and nitrous oxide (N_2O), retain heat from the sun, resulting in global warming and substantial alterations in weather patterns. The reduction of greenhouse gas emissions is critical in mitigating these effects, necessitating a transition towards more sustainable and renewable energy sources [1], [2].

To address this issue, the Kyoto Protocol was created as a significant international treaty, obligating its signatories to cut greenhouse gas emissions. This agreement is based on the understanding that global warming is real and that human-produced CO_2 emissions are a contributing factor. This protocol underscores the importance of global cooperation in addressing climate change, setting legally binding emission reduction targets for participating countries [3], [4].

The Intergovernmental Panel on Climate Change (IPCC) is crucial in evaluating the scientific aspects of climate change, offering a foundation of scientific evidence for governments at various levels to formulate climate policies. The IPCC's reports highlight the critical need for immediate and substantial reductions in greenhouse gas emissions to limit global warming, emphasizing the role of renewable energy technologies in achieving these objectives [5], [6].

The Conference of the Parties (COP) acts as the highest decision-making authority of the United Nations Framework Convention on Climate Change (UNFCCC), bring-

ing countries together to assess and promote the execution of the Convention and its Kyoto Protocol. These conferences have been crucial in setting global agendas for reducing carbon emissions and transitioning towards low-carbon economies, with significant discussions focused on enhancing the role of renewable energy sources and improving energy efficiency [7], [8], [9].

The challenge of integrating renewable energy sources into the power grid is further compounded by the need for precise sizing of hybrid systems. This process is critical to ensuring that the combination of wind turbines, solar photovoltaics (PVs), and battery energy storage systems (BESS) operates at optimal efficiency and reliability. The sizing of these components is a complex undertaking that requires a careful balance between technical feasibility, economic viability, and environmental sustainability [10], [11], [12], [13].

Wind turbines, as a cornerstone of hybrid microgrid systems, must be selected and sized based on local wind resource assessments to maximize energy capture and minimize variability [14]. The design and sizing of solar PV installations, on the other hand, depend on solar irradiance levels, available space, and the intended load profile of the microgrid [16]. These renewable sources are inherently intermittent, necessitating the integration of BESS to regulate the energy supply, manage peak loads, and enhance system resilience [15].

The sizing of BESS is particularly critical in hybrid microgrids [17]. It involves determining the optimal storage capacity and discharge rate to ensure that energy is available during periods of low wind or solar generation, thereby guaranteeing a continuous and reliable power supply. The integration of BESS not only provides a buffer against the variability of renewable energy sources but also plays a pivotal role in grid stabilization, energy management, and emergency backup.

Furthermore, the economic and environmental implications of hybrid system sizing cannot be overlooked. Proper sizing ensures that the system is cost-effective, minimizing wasted capacity while maximizing the utilization of renewable energies. This balance is essential for the long-term sustainability of microgrids, enabling them to deliver reliable energy solutions that are both financially viable and environmentally responsible [18], [20].

The broader economic impact of integrating renewable energy systems extends beyond immediate cost savings and environmental benefits [19], [18]. Economically, the transition towards renewable energy can stimulate job creation in the green technology sector, fostering innovation and economic growth [21]. Investments in renewable energy infrastructure, such as wind turbines and solar PVs, contribute to a more diversified and resilient economy, reducing dependence on fossil fuels and mitigating the risks associated with global commodity markets [22], [23].

Moreover, the economic implications of global warming — including the potential for significant financial losses due to increased natural disasters [24], health crises, and agricultural disruptions [25], [26] — make the case for reducing carbon emissions even more compelling. By decreasing reliance on fossil fuels and enhancing the efficiency and reliability of renewable energy sources, hybrid microgrids play a crucial role in mitigating these economic risks. The proactive reduction of carbon emissions through optimized renewable energy systems not only addresses the urgent challenges posed by climate change but also paves the way for sustainable economic development [27].

In summary, the optimization of hybrid microgrids through precise sizing of wind turbines, solar PVs, and BESS represents a critical area of research [28]. This endeavor aims to enhance the efficiency, reliability, and sustainability of renewable energy systems, making them capable of meeting the demands of modern energy consumption while addressing the urgent challenges posed by climate change [29]. The motivation behind this research is rooted in the vision of a future where energy systems are not only sustainable and efficient but also resilient in the face of evolving global environmental conditions, with significant positive impacts on economic growth and stability [30].

1.2 Research Objectives

This study proposes to use Generalized Reduced Gradient (GRG) to optimize hybrid renewable energy systems for microgrids. The optimization problem in the thesis focuses on designing an efficient hybrid microgrid system, with the primary goal of

minimizing the Weighted Average Cost of Energy ($waCOE$) to balance economic efficiency with sustainability. The decision variables include the quantity of 2 MW wind turbines, 250 W solar PV panels, and the capacity of battery energy storage systems, all fine-tuned to achieve the optimal design. The key constraint is maintaining a Renewable Energy Fraction (F_{RES}) greater than 60% whenever applicable, ensuring high sustainability. The research objectives are to optimize economic efficiency by minimizing ($waCOE$), ensure sustainability by keeping (F_{RES}) above 60%, and enhance system performance by optimizing the decision variables within the constraints.

To incorporate climate data and predictions, the study will utilize Multivariate Adaptive Regression Splines (MARS) to develop load and renewable power forecasting models. MARS is a powerful machine learning algorithm that can effectively capture nonlinear relationships between variables and is well-suited for modeling complex systems. The MARS models will integrate climate data from NOAA (National Oceanic and Atmospheric Administration) to account for the impact of global warming on renewable energy sources' performance and improve the accuracy of load and renewable power forecasting.

The novelty of this research lies in its comprehensive optimization of hybrid renewable energy systems for microgrids using advanced techniques. It employs the GRG algorithm to maximize renewable power output while minimizing costs. A key innovation is the use of MARS for accurate load and renewable power forecasting, integrating NOAA climate data to predict load, solar irradiation, and wind speed, incorporating the effects of global warming. This dual approach enhances the efficiency and reliability of microgrids and ensures robust adaptation to global warming, setting a new standard for sustainable energy design.

The proposed methodology will involve developing a simulation model of a microgrid system with hybrid renewable energy sources and energy storage systems. The simulation will be carried out using Excel, and the performance of the system will be evaluated based on various performance metrics, including renewable energy ($waCOE$) and (F_{RES}).

In summary, this study proposes a methodology that combines GRG optimization

with MARS load and renewable power forecasting models to improve the efficiency and reliability of hybrid renewable energy systems for microgrids. The methodology aims to account for the impact of global warming on the microgrid system's components.

1.3 Thesis Structure

The primary objective of this study is to optimize hybrid renewable energy systems for microgrids using GRG optimization techniques while incorporating MARS load and renewable energy forecasting models that account for global warming. The thesis is organized into five main chapters, beginning with the current chapter which sets the stage for the research.

- Chapter 2 delves into the literature, providing context and background on hybrid microgrids, the effect of climate change on energy systems, and the current state of renewable technologies.
- Chapter 3 describes the theoretical underpinnings and the methodology used for modeling and analysis.
- Chapter 4 presents the results of this research and discusses their implications.
- The final chapter, Chapter 5, summarizes the findings, reflects on the limitations of the study, and proposes avenues for future research.

CHAPTER 2

LITERATURE REVIEW

2.1 Overview of Microgrids and Their Benefits

Microgrids are compact, localized energy networks capable of functioning autonomously or in coordination with the main grid. They comprise distributed energy resources (DERs) like energy storage solutions, renewable energy sources, and controllable loads, all linked to create a localized grid. Microgrids provide numerous advantages over conventional centralized power systems [31], [32].

Microgrids increase the resilience and reliability of energy supply by reducing reliance on centralized power plants and transmission lines. In the event of disruptions or outages in the main grid, microgrids can continue to supply power to critical loads, ensuring uninterrupted electricity supply [33], [34].

By integrating DERs closer to the point of consumption, microgrids minimize transmission losses and optimize energy distribution. This results in increased energy efficiency and reduced overall energy consumption [35], [36].

Microgrids enable the incorporation of renewable energy sources, such as solar photovoltaics (PV), wind turbines, and hydropower, into the energy portfolio. This enhances the use of clean, sustainable energy resources and helps lower greenhouse gas emissions [37].

Optimizing the operation of DERs within microgrids can lead to cost savings for consumers and utilities [40]. By utilizing locally available renewable resources and implementing demand-side management strategies, microgrids can lower electricity bills and reduce infrastructure investments [38], [99].

Microgrids are capable of offering ancillary grid support services, including frequency regulation, voltage control, and peak shaving, which enhance grid stability and reliability. Moreover, microgrids can engage in demand response programs and deliver grid services to the main grid, thereby increasing overall system flexibility [41]. Microgrids empower local communities to take control of their energy supply and promote sustainability initiatives. They enable community-based energy generation, storage, and consumption, fostering resilience in the face of climate change and other external challenges [42].

In summary, microgrids offer a viable approach to tackling the challenges of modern energy systems, including climate change mitigation, energy security, and grid reliability.

2.2 Wind Speed Predictions

In recent years, significant strides have been made in wind speed prediction, leveraging machine learning algorithms and hybrid modeling techniques. Studies since 2020 showcase the efficacy of methodologies such as Random Forests, Long Short-Term Memory (LSTM) networks, Artificial Neural Networks (ANNs), and Multiple-Layer Perception Regressors (MLPR) in accurately forecasting wind speeds. Random Forest (RF) was used for short-term wind speed prediction, highlighting its significance in forecasting for wind energy systems [43].

These single algorithm applications underscore the diverse capabilities of machine learning techniques in handling the complexity and variability of wind speed data. They contribute valuable insights for enhancing wind power forecasting and management systems, crucial for optimizing the reliability and efficiency of wind energy generation.

Significant strides also have been made in the field of wind speed prediction, driven by the adoption of machine learning algorithms and hybrid modeling techniques.

Zhou et al. [44] proposed a hybrid forecasting method combining RF with Variational Mode Decomposition and Principal Component Analysis, enhancing the accuracy of

wind speed predictions generated by numerical weather models like the Weather Research and Forecasting (WRF) model. Reynolds et al. [45] leveraged Artificial Neural Networks (ANNs) to develop a retrieval algorithm for estimating wind speeds from satellite data, exemplifying the potential of machine learning in improving satellite-derived wind speed products.

Ruiz-Aguilar et al. [46] introduced a hybrid approach combining Empirical Mode Decomposition with Permutation Entropy and ANNs, demonstrating significant improvements in wind speed forecasting performance. López et al. [47] introduced a method utilizing Empirical Mode Decomposition, Least-squares support vector machines, and Wavelet Transform for forecasting wind speeds a day in advance across various regions, highlighting the efficacy of hybrid approaches in different geographical settings. Elsaraiti et al. [48] highlighted Long Short-Term Memory (LSTM) networks for accurate short-term wind speed forecasting. This study utilized weather data from Halifax, Canada, to train and test the forecasting model for different seasons, highlighting the effectiveness of LSTM in improving wind speed prediction accuracy. Jahangir et al. [49] developed a framework combining Stacked Denoising Auto-encoders and Rough Artificial Neural Networks for short-term wind speed prediction, aimed at reducing data noise and enhancing prediction accuracy.

These studies collectively illustrate the rapid evolution of wind speed prediction methodologies, emphasizing the role of machine learning and hybrid modeling approaches in addressing the inherent variability and unpredictability of wind speeds. Such advancements are crucial for enhancing the reliability and efficiency of wind power generation systems worldwide.

2.3 Solar Irradiation Predictions

Solar irradiation predictions have been the subject of numerous studies, employing a variety of methods, time periods, and environmental considerations. Predictive models play a crucial role in the planning and operation of microgrids, with solar radiation and irradiation forecasting being pivotal for sizing renewable energy components. In the literature, a plethora of statistical and machine learning methods have been ap-

plied, particularly on an hourly basis, to forecast these factors with high accuracy, while also considering their respective strengths and limitations [50]. For example, Obiora et al. employed Artificial Neural Networks (ANN), Support Vector Regression (SVR), and Random Forest methods to forecast hourly solar irradiance based on historical meteorological data. Similarly, Şahin et al. [52] developed a MARS model aimed at achieving precise forecasts of solar irradiance parameters, leveraging coefficients of determination (R^2). Additionally, environmental parameters relevant to solar irradiation, such as those investigated by Kuter et al. [53, 54] and Ewertowski et al. [55], have been incorporated into predictive models.

2.4 Electricity Demand Forecasting

Electricity demand forecasting is a critical aspect of energy planning and management, encompassing various methodologies tailored to different contexts and objectives. Yukseltan et al. [56] delve into a feedback-based forecasting approach, leveraging historical demand data from the Turkish power market spanning 2012–2017. Their study focuses on enhancing accuracy across hourly, daily, and yearly demand forecasts, showcasing improvements achieved through iterative feedback mechanisms. In a similar vein, Son et al. [57] present a forecasting model employing Long Short-Term Memory (LSTM) networks, tailored specifically for South Korea's residential sector. Their model incorporates social and weather-related variables to provide robust forecasts reflective of dynamic consumer behaviors and environmental influences. Additionally, Zhang et al. [58] propose a hybrid forecasting method integrating support vector regression with meteorological factors and electricity price information. Their approach, optimized using an enhanced adaptive genetic algorithm, aims to improve forecast accuracy by capturing multifaceted influences on electricity demand dynamics. Furthermore, Ilseven et al. [59] highlight the efficacy of Multivariate Adaptive Regression Splines (MARS) in medium-term monthly electricity demand forecasting for Turkiye. Their study demonstrates MARS's superiority over alternative models, including generalized additive models, multiple linear regression, and artificial neural networks, in terms of both forecast accuracy and stability. This section provides a comprehensive overview of diverse methodologies employed in

electricity demand forecasting, reflecting the ongoing efforts to enhance predictive capabilities in energy planning and management.

2.5 Wind Turbine Systems

Wind turbine systems are essential components of contemporary renewable energy infrastructure, converting wind's kinetic energy into electrical power. This subsection explores previous studies dedicated to the design and integration of wind turbines within microgrid systems. Understanding the operational characteristics, performance optimization, and integration challenges of wind turbines is essential for the effective planning and management of microgrid deployments relying on wind energy. The following review provides insights into key studies focused on wind turbine systems and their implications for microgrid design and operation. Tan et al. presents the design and control strategies for a microgrid incorporating a wind turbine and battery energy storage system. Integration challenges and control techniques to optimize the utilization of renewable energy sources while ensuring grid stability and reliability are addressed.

Numerous studies have been conducted to explore the intricacies of wind turbine systems and battery energy storage systems (BESS). Nascimento et al. [60] analyzed the performance of a microgrid with a hybrid unit composed of a PMSG-based wind turbine and BESS, focusing on the BESS's ability to manage power unbalances. The control strategies employed enable effective regulation of voltage and frequency levels in islanded mode.Barbaro et al. [61] proposed an optimized design for a high renewable penetration microgrid on Faial Island, focusing on wind turbines and BESS to ensure energy system stability and reliability. The optimal system design is robust against variability in wind speed and energy demand. Thakur et al. [62] discussed the creation of a wind turbine simulator designed for integration and coordination control within a microgrid, highlighting its effective performance in simulating realistic wind conditions and its ability to work in tandem with PV devices and battery storage. Mesbah Ul Huq et al. [63] explored challenges such as frequency deviation and voltage fluctuations in industrial microgrids with wind power integration. It discusses the role of BESS as a solution to these challenges. Yang et al. [64] addressed

the stability of microgrids with wind power and BESS, focusing on reducing grid power fluctuation and investigating the optimal sizing and selection of battery storage. Marchgraber et al. [65] explored the black-starting and islanding capabilities of Battery Energy Storage Systems (BESS) within a microgrid heavily integrated with wind turbines, emphasizing their role in supplying backup power during main grid outages.

2.6 Solar PV Systems

In recent years, optimizing microgrids has gained substantial interest because of its potential to improve the efficiency, reliability, and resilience of Solar PV energy systems. Various studies have explored optimization frameworks tailored to different microgrid configurations and objectives. In this section, several key contributions in the field of microgrid optimization will be reviewed.

Nasir et al. [66] created a framework for the optimal planning and design of low-voltage, low-power DC microgrids powered by solar PV. Their approach aims to minimize initial costs while optimizing component sizing and distribution architecture. Bandy [67] introduced an optimization model for sizing PV and battery systems in microgrids, aiming to enhance self-sufficiency and cost-effectiveness by balancing multiple objectives, including energy autonomy and capital expenses. Ahamad et al. [68] outlined the optimal design and performance evaluation of a microgrid for future seaports, using a case study in Copenhagen, Denmark. It analyzes the microgrid's performance based on solar PV and battery storage using HOMER software. Bogado et al. [69] proposed a comprehensive model for microgrid optimization based on commercially available devices and specific topologies focusing on the optimal sizing of PV arrays and storage systems. Their approach incorporates microgrid conditions and integrates this detailed model into the optimization problem, balancing financial objectives and introducing new goals for a multi-objective strategy to size the PV plant and battery pack in terms of the required number of parallel and series panels and batteries.

2.7 Battery Energy Storage Systems (BESS)

A plethora of studies have emerged exploring the optimal sizing of Battery Energy Storage Systems (BESS) in microgrids across various regions and systems, highlighting the importance of BESS in enhancing the reliability, efficiency, and cost-effectiveness of microgrids integrating renewable energy sources. Xie et al. [70] offered a two-layer optimal sizing strategy for Battery Energy Storage Systems (BESS), considering the dispatch of a Virtual Energy Storage System (VESS) in a smart microgrid with high PV penetration. This strategy aims to minimize system costs while ensuring stable operation. Pham et al. [71] demonstrated a dual-layer optimization approach to determine the optimal BESS size, factoring in the Energy Management System (EMS) of a microgrid. Their method utilizes iterative techniques and dynamic programming to solve the optimization problems. Abdulgalil et al. [72] introduced a technique for optimal BESS sizing under wind uncertainties using stochastic optimization methods, which enhance power system efficiency by improving accessibility and reducing operating costs. Lee et al. [73] provided a BESS sizing optimization approach for microgrids by solving the Security Constrained Optimal Power Flow (SCOPF), taking into account stochastic errors in PV output forecasts and improving voltage and frequency regulation. Mohandes et al. [74] explored an optimal sizing strategy for an islanded microgrid that incorporates BESS, ice-Thermal Energy Storage System (ice-TESS), a rooftop Photovoltaic (PV) system, and various loads. This paper focuses on the BESS's role in balancing generation and load within the microgrid, optimizing sizes to reduce system costs effectively.Guerrero et al. [75] presented a methodology aimed at sizing a BESS to reduce load peaks for an industrial load connected to a microgrid. The study includes case studies considering different load profiles to demonstrate the methodology's effectiveness in reducing energy purchase costs and demand charges through peak shaving. Takano et al. [76] discussed the critical need for optimal BESS sizing in microgrids, accounting for cooperative operations with other microgrid components. El-Bidairi et al. [77] explored the use of BESS for frequency support in microgrids with high renewable energy penetration, focusing on optimal sizing to enhance system reliability and security. The study uses the Flinders Island microgrid as a case study. Kumar et al. [78] focused on renewable energy resources, and included the optimal sizing of BESS in distributed

generation systems, particularly microgrids. It aims to minimize investment costs and discusses a two-constraint based linear programming technique for sizing solar photovoltaic systems, wind energy generation systems, and BESS to meet load demands effectively.

2.8 Hybrid Microgrids

Hybrid microgrids, which combine various forms of energy generation and storage technologies, have gained significant attention for their potential to enhance reliability and efficiency in energy systems. Yahaya et al. [79] present viable options for utilizing a hybridized microgrid system. The hybridization is achieved through an efficient design approach aimed at enhancing load and system reliability indices by intelligently placing and sizing hybrid distributed generation (DG) systems. Real-time models of solar photovoltaics, wind turbines, batteries, and thermal DGs are introduced and implemented. Dobrescu [80] explores an optimal control strategy for hybrid microgrids integrating thermal and electrical energy, emphasizing efficient energy generation and the maintenance of thermal comfort through advanced control of HVAC systems. The study integrates solar PV with combined heat and power generation systems. Ahmed et al. [81] propose an optimal power flow formulation for islanded AC/DC hybrid microgrids, addressing issues such as voltage and frequency limit violations and increased operational costs, and validate their approach through extensive simulations. This research highlights the significance of distributed generators (DGs) like solar photovoltaics (PV), battery storage systems, and fuel cells—primarily DC energy sources—as crucial components of modern microgrids. Murty et al. [82] discuss the integration of renewable sources in microgrids, proposing an optimal energy dispatch strategy to minimize operational costs and environmental impacts, demonstrating the techno-economic benefits through simulations. In this context, an optimal energy dispatch strategy is developed for both grid-connected and standalone microgrids incorporating photovoltaic (PV), diesel generator (DG), fuel cell (FC), wind turbine (WT), micro turbine (MT), and battery energy storage system (BESS). Krishna et al. [83] study the challenges in optimal planning of hybrid microgrids including wind turbines, solar PVs and batteries, highlighting various

optimization techniques and the importance of considering single and multi-objective optimization problems in hybrid microgrid design.

2.9 Optimization Methods

The optimization of microgrid components for optimal design encompasses a wide array of methodologies, each suited to specific objectives, constraints, and system characteristics. Mashayekh et al. utilized Mixed Integer Linear Programming (MILP) for optimal Distributed Energy Resources (DER) portfolio, sizing, and placement in multi-energy microgrids. It accounted electricity, heating, and cooling loads as well as sources, integrating operational constraints of electrical and thermal networks, [84]. Liu Zhengu suggested hybrid methodology that combines comprehensive optimization (including combination and capacity optimization) and dispatch optimization for distributed generations in microgrids, employing Multi-Objective Genetic Algorithm (MOGA) and MILP [85]. Balasubramaniam et al. applied quadratic programming in optimizing microgrid operation under conditions of uncertainty introduced by renewable energy sources, optimizing the combined objective of minimizing total operating cost and carbon emission [86]. Xie et al. utilized in multi-objective stochastic optimal planning method for microgrids, effectively handling the randomness of renewable resources and volatility of loads, employing NSGA-II algorithm for solving the model [87]. Particle Swarm Optimization (PSO) was used in a multi-objective optimal dispatch model for microgrids under grid-connected mode. Here, PSO is used to minimize system operation and environmental costs, incorporating batteries of electric vehicles as mobile energy storage devices [88]. Genetic Particle Swarm Optimization (GPSO)which is a hybrid optimization method that combines the strengths of Genetic Algorithm (GA) and Particle Swarm Optimization (PSO) for planning hybrid energy systems in microgrids, aiming to optimize generation capacities while considering reliability and cost was applied by Nasser et al. [89].

2.10 Global Warming Effects

The literature on optimal sizing of microgrid components amidst global warming effects underscores the necessity of incorporating climate change considerations into microgrid planning and operation strategies. The impact of global warming has become a central concern in energy systems design, particularly in the development and optimization of microgrids. Studies emphasize the importance of integrating climate projections, load profile analysis, and resilience metrics into optimization frameworks to ensure the reliability, flexibility, and sustainability of microgrid systems. Advanced optimization techniques, including mathematical programming and machine learning algorithms, are employed to address the multi-objective nature of microgrid optimization problems under climate uncertainty.

Zehra et al. [90] emphasized minimizing the impact of global warming by incorporating renewable energy sources and advanced storage systems in microgrid control, employing artificial intelligence techniques for efficient energy management. Jaganath et al. [91] focused on maximizing energy availability in microgrids by adapting component configurations in response to climate-induced changes, using techno-economic optimization models. Soykan et al. [92] evaluated the impact of weather conditions, intensified by global warming, on the optimal sizing of isolated microgrids, using cost optimization methods that account for the variability of renewable resources. Hannan et al. [93] reviewed methods for sizing energy storage systems in microgrids to achieve decarbonization, addressing global warming by optimizing energy storage to support renewable energy integration. Tabrizi [94] discussed the optimization of grid-connected microgrids with renewable sources to reduce carbon emissions, a direct response to global warming concerns, employing genetic algorithms and particle swarm optimization. Alvarez [95] proposed a Vectorial Microgrid Optimization method that includes reliability and energy efficiency as metrics, addressing the needs for sustainable power solutions in the face of global warming. Rahbar et al. [96] studied the impacts of energy cooperation among microgrids with renewable integration, optimizing operations to manage the intermittency of renewable resources under global warming scenarios Ouammi et al. [97] developed a predictive control model for a smart greenhouse integrated microgrid, focusing on optimizing the use of renewable

energy in response to climate variability linked to global warming. Praiselin et al. [98] reviewed control and optimization strategies for integrating renewable energy in microgrids, aiming to improve power quality and reduce emissions in light of global warming. Gao et al. [99] provided a comprehensive review of the optimization of microgrid operations, reflecting on how global warming has intensified the need for renewable energy integrations to mitigate environmental impacts.

The reviewed studies illustrate a growing trend of incorporating global warming considerations into the optimization of microgrid components. These approaches enhance the sustainability and resilience of microgrid systems in the face of increasing climate variability and energy demands. This literature survey underscores the critical role of innovative optimization techniques in addressing the dual challenges of energy efficiency and environmental sustainability. By synthesizing diverse methodologies and considering various objectives such as cost minimization and carbon footprint reduction, researchers strive to develop robust approaches capable of mitigating the adverse effects of global warming on microgrid performance and enhancing their adaptability to changing environmental conditions.

CHAPTER 3

THEORY AND METHODOLOGY

3.1 Theoretical Foundations

This study seeks to optimize the design of the METU NCC microgrid components by incorporating Wind Turbine, Solar PV, and BESS technologies, utilizing MARS prediction and GRG optimization techniques. To achieve this, accurate forecasts of wind speed, solar irradiation, campus electricity consumption, and other relevant variables are essential. The following subsections provide a detailed outline of the theoretical framework employed to obtain these predictions and subsequently optimize the microgrid's Distributed Energy Resources (DERs).

3.2 Data Collection and Processing

In this research, meteorological data for the METU NCC area were sourced from the NOAA Global Hourly - Integrated Surface Database (ISD) [100]. The variables retrieved from NOAA are outlined in Table 3.1. Additionally, campus electricity consumption data was sourced from the local electricity authority, Kib-Tek [101]. The meteorological data spans from January 1, 2017, to December 31, 2021, while the available electricity consumption data covers the period from January 1, 2017, to December 31, 2019.

After obtaining the dataset, it is processed by removing any missing or inaccurate data points. Subsequently, processing was conducted on the finalized datasets. In the prediction of wind speed, solar irradiation and campus load demand predictions, all variables were input to the MARS engine since it can eliminate the unnecessary

Table 3.1: Hourly weather and campus electricity consumption data.

Variable	Description	Date Range
$\mathbf{IRR_{solar}}$	All-Sky Surface Shortwave Downward Irradiance (W/m^2) - Total solar radiation reaching the Earth's surface under all-sky conditions.	January 01, 2017 - December 31, 2021
$\mathbf{T_{air}}$	Air Temperature - The air temperature measured at 2 meters above the Earth's surface.	January 01, 2017 - December 31, 2021
$\mathbf{HUMID_{rel}}$	Relative Humidity - The ratio of the actual moisture content of the air to the maximum moisture content it could hold at a given temperature at 2 meters.	January 01, 2017 - December 31, 2021
RAIN	Corrected Total Precipitation - The total amount of precipitation (rain, snow, etc.) corrected for various factors.	January 01, 2017 - December 31, 2021
PRES	Surface Pressure - The atmospheric pressure at the Earth's surface.	January 01, 2017 - December 31, 2021
$\mathbf{WIND_{spd}}$	10-Meter Wind Speed - The wind speed measured at a height of 10 meters above the Earth's surface.	January 01, 2017 - December 31, 2021
DEMAND	Campus electricity consumption	January 01, 2017 - December 31, 2019

variables by nature.

Normalization, particularly Z-score normalization, plays a pivotal role in the preprocessing of datasets for advanced machine learning algorithms like Multivariate Adaptive Regression Splines (MARS). MARS is a flexible regression technique capable of modeling complex non-linear relationships between the dependent and independent variables. This section elaborates on the significance of Z-score normalization within the context of MARS, illustrating how this method can optimize model performance by ensuring features contribute equally to the regression process [103].

Z-score normalization, is a process where each feature in the dataset is adjusted to have a mean of 0 and a standard deviation of 1. This normalization method is particularly beneficial for algorithms like MARS, which thrive on identifying and modeling intricate patterns in the data. In the context of MARS, Z-score normalization facilitates the algorithm's ability to efficiently partition the data space and apply linear fits within these partitions.

Standardizing the features contributes to the stability of the MARS model by reducing the chances of numerical instability during the calculation of basis functions.

Moreover, it enhances the interpretability of the model by aligning the scales of the coefficients, making it easier to understand the relative importance of each feature in the model.

When applying Z-score normalization in the context of MARS, it is crucial to calculate the mean and standard deviation from the training data only and then apply these parameters to normalize both the training and test datasets. This approach prevents data leakage and ensures that the model's performance is evaluated accurately on the unseen test data [102].

The Z-score normalization is used to scale the data so that it has a mean μ of 0 and a standard deviation σ of 1. The formula for calculating the Z-score of a value x in a dataset is given by:

$$z = \frac{x - \mu}{\sigma}, \tag{3.1}$$

where:

x is the value to be normalized, μ is the mean of the dataset, σ is the standard deviation of the dataset.

3.3 Multivariate Adaptive Regression Splines (MARS) as Forecasting Technique

MARS technique is a flexible method for forecasting that can model complex nonlinear relationships between variables. This subsection delves into how MARS can be applied to forecast energy production and demand in hybrid microgrid systems, addressing its capabilities and limitations.

Unlike frequently used model-driven or supervised learning methodologies and algorithms, MARS is primarily a regression model and, thus, data-driven. The original data-driven Basis Functions (BFs), or splines, provide extraordinarily diverse regression approaches as predictors. MARS tracks and discovers all potential knot positions, predictors, and possible interactions. Many BFs are used in conjunction with

one another to calculate interaction strength. Once MARS has determined the optimal number of basis functions and their corresponding knot placements, the least-squares estimator method is utilized to generate the final model, providing the best estimate of the dataset using the remaining basis functions. Using spline functions in dynamic modeling offers several advantages. Splines are piecewise polynomials in a single (input) dimension. If only polynomials were used and the absolute values of the input variables were extremely large, the polynomials would tend to infinity. However, to accurately model real-world processes within bounded margins, high-degree polynomials are often required, which is challenging due to the multivariate nature of real-world problems, resulting in a rapid increase in polynomial degree. In contrast, in multidimensional and spline models, the degree of polynomial segments can be kept relatively low. The term "elastic" aptly describes the flexibility of splines, and they are often referred to as "smoothing splines" because they smoothly approximate discrete data.

Many BFs are frequently included in the first forward stage, resulting in a possibly overfitted model. The model is discovered using a quick-searching technique, and the procedure is repeated until Mmax, the maximum number of basis functions that the user is permitted to select, is reached. All BFs are included in the base model created in the first phase, regardless of how much of a boost they provide to the model's overall performance. A second step, the MARS reverse stage, is necessary to eliminate the superfluous BFs from the forward stage model. In contrast, the overfitted model is simplified at the reverse stage by removing unnecessary features. Nonetheless, the model continues to exert control on overall performance via data fit. An optimum model is obtained by removing the BFs from the model at each stage with the least increase in the Residual Sum of Squares (RSS) [103], [104]. The BFs are deleted to obtain the optimal required amounts while accounting for their low contribution to the model. The backward-stage halting criterion seeks to reduce both bias and variance. MARS' multivariate BFs are piecewise expanded in one dimension, the BFs look like this, [105], [106]:

$$[x-t]_+ = \begin{cases} x-t, & \text{if } x > t, \\ 0, & \text{otherwise,} \end{cases} \tag{3.2}$$

$$[t-x]_+ = \begin{cases} t-x, & \text{if } x < t, \\ 0, & \text{otherwise,} \end{cases} \tag{3.3}$$

where t is a univariate knot calculated from the data. Truncated functions are called as the two mirrored functions.

Each function in the MARS method is represented as piece-wise linear with a knot at the value t; the two functions in Eq. (1) are known as a reflected pair. The objective is to represent reflected pairs at input data vectors $\mathbf{x}_{ij} = (x_{i1}, x_{i2}, ..., x_{in})^T$ for each x_j ($j = 1, 2, ..., N$) in n dimensions. Thus, the formula for the set B of BFs is

$$B = \{[x_j - t]_+, [t - x_j]_+ : t \in \{x_{1j}, x_{2j}, ..., x_{Nj}\}, j = 1, 2, ..., n\}, \tag{3.4}$$

where N represents the number of observations and n indicates the dimension of the input space; $2Nn$ BFs are generated if all input values are distinct.

In the forward stage of MARS, the data-adaptive model is developed using BFs from set B and their products. The model is represented as

$$Y = \alpha_0 + \sum_{m=1}^{M} \alpha_m \psi_m(\mathbf{X}) + \varepsilon, \tag{3.5}$$

with Y as the response variable and $\mathbf{X}$ as the vector of predictor variables. The additive stochastic noise component ε is assumed to have a zero-mean and constant-variance distribution. Additionally, M is the number of BFs included in the current model, $\psi_m(\mathbf{X})$ represents BFs from set B or products of two or more such functions, and the parameters denote the unknown coefficients for the constant 1 ($m = 0$) or for the mth BF. The general form of the mth BF is given by

$$\psi_m(\mathbf{x}) = \prod_{k=1}^{K_m} \left[s_{km} \cdot \left(x_{v(k,m)} - t_{km} \right) \right]_+ , \tag{3.6}$$

where K_m is the number of truncated linear functions multiplied by the mth basis function, $x_{v(k,m)}$ is the input variable for the kth truncated linear function multiplied by the mth basis function, t_{km} is the knot value corresponding to the variable $x_{v(k,m)}$, and $s_{km} = 1$. To evaluate the potential BFs, the lack-of-fit criteria is applied. Thus, a model with l terms is created by this procedure. Generalized cross-validation (GCV), also known as the lack of fit (LOF), determines the appropriate number of terms in the MARS model. The GCV formula, as presented by Friedman [107], is given by

$$LOF(f_\mu) = GCV(\mu) = \frac{\sum_{i=1}^{N} \left(y_i - f_\mu(\mathbf{x}_i) \right)^2}{1 - \left(\frac{M(\mu)}{N} \right)^2}, \tag{3.7}$$

where M refers to the actual number of parameters that the model uses, and N refers to the total number of observations.

In this study, the py-earth module was utilized to implement the Multivariate Adaptive Regression Splines (MARS) algorithm [108].

3.4 Comparison of Prediction Results

To evaluate the accuracy of prediction models for electricity demand, wind speed, and solar irradiation, we used four statistical indicators: Mean Absolute Error (MAE), Mean Squared Error (MSE), Root Mean Squared Error (RMSE), and Adjusted R-Squared (R^2_{adj}). These metrics were computed for normalized training and test sets to ensure comparability. The formulas and variables for each indicator are as follows:

Mean Absolute Error (MAE) is defined as the average magnitude of the errors in a set of predictions, without considering their direction:

$$\text{MAE} = \frac{1}{n} \sum_{i=1}^{n} |y_i - \hat{y}_i| \tag{3.8}$$

where n is the number of observations, y_i is the actual value, and $\hat{y}_i$ is the predicted value.

Mean Squared Error (MSE) measures the average of the squares of the errors, which is the average squared difference between the estimated values and the actual values:

$$\text{MSE} = \frac{1}{n}\sum_{i=1}^{n}(y_i - \hat{y}_i)^2 \tag{3.9}$$

where n, y_i, and $\hat{y}_i$ are defined as above.

Root Mean Squared Error (RMSE) is the square root of the average of squared differences between predictions and actual observations, providing a sense of the magnitude of the error:

$$\text{RMSE} = \sqrt{\frac{1}{n}\sum_{i=1}^{n}(y_i - \hat{y}_i)^2} \tag{3.10}$$

where n, y_i, and $\hat{y}_i$ are defined as above.

Adjusted R-Squared (R^2_{adj}) is a modified version of R-Squared that accounts for the number of predictors in the model, offering a measure of how accurately the model replicates outcomes, based on the proportion of total outcome variation explained by the model:

$$R^2_{\text{adj}} = 1 - \left(\frac{(1 - R^2)(n - 1)}{n - p - 1}\right) \tag{3.11}$$

where R^2 is the coefficient of determination, n is the number of observations, and p is the number of predictors.

These indicators all together provide a thorough assessment of the model's performance, highlighting the accuracy and effectiveness of the predictions for electricity demand, wind speed, and solar irradiation. Lower values of MSE, RMSE, and MAE indicate better model performance, whereas a higher Adjusted R-Squared (R^2_{adj}) signifies greater accuracy. It is important to consider all metrics together to determine the best performing model, as relying on a single measure is insufficient to evaluate the model's overall quality.

3.5 Modeling of Hybrid Microgrid Components

In recent years, Distributed Energy Resources (DERs) have emerged as viable options for power generation, allowing designers to leverage the strengths of both conventional and renewable energy sources. Typically, DERs incorporate battery storage to address peak demand or periods when renewable sources are unavailable, effectively balancing the disparity between peak load times and maximum power generation and a sample sketch for these components is given at Fig. 3.1. Microgrid component design heavily relies on the performance of each individual system. To ensure accurate performance forecasting, components must undergo individual modeling, enabling evaluation of their combination to reliably meet demand. If the predictions of power output from these components are sufficiently precise, the resulting combination can deliver power at minimal cost [114].

Figure 3.1: Reproduction image of a sample campus microgrid with Wind Turbine, Solar PV and BESS. [128]

3.5.1 Wind Turbine Energy Output

The energy output from wind turbines is contingent upon a myriad of factors, including wind speed, air density, and turbine characteristics. This subsection discusses the mathematical model that translate these variables into predictable energy outputs, which are vital for designing an efficient hybrid microgrid.

The wind speed at hub height is influenced by the hub's height, time, wind speed at ground level, ambient temperature, and terrain characteristics. These factors can be consolidated into a single variable known as the wind shear coefficient or wind profile exponent, α. The values of α can be estimated using site-specific data; however, in the absence of such data, α is typically assumed to be $1/7$ [115]. The wind speed at hub height can then be calculated using Equation 3.12:

$$u_h = u_1 \left(\frac{Z_h}{Z_1} \right)^{\alpha}, \tag{3.12}$$

where u_h is the wind speed at hub height (m/s), u_1 is the wind speed at Z_1, Z_1 is the height of the level in meters, at which speed is measured.

The electrical power produced by a single wind turbine can be determined using Equation 3.13 [117]:

$$P_w = \begin{cases} 0, & \text{for } u_h < u_c \text{ or } u_h > u_f, \\ P_{w,R} \left(\frac{u_c}{u_R} \right)^{\gamma} - \left(\frac{u_h}{u_R} \right)^{\gamma}, & \text{for } u_c \leq u_h \leq u_R, \\ P_{w,R}, & \text{for } u_R < u_h \leq u_f, \end{cases} \tag{3.13}$$

where P_w is the generated electrical power (kW), u_c is the cut-in wind speed (m/s), u_f is the cut-out wind speed (m/s), u_R is the rated wind speed (m/s), $P_{e,R}$ is the rated electrical power of the wind turbine (kW), and γ is the shape parameter of the Weibull distribution. The shape parameter γ can be calculated using Justus' theory [116], and for $1 < \gamma < 10$, it is approximated as:

$$\gamma = \left(\frac{\sigma_{u_1}}{\bar{u_1}} \right)^{-1.086}, \tag{3.14}$$

where σ_{u_1} and $\bar{u_1}$ are the standard deviation and average of the long term wind speed at METU NCC Campus. For this study hourly wind speed data using [100] Integrated Surface Database (ISD) for the years between 2017-2021. The value of σ_{u_1} is found to be 2.4069 m/s and $\bar{u_1}$ is calculated to be 4.4143 m/s. Therefore, the resultant shape parameter for this study is calculated to be 1.9322 using Equation 3.14.

Available wind turbines for this study are of type Vestas V90-2.0MW™ [118, 109]. The technical specifications of the wind turbine are given in Table 3.2.

Table 3.2: Technical details of the VESTAS V90-2.0 MW IEC IIA/IEC S wind turbine [118].

Parameter	**Value**	**Unit**
Hub height	80	m
Cut-in speed	4	m/s
Cut-out speed	25	m/s
Rated speed	15	m/s
Rated power	2	MW

3.5.2 Solar PV Output Calculation

Calculating the energy output of a photovoltaic system requires knowledge of the solar irradiation on the PV module. The method proposed by Duffie and Beckman [119], [120] was used to estimate solar insolation on a tilted surface under the isotropic sky assumption. The detailed methodology is omitted here for brevity. Both ambient temperature and solar insolation on the modules influence the efficiency of the PV module, which can be calculated using Equation 3.15:

$$\eta_{PV} = \eta_{PV,STC} \times [1 - \beta_p \times (T_{PV} - T_{STC})]. \tag{3.15}$$

where T_{PV} can be estimated using Equation 3.16:

$$T_{PV} = T_{amb} + (NOCT - T_{aNOCT}) \times \frac{I_T}{I_{ref}}. \tag{3.16}$$

where T_{PV} is the module temperature, $\frac{I_T}{I_{ref}}$ is the ratio of total irradiance on the tilted surface to the reference irradiation under nominal conditions, $NOCT$ is the nominal operating cell temperature, and T_{aNOCT} represents the reference ambient temperature at the nominal operating conditions.

After determining the module's efficiency and the total insolation on the module's surface, the energy generated by the PV system can be calculated using Equation 3.16:

$$E_{PV} = \eta_{PV} \times I_T \times A_m \times N_m \times \eta_{sys}, \tag{3.17}$$

where η_{sys} accounts for system losses such as shading, soiling, wiring, and inverter losses. η_{amb} and A_m were obtained from the manufacturer, while η_{sys} was assumed based on literature. The AXIPower-AC-250P/156-60S PV module is used in this study [127], as it is the module installed on the campus. Table 3.3 provides the technical specifications of the PV module utilized.

Table 3.3: AXIPower-AC-250P/156-60S PV module technical specifications [109], [127].

Parameter	**Symbol**	**Value**	**Unit**
Temperature coefficient for power	β_{ref}	0.0042	$\%/°C$
Single module area	A_m	1.63	m^2
Reference module temperature at nominal conditions	$T_{Ref,NOCT}$	20	$°C$
Reference module temperature at standard conditions	$T_{Ref,STC}$	25	$°C$
Nominal output	P_{mpp}	250	W_p
NOCT	$NOCT$	45	$°C$
Module conversion efficiency	η_{PV}	15.37	$\%$

3.5.3 Battery Storage Energy Calculations

Methods for calculating the charge and discharge cycles of battery storage systems are crucial. These methods consider the depth of discharge, efficiency, and other key

parameters that impact energy storage and availability within microgrids.

The proposed renewable energy systems (RESs) are integrated with a battery energy storage system (BESS). In this integrated system, the charge/discharge power is dependent on the energy storage capacity [109]. The depth of discharge (DOD) of the battery indicates the maximum fraction of energy that can be extracted without adversely affecting its lifespan. Table 3.4 lists the technical specifications of the battery used.

Table 3.4: Technical specifications of BESS [109].

BESS property	**Symbol**	**Value**
Depth of Discharge	DOD	95%
Charge efficiency	η_{ch}	92%
Discharge efficiency	η_{dch}	92%

3.6 Generalized Reduced Gradient (GRG) Optimization

The Generalized Reduced Gradient (GRG) method is an advanced optimization technique well-suited for nonlinear programming problems that involve constraints. Originally developed to address efficient constraint handling in optimization, the GRG method operates by maintaining a feasible direction of movement within the constraint boundaries to iteratively approach the optimal solution. This method manages constraints effectively by focusing on the gradient of the objective function with respect to the variables that are free to change, hence the term "reduced gradient" [121].

The process initiates with an initial guess of the variables that meet all constraints, followed by adjustments to ensure continued satisfaction of these constraints. The reduced gradient is computed concerning the free (non-basic) variables while keeping the basic (dependent) variables that meet the constraints constant. This selection of basic and non-basic variables is dynamic, adapting to the problem's structure through the optimization process. A line search then determines the optimal step size that advances the objective function while maintaining constraint compliance. This iterative process repeats until convergence criteria such as minimal changes in the objective

function or a near-zero gradient are met.

The theoretical basis of the GRG involves a variant of the gradient descent method, where the gradient is only computed for a subset of variables that do not violate any constraints. Mathematically, consider a nonlinear optimization problem defined as follows:

$$\min f(x) \quad \text{subject to} \quad g(x) = 0 \quad \text{and} \quad h(x) \leq 0,$$

where $f(x)$ is the objective function, and $g(x)$ and $h(x)$ represent the equality and inequality constraints, respectively. In GRG, the reduced gradient is calculated by fixing dependent variables and allowing the independent variables to vary, thus navigating the feasible region defined by the constraints.

The GRG method addresses nonlinear optimization problems as follows [122]:

$$\begin{aligned} &\text{minimize} \quad g_{m+1}(X), \\ &\text{subject to} \quad g_i(X) = 0, \quad i = 1, \ldots, \text{neq}, \\ &0 \leq g_j(X) \leq \text{ub}(n - k_i), \quad j = \text{neq} + 1, \ldots, m, \\ &\text{lb}(i) \leq X_i \leq \text{ub}(i), \quad i = 1, \ldots, n. \end{aligned} \tag{3.18}$$

Here, X is a vector of n variables, neq represents the number of equality constraints, and g_i are differentiable functions representing the constraints and objective function.

The GRG method transforms the problem into an equality form by introducing slack variables $X_{n+1}, \ldots, X_{n+m}$ to manage the inequality constraints:

$$\begin{aligned} &\text{minimize} \quad g_{m+1}(X), \\ &\text{subject to} \quad g_i(X) - X_{n+i} = 0, \quad i = 1, \ldots, m, \\ &\text{lb}(i) \leq X_i \leq \text{ub}(i), \quad i = 1, \ldots, n + m, \\ &\text{lb}(i) = \text{ub}(i) = 0, \quad i = n + 1, \ldots, n + \text{neq}, \\ &\text{lb}(i) = 0, \quad i = n + \text{neq} + 1, \ldots, n + m. \end{aligned} \tag{3.19}$$

The method uses the binding constraints to solve for a subset of variables in terms of the others. Let y be the vector of basic variables and x the vector of nonbasic variables; the binding constraints can be expressed as:

$$g(y, x) = 0, \tag{3.20}$$

where g represents the vector of binding constraint functions. The solution yields a function $y(x)$ valid near the initial feasible solution, reducing the objective to:

$$g_{m+1}(y(x), x) = F(x), \tag{3.21}$$

where $F(x)$ is known as the reduced objective, and the reduced problem is then:

$$\text{minimize} \quad F(x) \quad \text{subject to} \quad l \leq x \leq u. \tag{3.22}$$

The Generalized Reduced Gradient (GRG) method, renowned for its robustness and efficacy in nonlinear optimization, offers significant advantages for the energy sector. This method excels in handling complex constraints and optimizing multiple parameters, which is essential for improving operational efficiencies and decision-making in energy-related applications. GRG techniques can accelerate convergence rates in stochastic optimization tasks, crucial for dynamic energy management systems [123]. The flexibility of GRG in adapting to various problem structures allows for enhanced accuracy and convergence in optimization tasks, where GRG was integrated with deep learning to predict energy consumption accurately [124]. As the energy industry faces increasing complexities and stringent efficiency demands, GRG's capability to efficiently navigate multidimensional decision spaces becomes invaluable, aiding in the sustainable management and optimization of energy resources. This method has been shown to improve the efficiency and economic viability of cogeneration plants through the optimization of salinity gradient power-heat engines [125] and has enhanced policy gradient methods for energy management systems [126].

In this study the primary goal is to minimize the Weighted Average Cost of Energy (waCOE), combining economic efficiency with sustainability in energy production. Decision variables include the quantity of wind turbines, each with a 2 MW rated power, the quantity of solar PV panels, each capable of delivering 250 W maximum power, and the capacity of battery energy storage systems. These variables are fine-tuned to achieve the optimal design within imposed constraints, ensuring that the Renewable Energy Fraction (Fres) remains above 60% whenever applicable.

3.7 Economic Evaluation Methods

An economic assessment is crucial in determining the feasibility of microgrid projects. This section introduces the economic evaluation methods utilized in this research.

Calculating the Cost of Self-Consumed Produced Electricity (CosE) in €/kWh involves an analysis of the costs associated with generating and consuming electricity on-site. This subsection discusses the formulae and factors considered in calculating CosE, including capital investment, operational costs, and energy yields.

The Weighted Average Cost of Electricity (waCOE) in €/kWh provides a measure of the average cost per unit of energy produced by the microgrid. This subsection covers the methodology for calculating waCOE and its significance in the economic evaluation of microgrid systems.

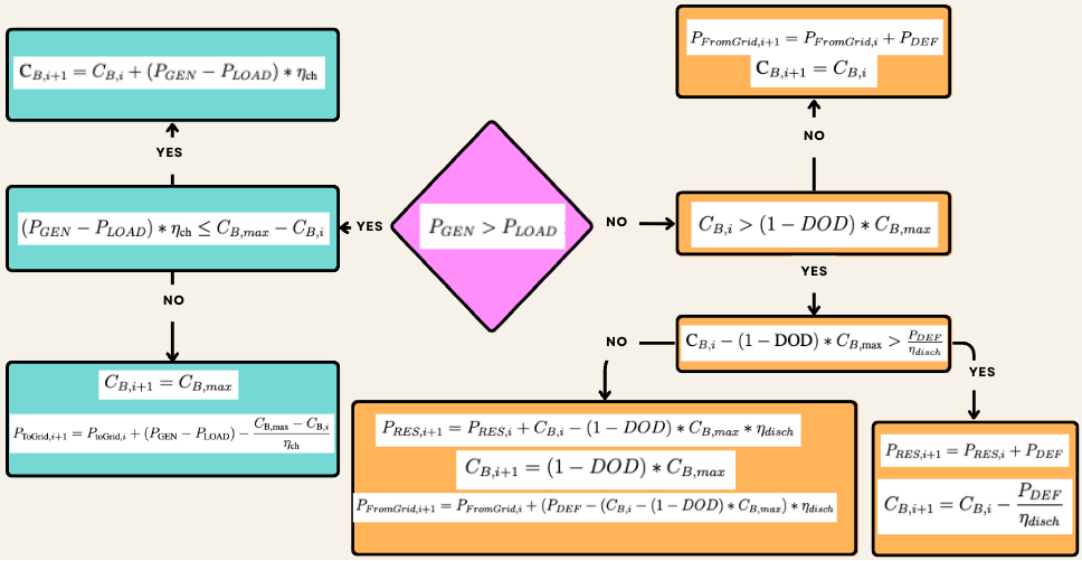

Figure 3.2: Flowchart of BESS (Battery Energy Storage System).

Figure 3.2 illustrates the energy management strategy employed by the system with BESS. The model assesses whether the energy generated by the RES during the time step meets the demand. If the demand exceeds the energy produced during the time step, the energy storage system compensates for the shortfall. If the stored energy is insufficient, the grid supplies the remaining energy needed. Conversely, if the RES generates more energy than the demand, the model checks if the storage sys-

tem can store the excess energy, considering the capacity of the battery. The RES Fraction (F_{RES}) and Demand-Supply Fraction (DSF) are technical metrics that allow decision-makers to evaluate and compare different systems, and they are used in this study. F_{RES} represents the proportion of demand energy supplied by the RES with or without ESS, while DSF indicates the system's autonomy over time. These parameters are derived from Equations 3.23 and 3.24, respectively [109].

$$F_{RES} = \frac{P_{RES}}{D} \tag{3.23}$$

$$DSF = \frac{S}{H} = \frac{S}{24 \times 365} \tag{3.24}$$

where S is the yearly number of hours during which the energy system met the demand. In this study, the time step is considered to be one hour.

In the study, it's vital to delineate between the Renewable Energy Fraction F_{RES} and the Demand-Supply Fraction (DSF) due to their distinct roles and implications in hybrid microgrid systems. Fres, which represents the portion of the total electrical energy demand met directly by renewable sources over a specified period, typically a year, is utilized to assess the contribution of renewable sources like wind turbines and solar PV to the microgrid's energy mix. It quantifies the amount of the microgrid's total energy requirement supplied by renewable sources, thereby indicating the sustainability of the energy supply. In this context, F_{RES} is used as a constraint to steer the system design towards sustainability goals, promoting the integration of renewable energy sources and potentially increasing the system's complexity due to the intermittent nature of these sources. F_{RES} is calculated by dividing the total annual energy supplied by renewable sources by the total annual energy demand of the microgrid.

Conversely, DSF measures the microgrid's ability to autonomously meet its energy demand, focusing on the temporal aspect—specifically, the number of hours per year the microgrid can satisfy its demand entirely through its internal generation and storage systems, without external power sources. DSF provides insight into the reliability and autonomy of the microgrid system, evaluating its effectiveness in ensuring energy

availability throughout different periods, considering the variability in renewable energy generation and the capacity of energy storage systems. DSF is calculated as the number of hours per year that the microgrid meets its own energy demand divided by the total hours in the year. It offers a basis for assessing operational reliability and can guide investments in energy storage solutions and advanced management systems to enhance grid independence and emergency preparedness.

In this study, while Fres was used as a constraint to ensure sustainable energy generation within the microgrid, DSF was also provided as a comparison criterion to benchmark against similar studies in the future. This approach not only underscores the importance of incorporating sustainability into microgrid design but also highlights the need for reliability and autonomy in energy systems, facilitating comprehensive evaluations of microgrid performance in future research.

The weighted-average cost of electricity ($waCOE$) is used to evaluate the economic feasibility of an energy system in this study. To calculate $waCOE$, the unit cost of self-consumed produced electricity ($CosE$) must first be defined. This considers the demand energy covered by renewable energy sources rather than the total generated energy typically used in LCOE calculations. This approach is used because the study implements a one-way tariff system, where excess energy is injected into the grid without generating revenue for the producer. To provide a more precise, realistic, and logical assessment, the concepts of $waCOE$ and $CosE$ are introduced and used, instead of traditional methods such as LCOE, which considers total generated and renewable energy. Equation 3.25 represents the calculation of $CosE$:

$$CosE = \frac{C_i + \sum_{n=1}^{N} \frac{M_n}{(1+r)^n}}{\sum_{n=1}^{N} \frac{P_{\text{RES}}}{(1+r)^n}} \tag{3.25}$$

In the proposed system, any energy shortfall that cannot be supplied by DERs is purchased from the grid at a tariff of 0.175 €/kWh. The metering system for this study is assumed to be unidirectional, meaning any surplus generation that cannot be stored in BESS is injected into the grid for free. Considering these circumstances, the final $waCOE$ can be calculated using Equation 3.26 [109]:

$$waCOE = \frac{P_{\text{RES}} \times CosE + P_{\text{Grid}} \times GT}{D} \tag{3.26}$$

All system components are assumed to have a lifespan of 25 years, except for the battery, which is envisaged to have a lifespan of 10 years [109]; thus, the cost of battery replacement is considered three times in the calculation of $CosE$. The investment cost includes both component and installation costs. Table 3.5 presents the economic parameters used in this study.

Table 3.5: Economic values of RES and ESS and discount rate [109].

Parameter	**Unit**	**Value**
PV system capital cost	€/kW	1547
Annual PV maintenance cost	€/kW	24
Wind system capital cost	€/kW	1155
Annual wind maintenance cost	€/kW	35.275
Battery capital cost	€/kWh	550
Annual battery maintenance cost	€/kWh	10
Discount rate	%	9

3.8 Methods for Environmental Impact and Decarbonization Assessment Calculation

The methodologies encompass a spectrum of techniques aimed at quantifying greenhouse gas emissions, delineating energy consumption patterns, and evaluating the overall environmental footprint associated with different microgrid configurations. Furthermore, the assessment extends to estimating carbon abatement potentials, incorporating considerations such as the integration of renewable energy sources, enhancements in energy efficiency, and the dynamics of grid interactions. Through a meticulous exploration of these calculation methods, this subsection endeavors to furnish a robust framework for appraising the environmental sustainability and carbon mitigation capabilities intrinsic to diverse microgrid designs, thereby facilitating informed decision-making processes directed toward fostering a more sustainable en-

ergy landscape.

The DERs deployment can significantly reduce greenhouse gas emissions such as CO_2 and combat climate change since RES are clean and environmentally friendly. The annual CO_2 emissions avoided by the implementation of RES, A_{CO_2}, are calculated using Equation 3.27.

$$A_{CO_2} = R_{CO_2} \times E_{RES} \tag{3.27}$$

where for Cyprus, the CO_2 intensity of electricity (R_{CO_2}) is 0.584 kg/kWh [129].

To provide a better assessment of the environmental benefits of RES, the avoided social carbon cost (A_{SCC}) and the number of urban trees (T_S) required to sequester the CO_2 emissions if the electricity were generated from a fossil fuel-based system are calculated using Equations 3.28 and 3.29, respectively. The social carbon cost is an estimate of the potential damages to sectors such as health and agriculture caused by carbon emissions [115].

$$A_{SCC} = \text{SCC} \times A_{CO_2} \tag{3.28}$$

$$T_S = \frac{A_{CO_2}}{S_R} \tag{3.29}$$

The social cost of carbon (SCC) is 37 €/ton [115] and the number of urban trees required for CO_2 sequestration (S_R) is 0.039 CO_2 ton/urban tree.

3.9 Site Description

In this subsection, a comprehensive description of the METU NCC campus is provided, which serves as the focus of the case study. The Middle East Technical University Northern Cyprus Campus (METU NCC) as given in Fig. 3.3 is situated in Northern Cyprus, [109],[113].

The institution, established in 2005, is located about 50 kilometers west of the capital city, Lefkosa (Nicosia), and 6 kilometers north of Guzelyurt (Morphou), a town with a population of 12,000. The campus is nestled in one of the greenest areas of the island, neighboring the expansive Kalkanli valley, which is an EU protected area moreover, the region enjoys an abundance of sunshine, with an average of 300 sunny days a year [110].

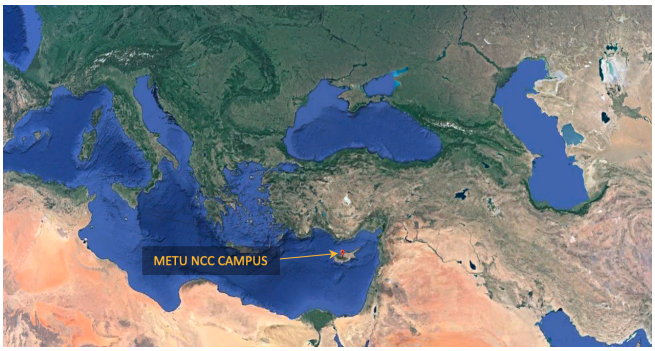

Figure 3.3: METU NCC Campus location.

3.10 Temperature, Solar Irradiation and Wind Speed Attributes in METU NCC

METU NCC campus is located in Mediterrean region. Using the NOAA (National Oceanic and Atmospheric Administration) archives, when we look at solar irradiation, temperature and wind speed values since 2004, the monthly averages are seen as follows. Hourly data since 1991 is available however for this study time periodd 2017-2021 were selected.

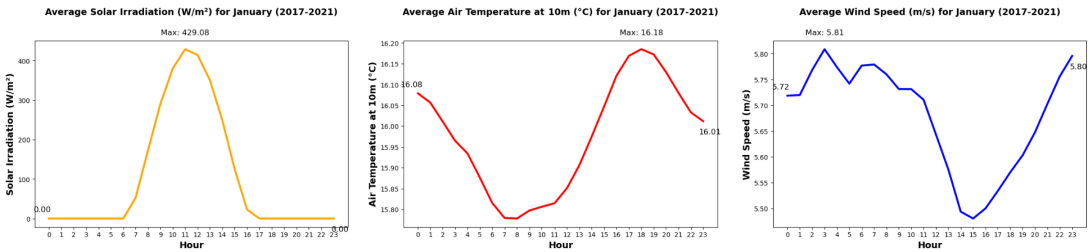

Figure 3.4: 2017-2021 Average Hourly Temperature, Wind Speed and Solar Irradiation for January

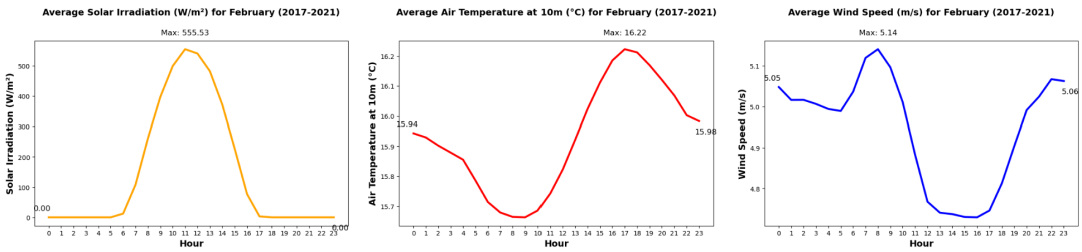

Figure 3.5: 2017-2021 Average Hourly Temperature, Wind Speed and Solar Irradiation for February

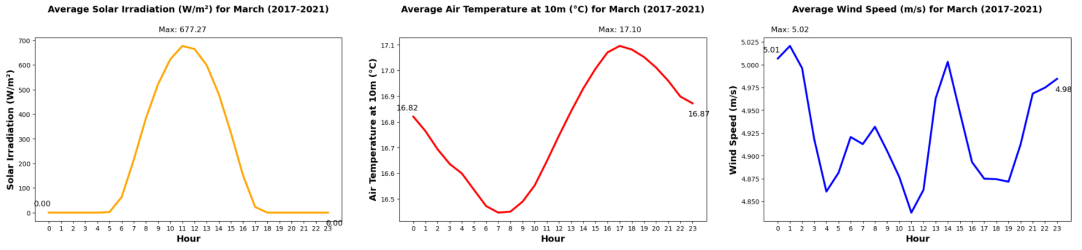

Figure 3.6: 2017-2021 Average Hourly Temperature, Wind Speed and Solar Irradiation for March

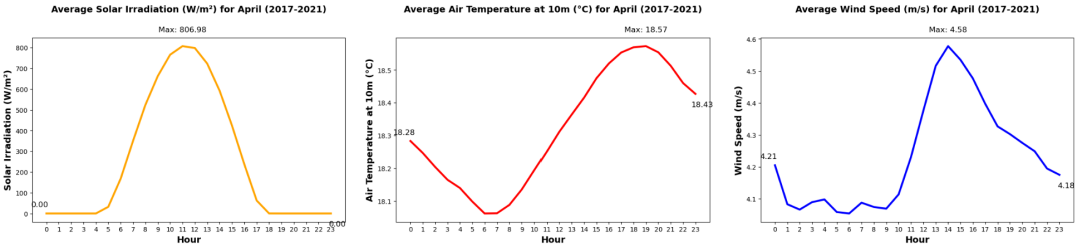

Figure 3.7: 2017-2021 Average Hourly Temperature, Wind Speed and Solar Irradiation for April

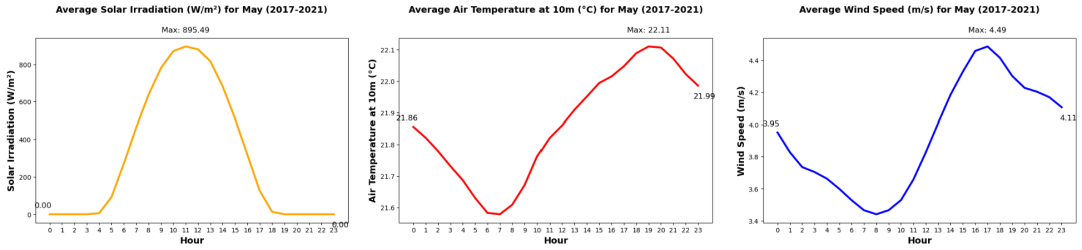

Figure 3.8: 2017-2021 Average Hourly Temperature, Wind Speed and Solar Irradiation for May

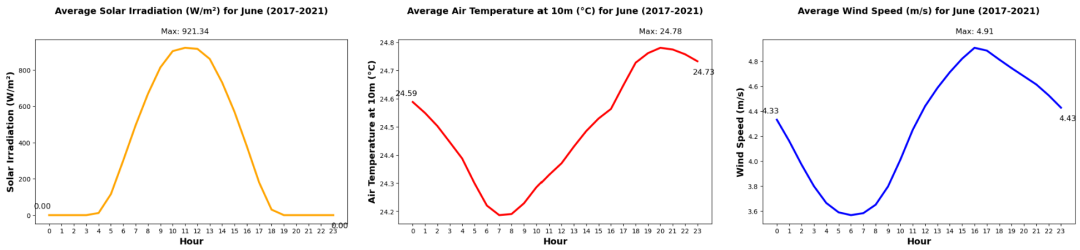

Figure 3.9: 2017-2021 Average Hourly Temperature, Wind Speed and Solar Irradiation for June

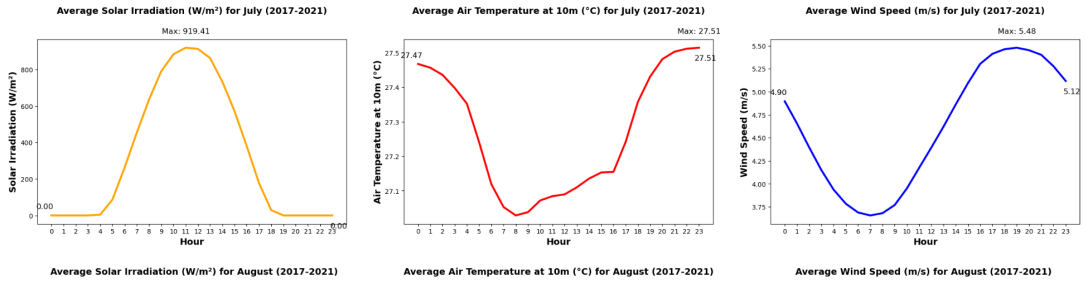

Figure 3.10: 2017-2021 Average Hourly Temperature, Wind Speed and Solar Irradiation for July

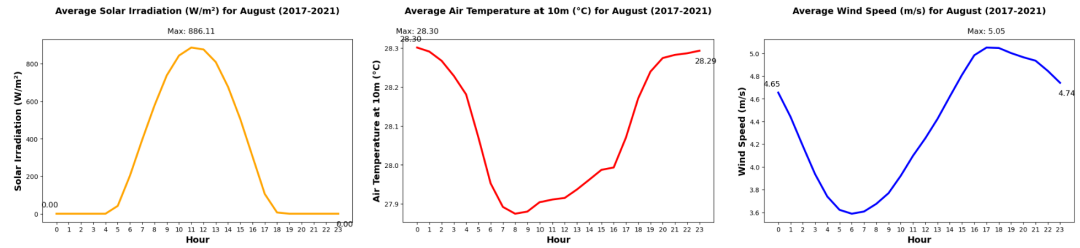

Figure 3.11: 2017-2021 Average Hourly Temperature, Wind Speed and Solar Irradiation for August

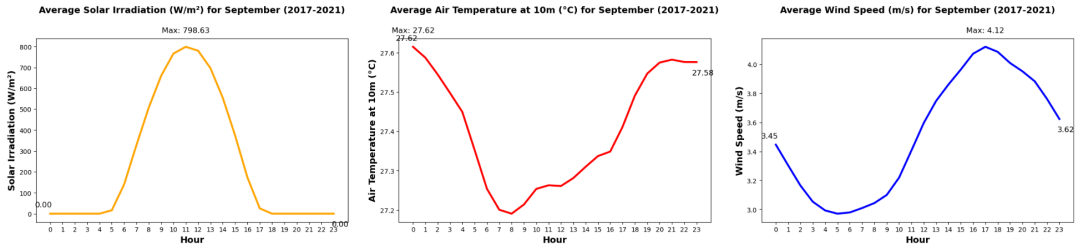

Figure 3.12: 2017-2021 Average Hourly Temperature, Wind Speed and Solar Irradiation for September

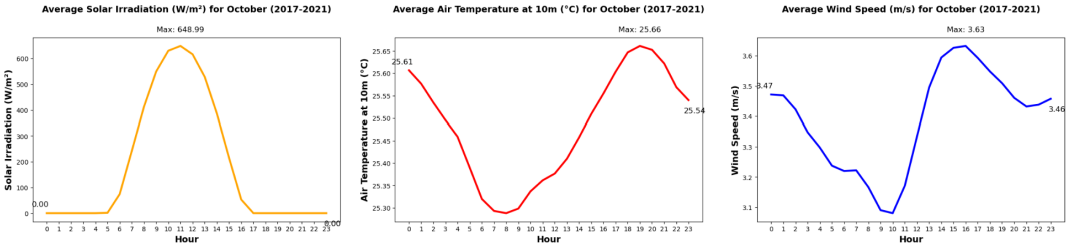

Figure 3.13: 2017-2021 Average Hourly Temperature, Wind Speed and Solar Irradiation for October

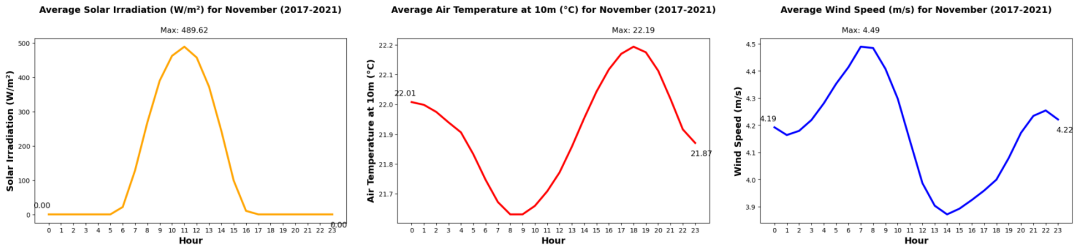

Figure 3.14: 2017-2021 Average Hourly Temperature, Wind Speed and Solar Irradiation for November

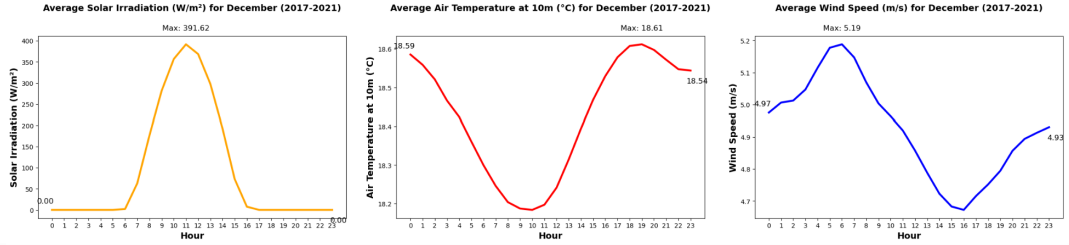

Figure 3.15: 2017-2021 Average Hourly Temperature, Wind Speed and Solar Irradiation for December

3.11 Electricity Demand in METU NCC

Campus load varies monthly, as shown in the average hourly load plots below.

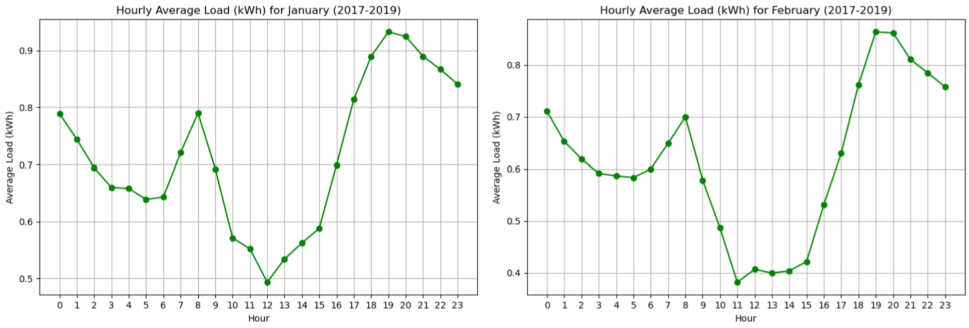

Figure 3.16: 2017-2019 Average Hourly Load for January and February

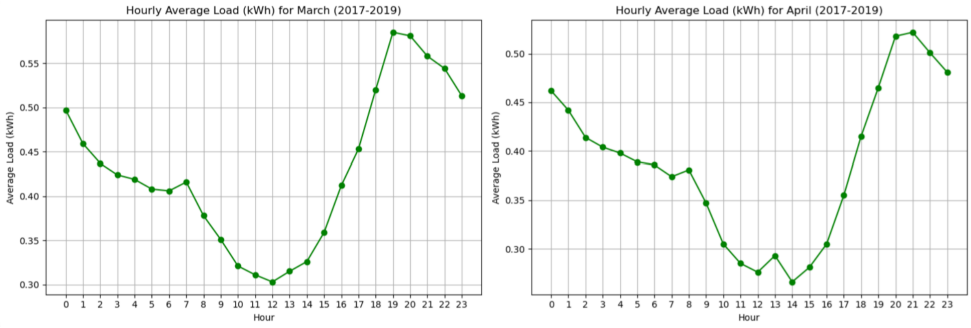

Figure 3.17: 2017-2019 Average Hourly Load for March and April

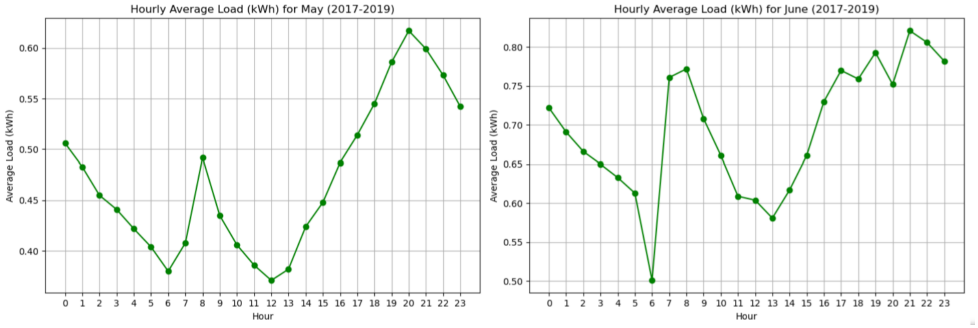

Figure 3.18: 2017-2019 Average Hourly Load for May and June

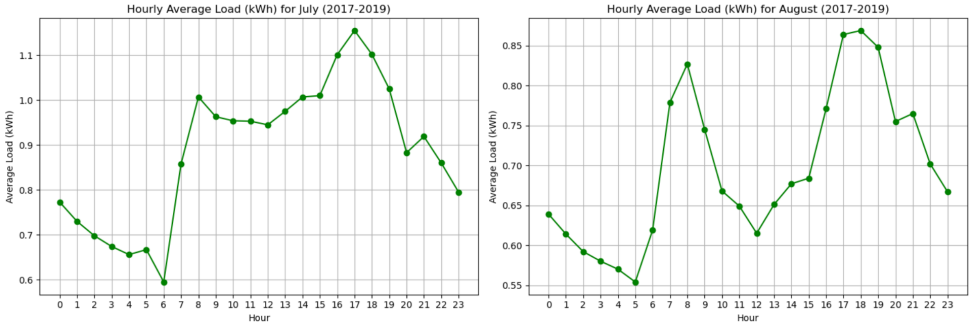

Figure 3.19: 2017-2019 Average Hourly Load for July and August

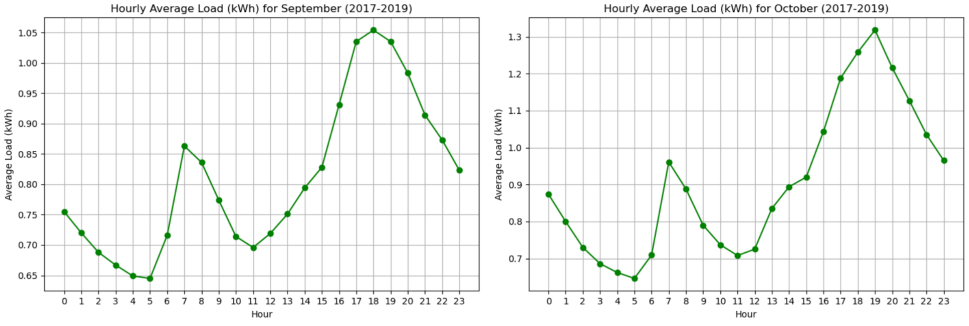

Figure 3.20: 2017-2019 Average Hourly Load for September and October

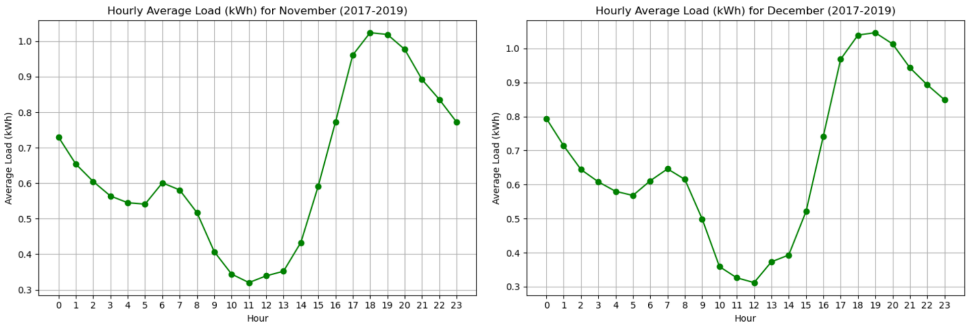

Figure 3.21: 2017-2019 Average Hourly Load for November and December

3.12 Optimization Scenarios

The scenarios help to understand the impact of changing environmental factors and guide strategic planning for future microgrid implementations. This study aims to find and compare the optimum design for a system with 6 different scenarios for 3 mentioned conditions, for Normal Conditions in 2041, Global Warming Effecting 2039 and Global Warming Effected 2050 :

Table 3.6: Scenarios considered for Normal Consitions 2041, Global Warming Condition 2039, and Global Warming 2050 Cases.

Scenario	**Configuration**
1	WT only
2	PV only
3	WT + PV
4	WT + BESS
5	PV + BESS
6	WT + PV + BESS

3.13 Optimization Structure of the Study

The primary goal is to minimize the Weighted Average Cost of Energy (waCOE).

The decision variables include:

- Quantity of Wind Turbines: Each wind turbine has a 2 MW rated power.
- Quantity of Solar PV Panels: Each panel delivers a maximum power of 250 W.
- Capacity of Battery Energy Storage Systems: The storage capacity is optimized to ensure efficient energy use and availability.

The key constraint is ensuring that the Renewable Energy Fraction (Fres) remains above 60% whenever applicable for sustainability.

The research objectives are:

- Economic Efficiency: Optimize the hybrid microgrid design to minimize the waCOE, ensuring cost-effective energy production.
- Sustainability: Ensure a high renewable energy fraction (Fres > 60%) to promote sustainable energy use.
- System Performance: Fine-tune the decision variables (wind turbines, solar PV panels, and battery storage) to achieve optimal system performance within the given constraints.

CHAPTER 4

RESULTS AND DISCUSSION

4.1 Electricity Load, Available Wind and Solar Energy Forecasts

In the study, an immediate increase of +0.7°C was applied to each hourly temperature data point for the years 2026-2041, uniformly adjusting upwards regardless of the time of day or season to model the initial phase of projected global warming impacts. For the period from 2041-2050, each hourly temperature was further adjusted by an additional +2.12°C over the base temperatures, reflecting a cumulative and significant impact of global warming as projected for the later phase of the study period. This method directly influenced the input conditions for the system's performance simulations, ensuring accurate capture of the effects of temperature fluctuations on component efficiency and energy output, and provided a stringent test of the microgrid's resilience and efficiency under escalated climate change conditions. By simulating a worst-case scenario where the effects of global warming are instantly realized, the study helps prepare for the most severe impacts on energy systems, ensuring that planning and design consider potential future extremes rather than gradual changes, which might underestimate the urgency of adaptations needed. The approach ensures that the findings are grounded in a realistic assessment of how increased temperatures could stress current and future microgrid configurations, offering valuable insights into necessary adaptations or improvements in technology and management strategies for future resilience and providing a robust understanding of potential operational challenges and adaptation strategies required to maintain reliability and efficiency in a warmer world.

The MARS methodology was selected for its robust capability to handle complex,

non-linear interactions between variables, particularly apt for the hybrid microgrid optimization explored in this thesis. MARS excels by not only accommodating but systematically evaluating all input variables, ultimately retaining those that most significantly impact the model's predictive accuracy. This method is preferable to traditional regression because it automates the detection of relevant interactions, thereby minimizing manual input and potential bias/characteristics highlighted in Friedman's seminal 1991 study on MARS [107]. For this research, for load, wind speed and solar irradiation forecasts the MARS model was configured to test up to two interactions; empirical tests showed that two interactions provided slightly better predictions than a single interaction, supporting a more nuanced understanding of the data's underlying patterns. This approach aligns with recommendations by [111] for conducting comprehensive sensitivity analysis, which was rigorously applied to each parameter within the model to ensure robustness and reliability in the predictions, confirming the findings are based on a thorough examination of all possible influences, as detailed by Saltelli et al. in their sensitivity analysis guidelines [112]. The systematic methodological rigor adopted in this thesis is reflective of the best practices in the field, ensuring that recommendations given for microgrid optimization are both scientifically robust and practically applicable.

4.1.1 Demand Forecasting of the Campus

The campus hourly electricity load was predicted for 2019 (Test Set). Hourly electricity demand data from 2017 and 2018 years is used as the Training Set. MARS algorithm was used to make prediction using the normalized datasets. The MARS equation is obtained as in Equation 4.1 for which the explanation of the variables are provided at Table 4.1:

$$
\begin{aligned}
\textbf{LOAD} = {} & 0.0516 \times \textbf{Hour\_13} + 0.0701 \times \textbf{Hour\_14} + 0.0667 \times \textbf{Hour\_15} \\
& - 14.5768 \times \textbf{Hour\_16} \times \max(0, -\textbf{SOLAR\_2} - 0.6838) \\
& - 0.0543 \times \textbf{Hour\_16} \times \max(0, \textbf{SOLAR\_2} + 0.6838) \\
& + 0.1972 \times \textbf{Hour\_16} + 0.1365 \times \textbf{Hour\_17} \times \max(0, 0.9465 - \textbf{SOLAR\_2}) \\
& + 0.1624 \times \textbf{Hour\_17} \times \max(0, \textbf{SOLAR\_2} - 0.9465) \\
& + 0.0521 \times \textbf{Hour\_17} + 0.1853 \times \textbf{Hour\_18} \times \max(0, 0.2192 - \textbf{SOLAR\_2}) \\
& + 0.1322 \times \textbf{Hour\_18} \times \max(0, \textbf{SOLAR\_2} - 0.2192) \\
& + 0.0291 \times \textbf{Hour\_18} + 1.3154 \times \textbf{Hour\_19} \times \max(0, -\textbf{SOLAR\_2} - 0.6498) \\
& + 0.1165 \times \textbf{Hour\_19} \times \max(0, \textbf{SOLAR\_2} + 0.6498) \\
& + 0.0293 \times \textbf{Hour\_19} + 0.0205 \times \textbf{Hour\_20} \times \max(0, \textbf{LOAD\_2} + 1.4459) \\
& + 0.0550 \times \textbf{Hour\_7} \times \textbf{TEMP\_2} \\
& + 0.0823 \times \textbf{Hour\_7} \times \max(0, \textbf{LOAD\_2} + 1.4459) \\
& - 0.0841 \times \textbf{Hour\_8} \times \max(0, 0.1767 - \textbf{SOLAR\_2}) \\
& + 0.0968 \times \textbf{Hour\_8} \times \max(0, \textbf{LOAD\_2} + 1.4459) \\
& + 1.4249 \times \textbf{Month\_7} \times \max(0, -\textbf{LOAD\_2} - 1.4459) \\
& - 0.2421 \times \textbf{TEMP\_2} \times \max(0, 0.1885 - \textbf{SOLAR\_2}) \\
& - 0.0833 \times \textbf{TEMP\_2} \times \max(0, \textbf{SOLAR\_2} - 0.1885) \\
& + 0.2252 \times \textbf{TEMP\_2} \\
& + 0.2830 \times \max(0, 0.0627 - \textbf{SOLAR\_2}) \times \max(0, \textbf{LOAD\_2} + 1.4459) \\
& - 0.1592 \times \max(0, 0.1767 - \textbf{SOLAR\_2}) \\
& - 34.4652 \times \max(0, -\textbf{LOAD\_2} - 1.8663) \times \max(0, \textbf{SOLAR\_2} - 0.1767) \\
& + 80.5697 \times \max(0, -\textbf{LOAD\_2} - 1.8659) \times \max(0, -\textbf{LOAD\_2} - 1.4459) \\
& - 4.2672 \times \max(0, -\textbf{LOAD\_2} - 1.4459) \times \max(0, \textbf{LOAD\_2} + 1.8659) \\
& - 0.9584 \times \max(0, -\textbf{LOAD\_2} - 1.4459) \\
& + 0.7632 \times \max(0, \textbf{LOAD\_2} + 1.4459) \times \max(0, \textbf{SOLAR\_2} - 0.0627) \\
& + 0.5710 \times \max(0, \textbf{LOAD\_2} + 1.4459) \\
& - 0.5680 \times \max(0, \textbf{LOAD\_2} + 1.8663) \times \max(0, \textbf{SOLAR\_2} - 0.1767) \\
& - 0.9630;
\end{aligned}
\tag{4.1}
$$

Table 4.1: Definitions of Variables in the Load Prediction Model.

Variable	**Definition**
LOAD	The predicted hourly electricity demand.
LOAD_2	The electricity demand in MW 2 hours before the load to be predicted, normalized.
Hour_13, **Hour_14**, ..., **Hour_20**	Normalized categorical variables indicating whether the prediction is for the respective hour.
SOLAR_2	Solar irradiation 2 hours before the load to be predicted, normalized.
TEMP_2	Temperature 2 hours before the load to be predicted, normalized.
Month_7	A binary indicator for July, indicating if the target LOAD is predicted in July or not.

The performance matrices are at Table 4.2:

Table 4.2: Evaluation Metrics for Hourly Demand Forecasting Training and Test Sets.

Metric	Training Set	Test Set
MAE	0.265	0.341
MSE	0.157	0.245
RMSE	0.396	0.50
Adjusted R-square	0.843	0.744

The scatter plots at Figures 4.1 and 4.2 compare true and predicted (scaled) values for the load forecasting model on training and test sets. Each point represents an instance in the dataset, showing how closely predictions align with actual values. These visualizations help assess the model's performance and accuracy in real-world applications.In both plots, the true values (black dots) and predictions (green crosses) generally cluster around the mean, indicating that the model captures the central trend

well. However, noticeable scatter exists, particularly in the range between -2 and 2, with the training data showing a wider spread of values from -2 to 4. This suggests the model fits the training data better, but exhibits signs of overfitting, as evidenced by the tighter clustering around the true values in the training plot compared to the test plot. Outliers are more prominent in the test data, where the model's predictions deviate significantly for extreme values, highlighting the model's struggle with less frequent, higher, and lower demand values. Overall, while the model performs well for average demand predictions, it shows decreased performance on new, unseen data, particularly at the extremes, indicating a need for improved generalization and handling of variability in electricity demand.

To address these issues, several strategies can be implemented. Enhancing feature engineering by including additional features such as weather data, campus population, calendar effects, and economic indicators can provide the model with more context when theya are able to be included. Increasing the training data size by gathering more historical data or using synthetic data generation techniques can help the model learn better patterns. Regularization techniques can be applied to prevent overfitting, and more advanced algorithms like ensemble methods or deep learning models might better capture temporal patterns. Hyperparameter tuning through grid search or random search and cross-validation ensures the model generalizes well to different data subsets. Employing ensemble methods to combine multiple models can improve overall performance. By implementing these strategies, the model's ability to generalize and accurately predict both average and extreme electricity demand values can be significantly enhanced.

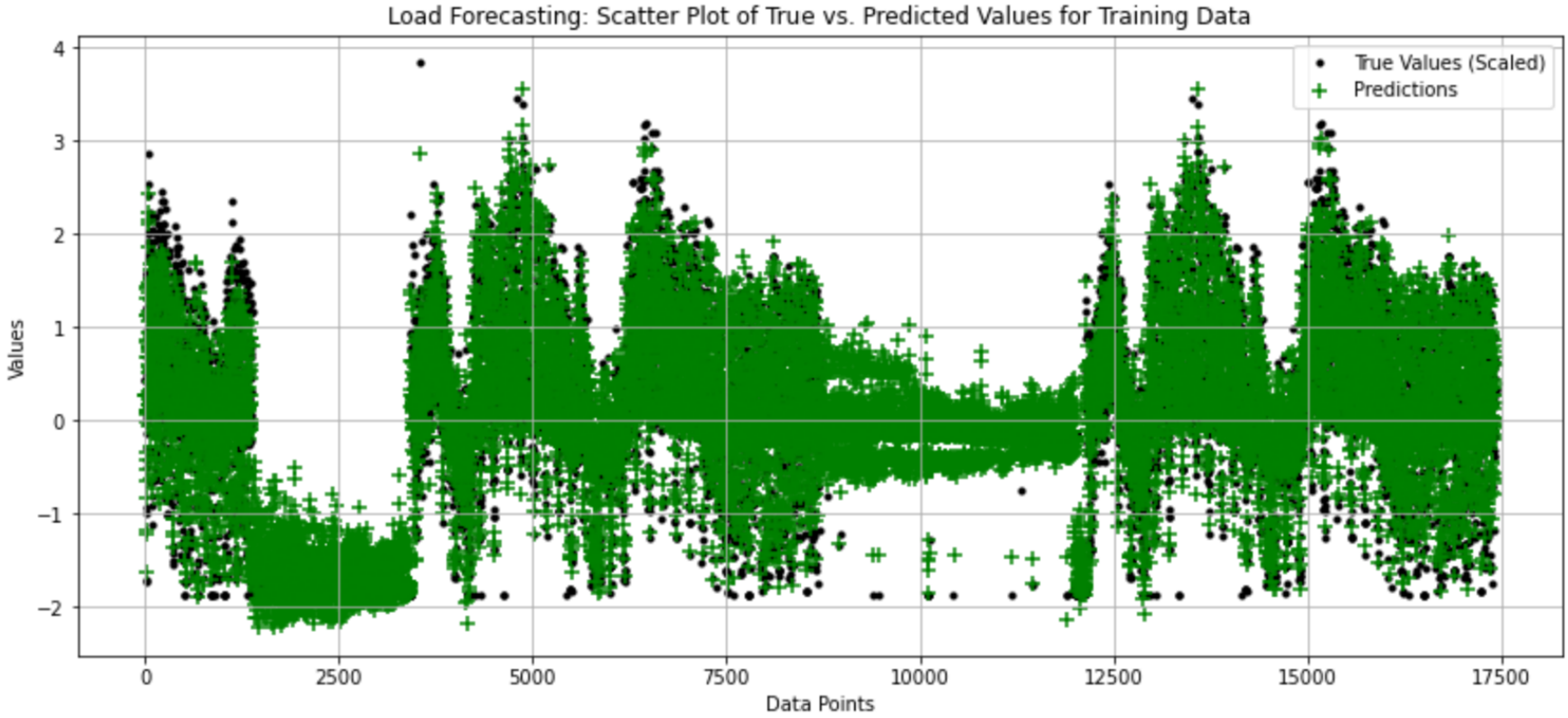

Figure 4.1: Load Forecasting: Scatter Plot of True vs. Predicted Values for Training Data

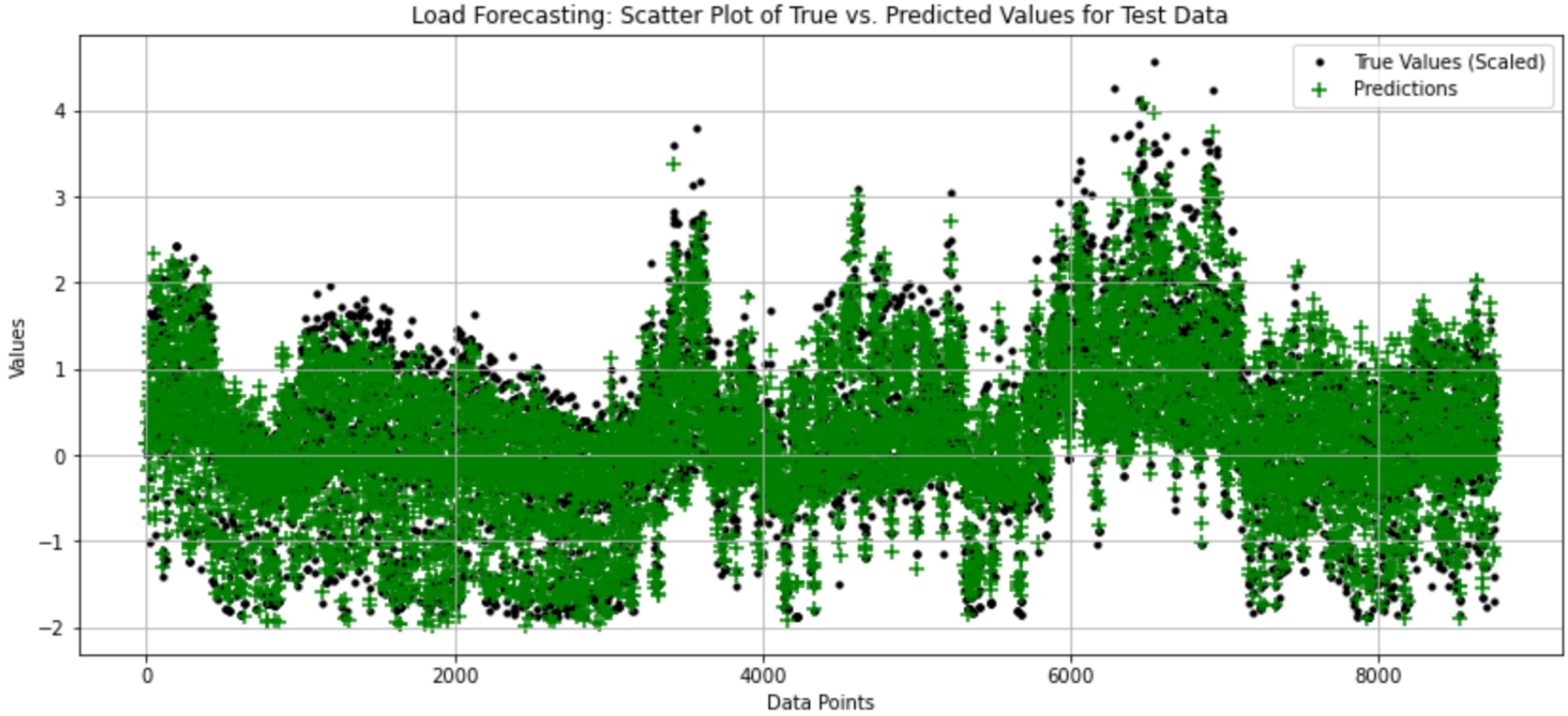

Figure 4.2: Load Forecasting: Scatter Plot of True vs. Predicted Values for Test Data

Scatter Plot is a type of chart that displays values for two variables as points on a Cartesian plane. Each point corresponds to the value of one variable relative to the value of the other variable. In this context, the x-axis represents the true (scaled) values of the load forecasting data, while the y-axis represents the predicted values.

These plots are used for Model Performance Evaluation in Load Forecasting. The scatter points represent the actual (true) values of the load forecasting data (scaled) and the predicted values generated by the model. By comparing these points, one can visually assess the model's prediction accuracy. The diagonal dashed line represents the ideal scenario where the predicted values perfectly match the true values.

Deviations from this line indicate the model's accuracy and performance. In both the training and test data plots, the purple and orange colors respectively differentiate between the true values and the model predictions. The titles of the plots indicate that they are specifically evaluating the performance of a model in predicting load forecasting, with one plot dedicated to training data and the other to test data. The grid lines provide additional reference points for interpretation. Overall, these plots are essential tools for evaluating the effectiveness of the load forecasting model and making any necessary adjustments to improve its performance.

The scattered plots at Figures at 4.3 depict the normalized true versus predicted hourly electricity demand values for both training and test datasets. In both plots, the true values (black dots) and predictions (green crosses) generally cluster around the mean, indicating that the model captures the central trend well. However, noticeable scatter exists, particularly in the range between -2 and 2, with the training data showing a wider spread of values from -2 to 4. This suggests the model fits the training data better, but exhibits signs of overfitting, as evidenced by the tighter clustering around the true values in the training plot compared to the test plot. Outliers are more prominent in the test data, where the model's predictions deviate significantly for extreme values, highlighting the model's struggle with less frequent, higher, and lower demand values. Overall, while the model performs well for average demand predictions, it shows decreased performance on new, unseen data, particularly at the extremes, indicating a need for improved generalization and handling of variability in electricity demand. The measure mentioned for Figures 4.1 and 4.2 suggested will help to improve this

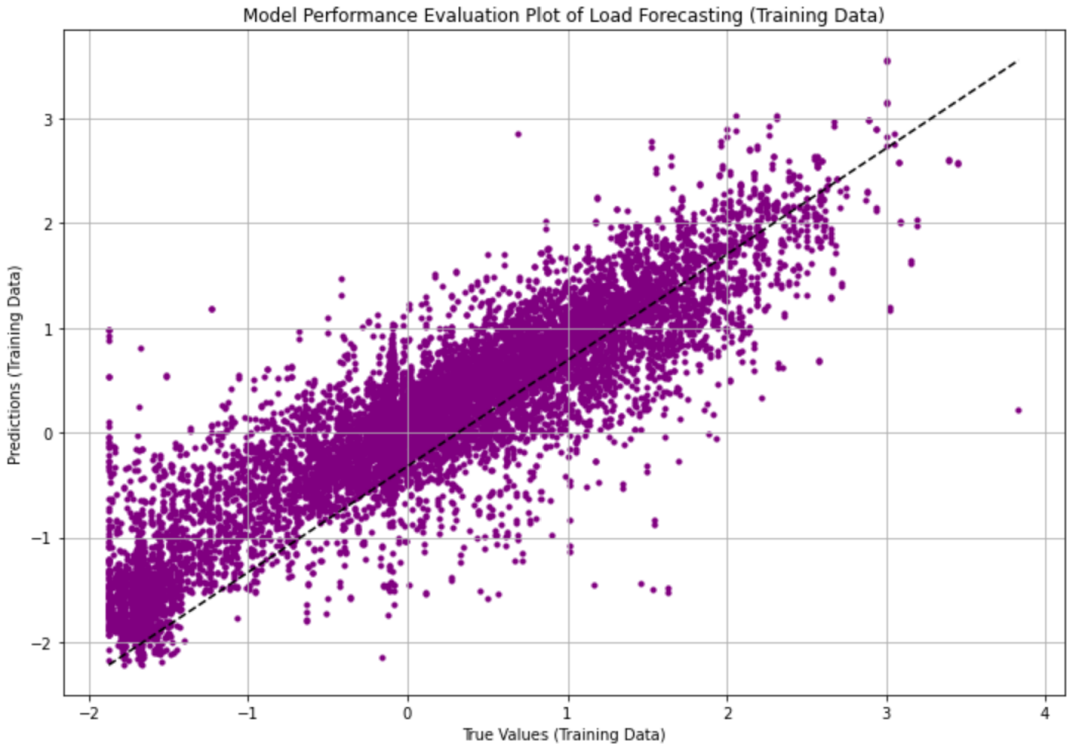

(a) Training Data

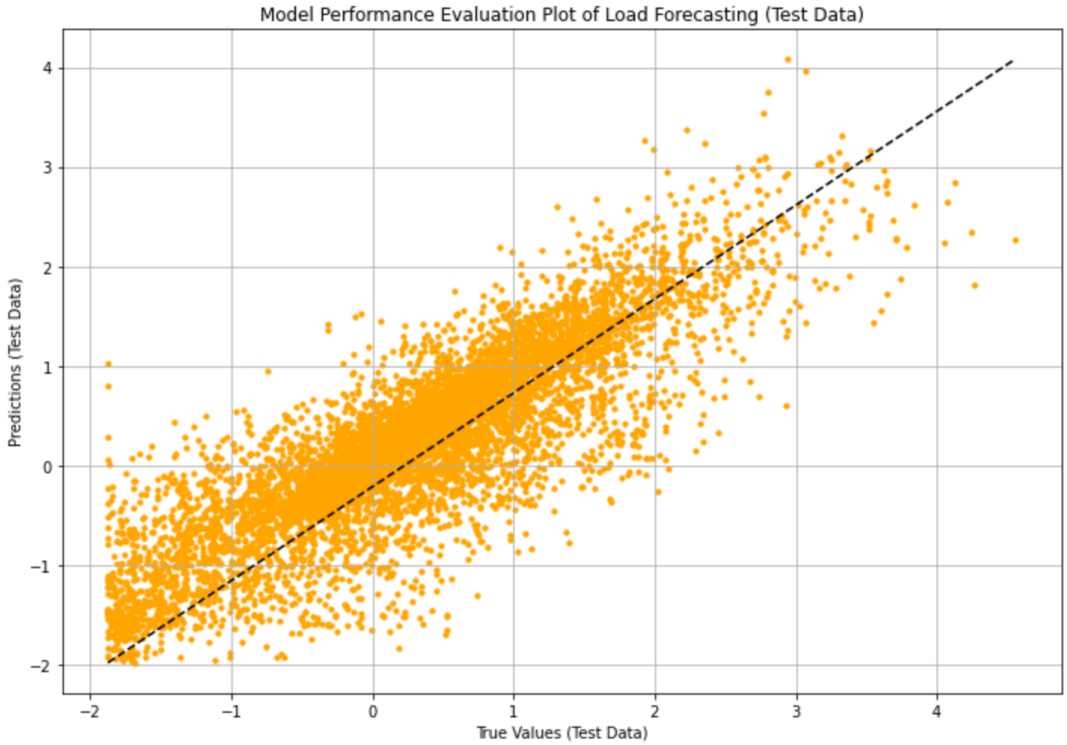

(b) Test Data

Figure 4.3: Model Performance Evaluation Plots for Load Forecasting.

plot too.

4.1.2 Wind Speed Forecast

The wind speed at the Campus level was predicted for 2020 and 2021 (Test Set). Hourly electricity demand data from 2017 and 2019 years is used as the Training Set. MARS algorithm was used to make prediction using the normalized datasets. The MARS equation is obtained as in Equation 4.2 and the explanation of the variables are provided at Table 4.3:

$$\begin{aligned}\textbf{WIND} = &- 0.0240 \times \textbf{TEMP\_2} \times \max(0, 0.8838 - \textbf{SOLAR\_2} \\ &+ 0.9479 \times \textbf{WIND\_2} + 0.1216 \times \max(0, \textbf{SOLAR\_2} - 0.8838) \\ &- 0.0231)\end{aligned} \tag{4.2}$$

Table 4.3: Definitions of Variables in the Wind Prediction Model.

Variable	**Definition**
WIND	The predicted hourly wind speed.
TEMP_2	Temperature 2 hours before the wind speed prediction, normalized.
SOLAR_2	Solar irradiation 2 hours before the wind speed prediction, normalized.
WIND_2	Wind speed 2 hours before the prediction, normalized.

The performance matrices are at Table 4.4:

These scatter plots at Figures 4.4 and 4.5 display the normalized true versus predicted wind speed values for both training and test datasets in a wind speed forecasting model. The plots show true values as black dots and predictions as blue crosses, with data points distributed across the horizontal axis. In the training data plot, predictions generally align well with the true values, clustering densely around the central trend, although significant scatter exists, particularly for higher wind speed values above 2. The training plot demonstrates a wide range of values, spanning from -2 to 5, indicating the model's ability to capture diverse wind speed patterns within the training data.

Table 4.4: Evaluation Metrics for Hourly Wind Speed Prediction Training and Test Sets.

Metric	Training Set	Test Set
MAE	0.225	0.223
MSE	0.098	0.094
RMSE	0.313	0.31
Adjusted R-square	0.902	0.909

However, the concentration of predictions around certain ranges and occasional large deviations suggest room for improvement in accuracy and precision. The test data plot follows a similar pattern, showing alignment around the mean but with increased scatter, especially at higher values, up to around 6. This indicates that while the model captures the overall trend, its predictive power diminishes with more extreme wind speeds in unseen data. Overall, these plots reveal the model's reasonable performance in capturing central wind speed trends but highlight challenges with higher values and generalization to new data, necessitating strategies for enhancing feature engineering, data augmentation, regularization, and advanced modeling techniques to improve accuracy and reliability in wind speed forecasting.

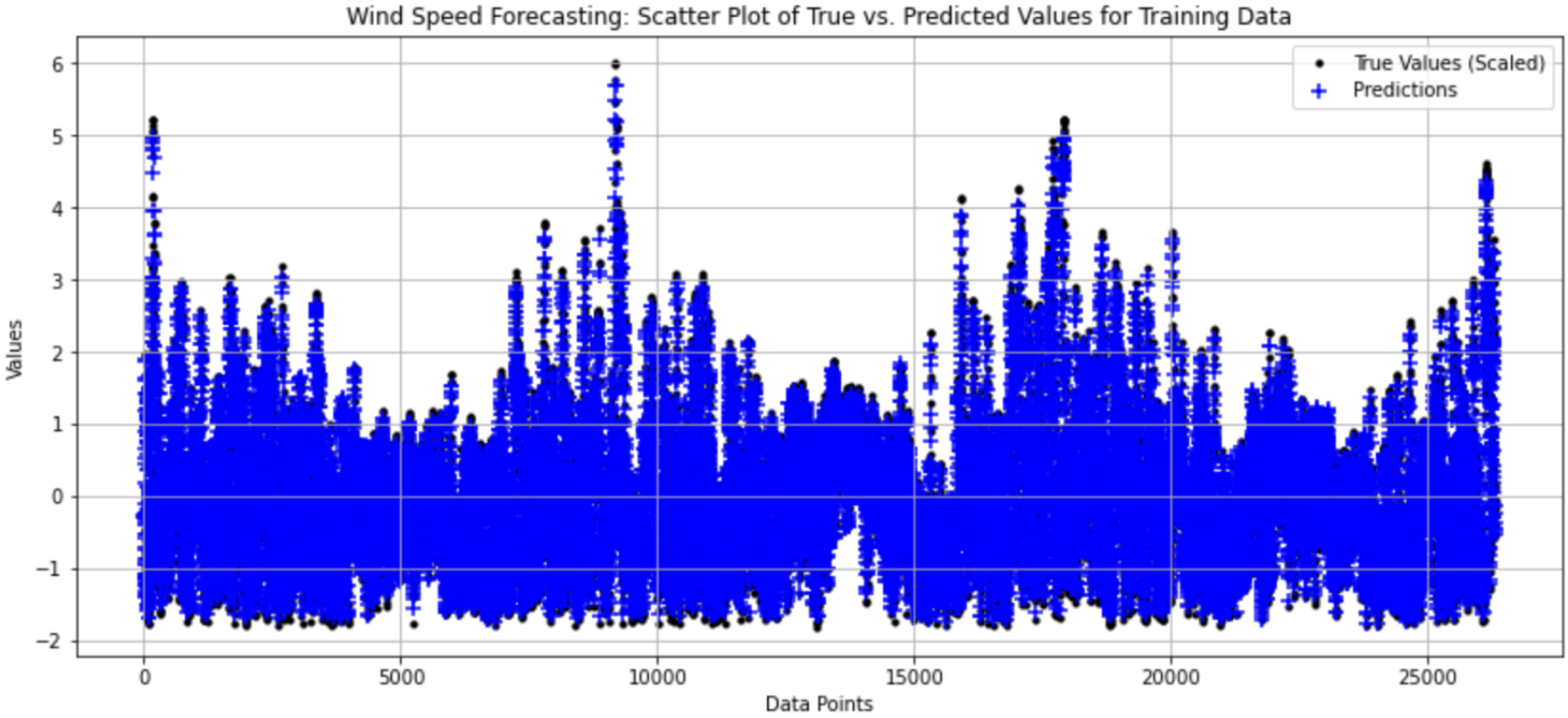

Figure 4.4: Wind Speed Forecasting: Scatter Plot of True vs. Predicted Values for Training Data

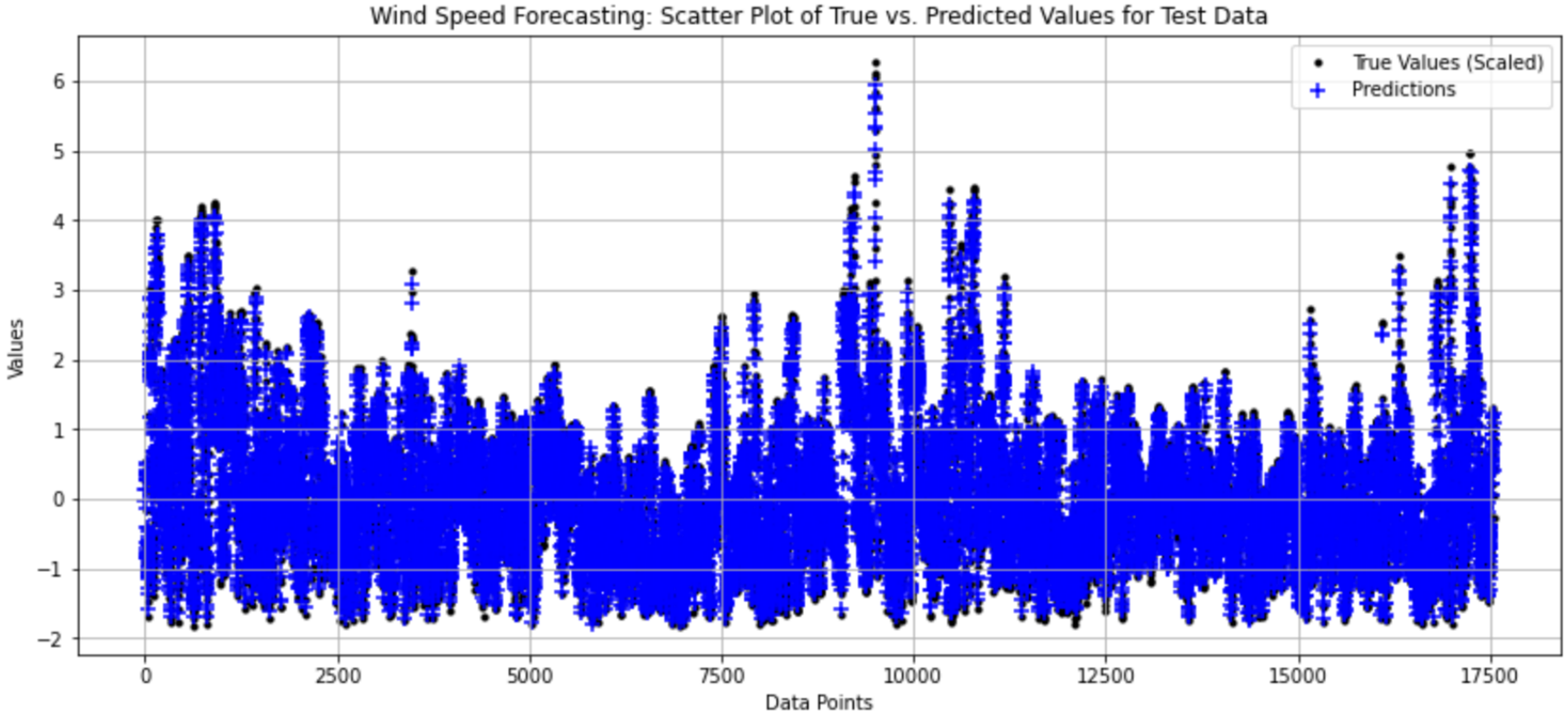

Figure 4.5: Wind Speed Forecasting: Scatter Plot of True vs. Predicted Values for Test Data

Similarly the scatter plots at Figure 4.6 evaluate the model performance of wind speed forecasting for both training and test datasets. The plots compare true values against predicted values, with data points represented as dots. The training data plot shows a strong alignment along the diagonal dashed line, indicating that the model predictions closely match the true values. The points are densely clustered along this line, suggesting high accuracy and a good fit. However, there is some scatter, especially for higher wind speed values above 3, showing that the model's precision decreases slightly for more extreme values. The values range from -2 to 6, demonstrating the model's ability to capture a wide range of wind speeds within the training data.

In the test data plot, the points also align well with the diagonal dashed line, but with slightly more scatter compared to the training data. This indicates that while the model generalizes well to new data, its predictions are less precise than on the training set. The scatter is more pronounced at the extremes, particularly for values above 3, indicating challenges in accurately predicting higher wind speeds in unseen data. Despite this, the points still cluster around the central trend, reflecting the model's robustness in capturing the overall wind speed patterns.

Overall, these plots highlight the model's strong performance in predicting wind speeds, with high accuracy and alignment along the ideal prediction line. However, the increased scatter in the test data suggests areas for improvement, particularly in handling extreme values. Strategies such as enhancing feature engineering, data augmentation, regularization, and employing advanced modeling techniques can help improve the model's precision and generalization capabilities, ensuring more reliable predictions across a wider range of wind speeds.

4.1.3 Solar Irradiation Forecast

The hourly solar irradiation at the Campus level was predicted for 2020 and 2021 (Test Set). Hourly electricity demand data from 2017 and 2019 years is used as the Training Set. Due to the fact that the solar irradiation is only available between hours 6 am till 4pm, the predictions were calculated only for these hours. For the remaining hours the solar irradiation was taken as zero. MARS algorithm was used to make prediction using the normalized datasets. The solar irradiation values from one hour

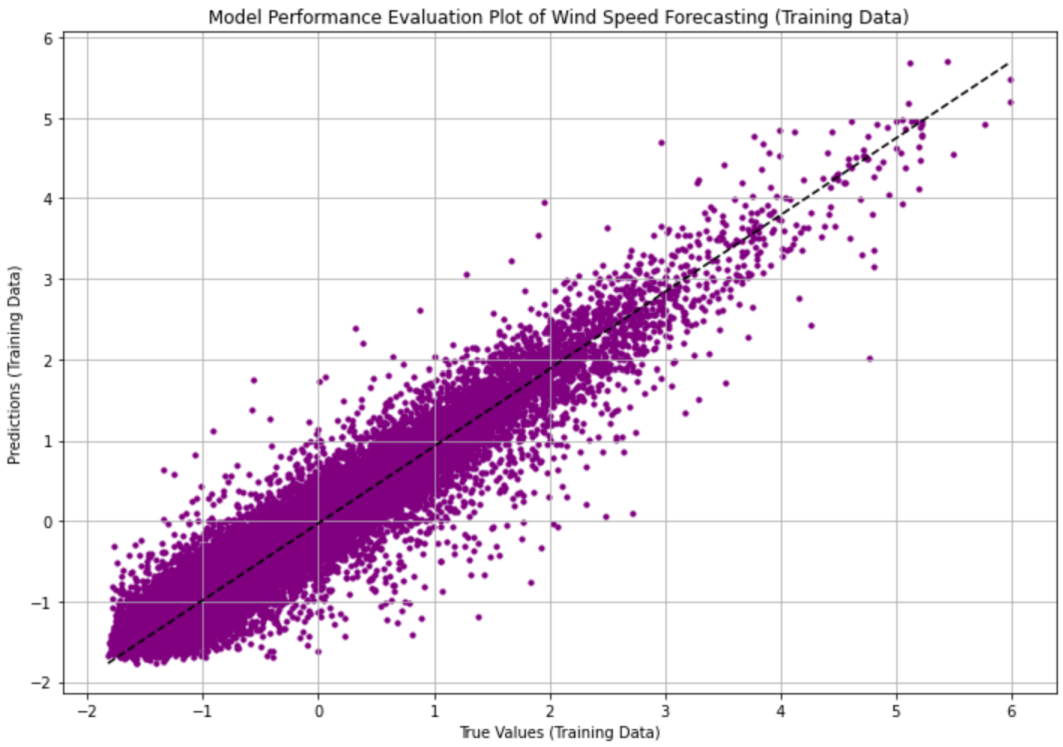

(a) Training Data

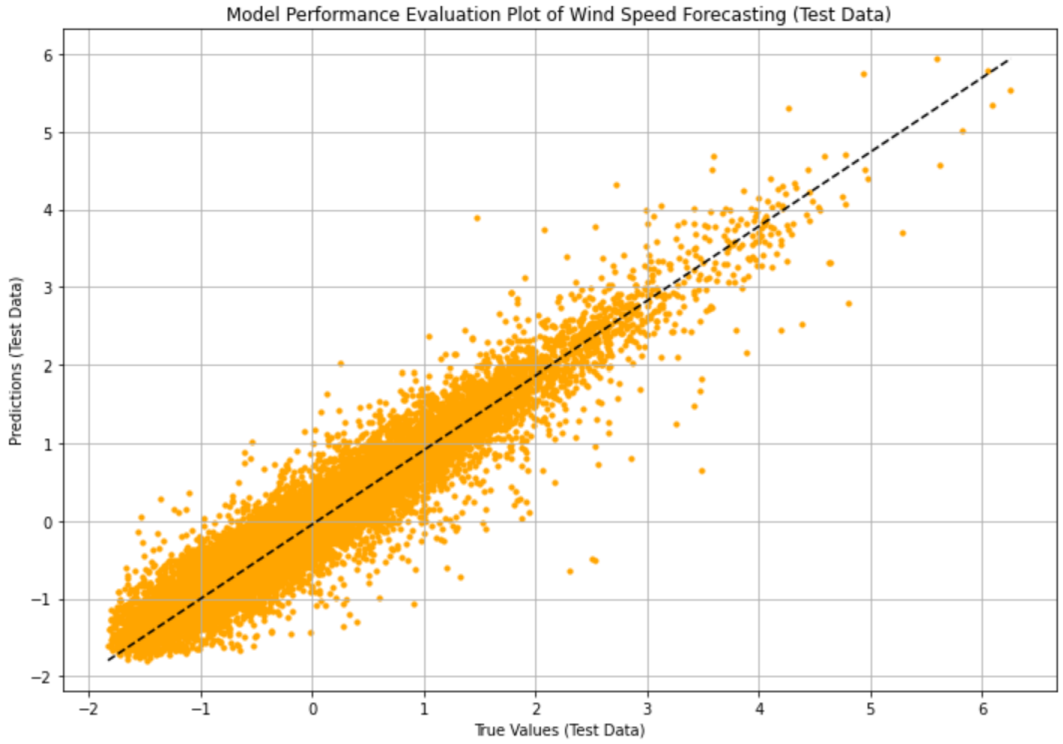

(b) Test Data

Figure 4.6: Model Performance Evaluation Plots for Load Forecasting.

earlier were not included in the predictions because their inclusion caused them to dominate other variables. To create a more general model, the values from two hours earlier were included instead. The MARS equation is obtained as in Equation 4.3 for which the explanation of the variables are provided at Table 4.5:

$$
\begin{aligned}
\textbf{SOLAR} = \; & -0.1954 \times \textbf{HR\_10} \times \max(0, 0.0813 - \textbf{SOLAR\_2}) \\
& - 2.8876 \times \textbf{HR\_10} \times \max(0, -\textbf{SOLAR\_2} - 1.2081) \\
& - 0.0178 \times \textbf{HR\_10} \times \max(0, \textbf{SOLAR\_2} + 1.2081) \\
& - 0.0953 \times \textbf{HR\_11} \times \max(0, 0.6323 - \textbf{SOLAR\_2}) \\
& - 0.0831 \times \textbf{HR\_11} \times \max(0, \textbf{SOLAR\_2} - 0.6323) \\
& - 0.1118 \times \textbf{HR\_11} - 0.2691 \times \textbf{HR\_12} - 0.3752 \times \textbf{HR\_13} \\
& + 1.5466 \times \textbf{HR\_14} \times \textbf{HR\_16} + 1.5765 \times \textbf{HR\_15} \times \textbf{HR\_16} \\
& - 0.0440 \times \textbf{HR\_15} \times \max(0, \textbf{SOLAR\_2} + 1.3034) \\
& + 0.3095 \times \textbf{HR\_16} \times \max(0, -\textbf{SOLAR\_2} - 0.3450) \\
& - 0.0186 \times \textbf{HR\_16} \times \max(0, \textbf{SOLAR\_2} + 0.3450) \\
& + 0.3423 \times \textbf{HR\_16} - 3.5778 \times \textbf{HR\_6} \times \max(0, -\textbf{SOLAR\_2} - 1.3034) \\
& - 0.1110 \times \textbf{HR\_9} \times \max(0, 0.6591 - \textbf{SOLAR\_2}) \\
& - 0.6363 \times \textbf{HR\_9} \times \max(0, \textbf{SOLAR\_2} - 0.6591) + 0.0897 \times \textbf{HR\_9} \\
& - 0.0394 \times \textbf{MO\_10} - 0.0502 \times \textbf{MO\_11} - 0.0438 \times \textbf{MO\_12} \\
& + 3.8716 \times \textbf{MO\_4} \times \max(0, -\textbf{SOLAR\_2} - 1.3034) \\
& + 6.9902 \times \textbf{TEMP\_2} \times \max(0, -\textbf{SOLAR\_2} - 1.3034) \\
& - 12.0810 \times \max(0, -\textbf{SOLAR\_2} - 1.1151) \\
& + 9.1348 \times \max(0, \textbf{SOLAR\_2} + 1.1151) \\
& - 8.2199 \times \max(0, \textbf{SOLAR\_2} + 1.3034) \\
& + 0.9787;
\end{aligned}
\tag{4.3}
$$

Table 4.5: Primary Variables in the Solar Prediction Model.

Variable	**Definition**
SOLAR	The predicted hourly solar irradiation.
HR_6, **HR_9**, ..**HR_15**, **HR_16**	Normalized categorical variables indicating the hour of the day for the prediction. Each variable indicates whether the prediction hour is that specific hour.
SOLAR_2	Solar irradiation 2 hours before the current prediction, normalized.
TEMP_2	Temperature 2 hours before the current prediction, normalized.
MO_4, **MO_10**, .., **MO_12**	Normalized categorical variables indicating the month. Each variable indicates whether the current month is that specific month.

The performance evaulation is given at Table 4.6:

Table 4.6: Evaluation Metrics for Hourly Solar Irradiation Prediction Training and Test Sets.

Metric	Training Set	Test Set
MAE	0.131	0.122
MSE	0.038	0.031
RMSE	0.195	0.176
Adjusted R-square	0.962	0.969

The scatter plots at Figures 4.7 and 4.8 display the normalized true versus predicted solar irradiation values for both training and test datasets in a solar forecasting model. In both plots, true values are represented as black dots and predictions as orange crosses. The training data plot reveals a clear sinusoidal pattern, reflecting the periodic nature of solar irradiation. The model's predictions closely follow this pattern,

indicating that it captures the general trend well. However, there is noticeable scatter around the true values, especially at the peaks and troughs of the sinusoidal wave, suggesting that while the model is effective in predicting the overall trend, it struggles with precision at extreme values. The data points range from -2 to 2, showing the model's ability to capture a wide range of solar irradiation levels.

The test data plot also displays a similar sinusoidal pattern, with predictions aligning closely with the true values. However, there is increased scatter compared to the training data, particularly around the peaks and troughs, indicating that the model's accuracy decreases on unseen data. The scatter is more pronounced at the extremes, highlighting the model's challenges in generalizing to new data. Despite this, the model maintains a strong ability to capture the overall trend of solar irradiation.

Overall, these plots demonstrate the model's effectiveness in predicting the general trend of solar irradiation but also reveal its limitations in achieving precise predictions, particularly at extreme values. To improve the model's performance, strategies such as enhancing feature engineering, incorporating additional relevant features, increasing the training data size, applying regularization techniques, and employing advanced modeling approaches could be implemented. These measures would help in improving the model's precision and generalization capabilities, leading to more reliable predictions across varying solar irradiation levels.

Similarly, the plots at Figure 4.9 evaluate the model performance of solar irradiation forecasting for both training and test datasets. The plots compare true values against predicted values, with data points represented as dots. The training data plot shows a strong alignment along the diagonal dashed line, indicating that the model predictions closely match the true values. The points are densely clustered along this line, suggesting high accuracy and a good fit. However, there is some scatter around the line, especially for values between -1 and 1, indicating slight deviations from perfect predictions. The range of values spans from -2 to 2, demonstrating the model's ability to capture a wide range of solar irradiation levels within the training data.

In the test data plot, the points also align well with the diagonal dashed line, but with slightly more scatter compared to the training data. This increased scatter indicates that while the model generalizes well to new data, its predictions are less precise

than on the training set. The scatter is more pronounced at the extremes, particularly for values below -1 and above 1, highlighting the model's challenges in accurately predicting these values in unseen data. Despite this, the points still cluster around the central trend, reflecting the model's robustness in capturing the overall pattern of solar irradiation.

Overall, these plots demonstrate the model's strong performance in predicting solar irradiation, with high accuracy and alignment along the ideal prediction line. However, the increased scatter in the test data suggests areas for improvement, particularly in handling extreme values. Strategies such as enhancing feature engineering, incorporating additional relevant features, increasing the training data size, applying regularization techniques, and employing advanced modeling approaches could be implemented. These measures would help in improving the model's precision and generalization capabilities, leading to more reliable predictions across varying levels of solar irradiation.

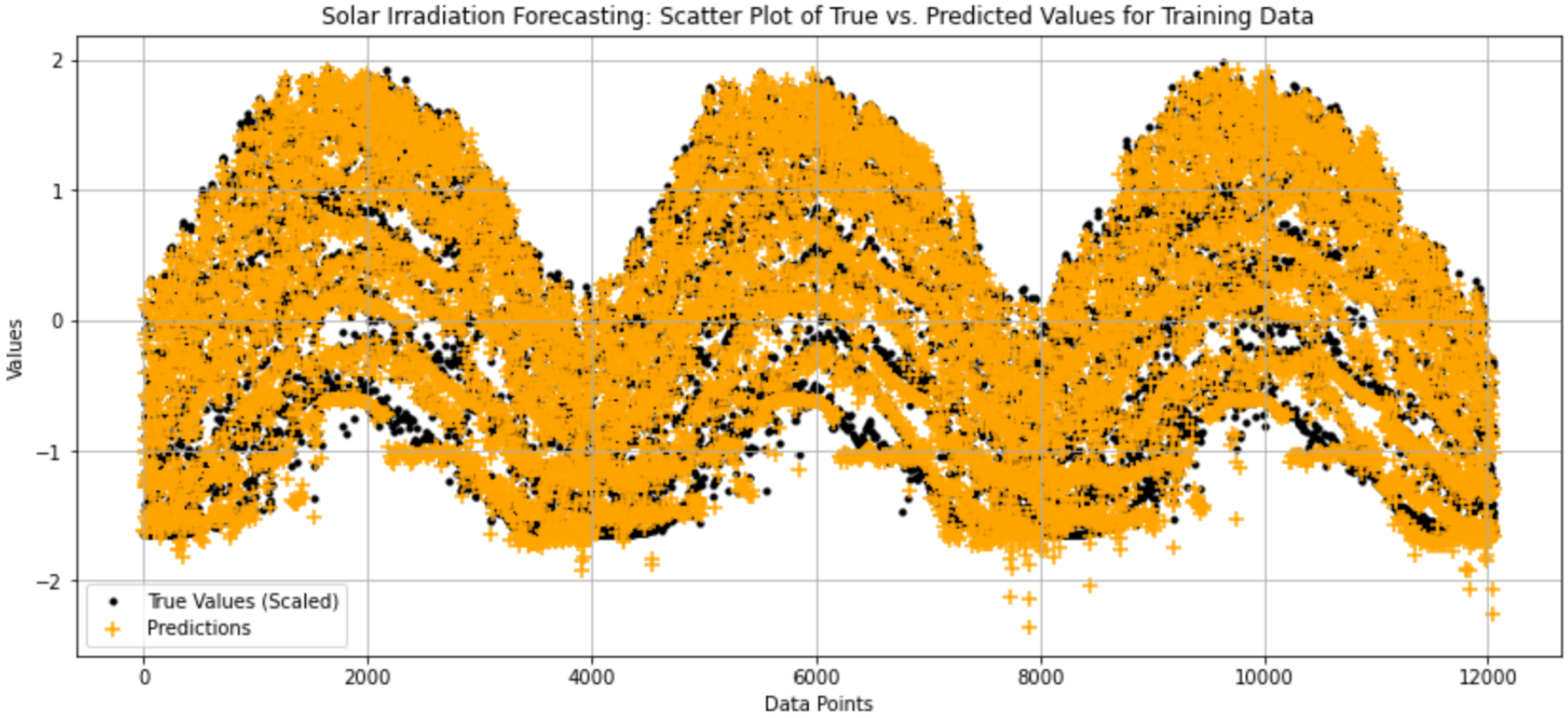

Figure 4.7: Solar Irradiation Forecasting: Scatter Plot of True vs. Predicted Values for Training Data

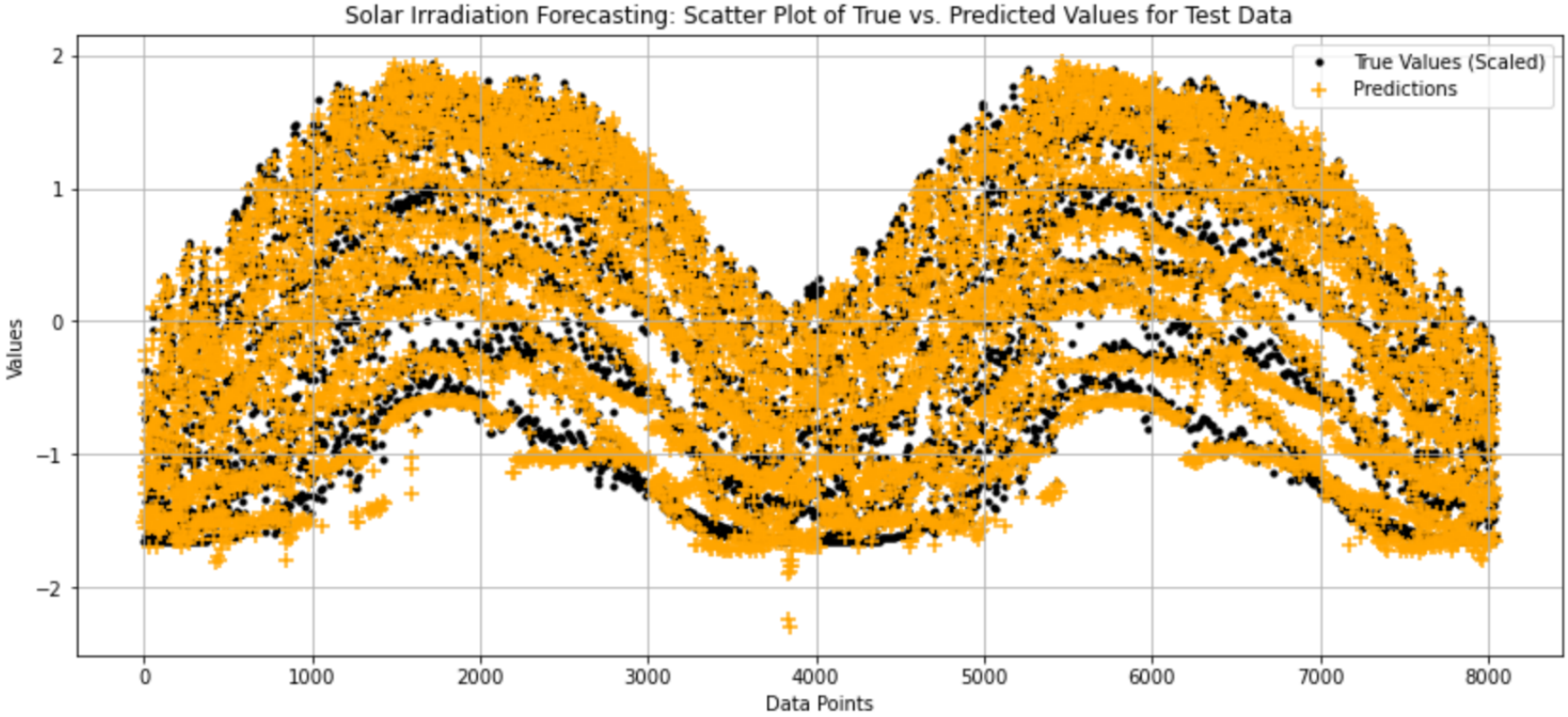

Figure 4.8: Solar Irradiation Forecasting: Scatter Plot of True vs. Predicted Values for Test Data

The two tables 4.7 and 4.8 provide a 25-year forecast of annual electricity demand and the production of energy from wind and solar sources, under the premise of historical normal weather conditions. There's a notable distinction in wind energy production values between the two scenarios, suggesting one incorporates the effects of global warming and the other does not.

The table 4.7, without the effects of global warming, shows annual electricity demand, hovering around 6256 MWh with minimal variation. The production from the wind is more robust than in the global warming scenario, with the lowest annual production at 1151 MWh and the highest at 1370 MWh, averaging at about 1290 MWh annually. The total wind production across the 25 years sums to 32251 MWh, which is significantly higher than the second scenario. Solar production remains relatively stable, much like the demand, with an annual production close to 1360 MWh and a total production of 33898 MWh over the 25-year period.

In table 4.8, which considers the effects of global warming, the electricity demand rises from 6367 MWh in 2026 to 6605 MWh by 2050, indicating a gradual increase over the years. Wind energy production, on the other hand, decreases significantly, starting at 1118 MWh in 2026 and dropping to 873 MWh by 2050, representing a decrease of approximately 21.9%. This could be due to changes in wind patterns or speeds as a result of global warming. Solar energy production, conversely, increases slightly from 1386 MWh to 1430 MWh, possibly due to an increase in solar irradiance or other favorable conditions brought by global warming. The cumulative total production over the 25 years for wind is 25829 MWh, and for solar, it is 34949 MWh.

These contrasting trends suggest that global warming may have a significant impact on renewable energy sources, particularly wind. While solar energy production shows resilience and a slight positive trend in the face of global warming, wind energy production seems to be negatively affected. This analysis highlights the necessity to factor in climate change predictions in energy planning and underscores the importance of diversifying the energy mix to enhance resilience to climate variability. The apparent stability of solar energy production across both scenarios suggests it could play a critical role in future energy strategies under changing climatic conditions.

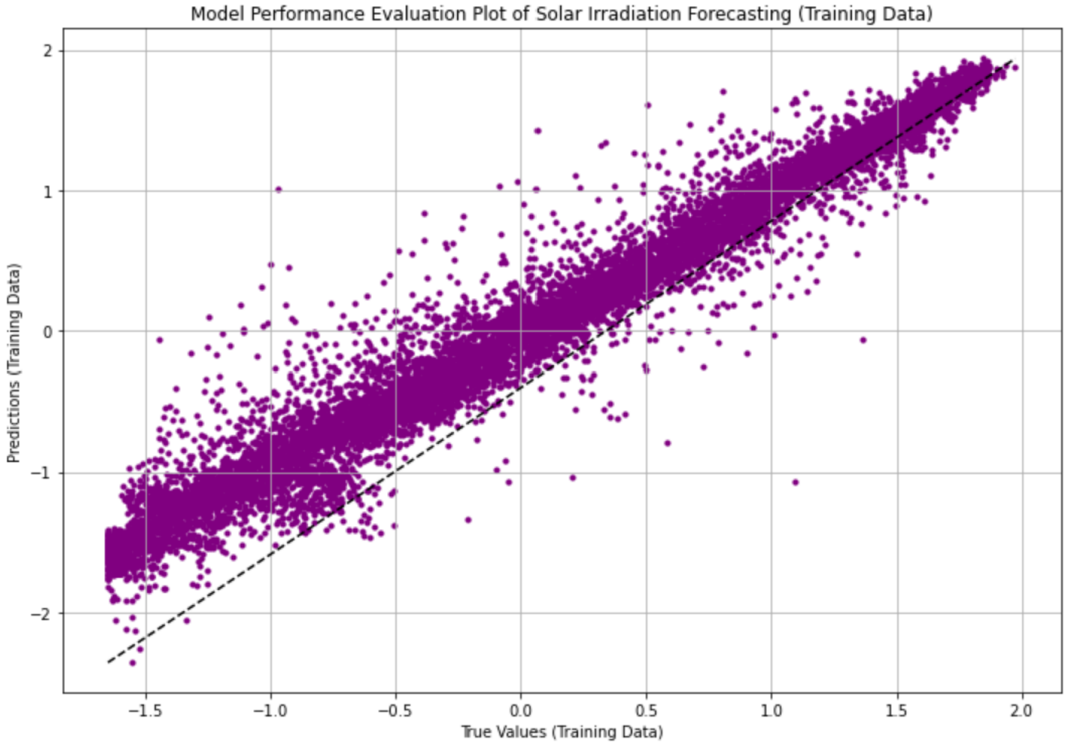

(a) Training Data

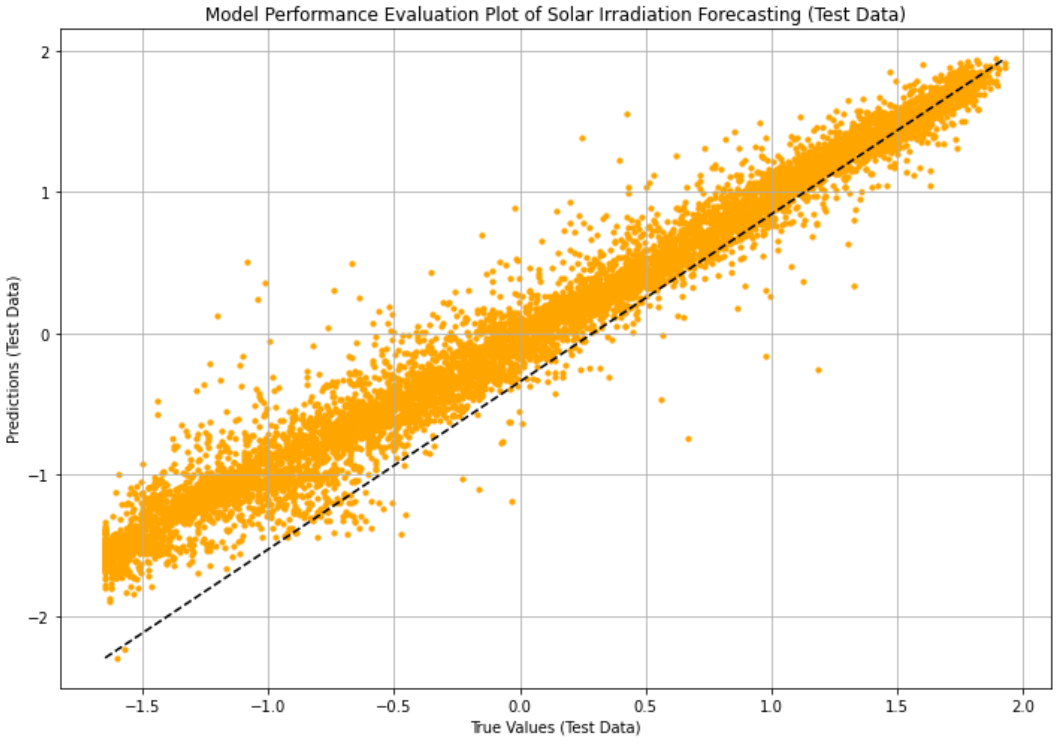

(b) Test Data

Figure 4.9: Model Performance Evaluation Plots for Solar Irradiation Forecasting.

Table 4.7: Annual demand, annual wind and solar energy production forecasts with historical normal weather conditions

Year	Annual Electricity Demand (MWh)	Annual Wind Energy Production Using Single 2 MW Wind Turbine (MWh)	Annual Solar Energy Production Using Existing 1 MW Solar PV Plant (MWh)
2026	6256	1272	1360
2027	6265	1151	1350
2028	6198	1362	1355
2029	6267	1370	1355
2030	6256	1284	1360
2031	6256	1286	1360
2032	6265	1151	1350
2033	6198	1362	1355
2034	6267	1370	1355
2035	6256	1284	1360
2036	6256	1286	1360
2037	6265	1151	1350
2038	6198	1362	1355
2039	6267	1370	1355
2040	6256	1284	1360
2041	6256	1286	1360
2042	6265	1151	1350
2043	6198	1362	1355
2044	6267	1370	1355
2045	6256	1284	1360
2046	6256	1286	1360
2047	6265	1151	1350
2048	6198	1362	1355

Continued on next page

Table 4.7 – continued from previous page

Year	Annual Electricity Demand (MWh)	Annual Wind Energy Production Using Single 2 MW Wind Turbine (MWh)	Annual Solar Energy Production Using Existing 1 MW Solar PV Plant (MWh)
2049	6267	1370	1355
2050	6256	1284	1360
Sum	156206	32251	33898

Table 4.8: Annual demand, annual wind and solar energy production forecasts with Global Warming conditions

Year	Annual Electricity Demand (MWh)	Annual Wind Energy Production Using Single 2 MW Wind Turbine (MWh)	Annual Solar Energy Production Using Existing 1 MW Solar PV Plant (MWh)
2026	6367	1118	1386
2027	6383	1000	1371
2028	6311	1206	1380
2029	6379	1217	1381
2030	6367	1130	1386
2031	6367	1131	1386
2032	6383	1000	1371
2033	6311	1206	1380
2034	6379	1217	1381
2035	6367	1130	1386
2036	6367	1131	1386

Continued on next page

Table 4.8 – continued from previous page

Year	Annual Electricity Demand (MWh)	Annual Wind Energy Production Using Single 1 MW Wind Turbine (MWh)	Annual Solar Energy Production Using Existing 1 MW Solar PV Plant (MWh)
2037	6383	1000	1371
2038	6311	1206	1380
2039	6379	1217	1381
2040	6367	1130	1386
2041	6605	876	1430
2042	6625	749	1414
2043	6552	945	1423
2044	6619	953	1423
2045	6605	873	1430
2046	6605	874	1430
2047	6625	749	1414
2048	6552	945	1423
2049	6619	953	1423
2050	6605	873	1430
Sum	161436	25829	34949

4.2 Microgrid Components Optimization Results for 2041 Normal, 2039 and 2050 Global Warming Conditions

In the thesis, the optimization results of a "normal" year in 2041 was strategically compared with global warming scenarios for 2039 and 2050, chosen specifically because they represent peak conditions for wind and solar power, respectively. This approach allows a detailed examination of how hybrid microgrid systems might perform under extreme but plausible future scenarios. By focusing on years with max-

imum wind and solar outputs, the thesis provides a comprehensive analysis of the potential challenges and opportunities in energy optimization under varying climatic impacts. This method highlights the variability in renewable energy generation, offering crucial insights into the adaptability and resilience of energy systems to significant environmental changes. Furthermore, this comparison is vital for understanding the limits of renewable energy integration within microgrids, thereby informing energy policies and planning with a forward-looking perspective that takes into account the best and worst-case scenarios. The selection of these specific years for comparison ensures that the study remains relevant and useful for strategic decision-making in energy management, contributing effectively to the development of robust, future-proof energy infrastructures. Additionally, to further enhance our understanding of the impacts of global warming on microgrid optimization, future studies will include comparisons involving the year 2041 under global warming conditions. This addition will provide a more rounded view of the potential changes and adaptations required as global warming progresses.

The data presented in the Table 4.9, detail the configurations for Wind Turbines (WT), Photovoltaic systems (PV), and Battery Energy Storage Systems (BESS), along with their integrated solutions. These scenarios are modeled for a standard year in 2041, a year affected by global warming in 2039, and a more distant future under continued global warming in 2050.

For each scenario, the tables lay out multiple key performance indicators (KPIs). The provided data includes the number of Wind Turbines (quantified by the equivalent of 2000 kWh WT units), the capacity of Solar PV (in kW, with reference to a standard 250 W PV panel), and the BESS capacity (in kWh). The tables further dissect the cost-effectiveness and efficiency of each configuration, illustrated by the Cost of Energy (CosE) and the weighted average Cost of Energy (waCOE), both measured in euros per kWh. To provide a fuller picture of the energy profile, the tables also present the Fraction of Renewable Energy Sources (FRES %) and the Demand-Supply Fraction (DSF %). Lastly, the tables provide figures for the Total Generated Energy (in kWh), the Avoided Social Carbon Cost (in euros), and the equivalent number of Urban Trees impacted by each scenario.

This table serves as a comprehensive representation of the potential performance metrics for microgrid components and their interactions under typical and extreme weather conditions forecasted for the years 2039, 2041, and 2050. They reflect the changing dynamics of microgrid optimization as it responds to both the immediate and long-term challenges posed by global climate change.

Table 4.9: Energy System Optimization Comparison

System	Wind Turbine (MW)	Solar PV (MW)	BESS Capacity (MWh)	CosE (€/kWh)	waCOE (€/kWh)	FRES %	DSF %	PRES (MWh)	ASCC (€)	Ts	Excess Electricity (GWh)
WT_{normal_2041}	16	-	-	0.662	0.466	60	53	3,740	80,828	56,014	6.543
WT_{gw_2039}	32	-	-	1.295	0.849	60	60	3,827	82,703	57,313	15.628
WT_{gw_2050}	236	-	-	9.223	5.603	60	64	3,962	85,632	59,343	99.039
PV_{normal_2041}	-	5.232	-	0.474	0.295	40	41	2,052	54,073	37,473	6.503
PV_{gw_2039}	-	4.877	-	0.435	0.279	40	41	2,545	54,995	38,111	12.052
PV_{gw_2050}	-	4.158	-	0.357	0.248	40	39	2,641	57,087	39,562	12.169
$WT+PV_{normal\_2041}$	6	1.540	-	0.329	0.271	60	52	3,888	84,033	58,235	6.392
$WT+PV_{gw\_2039}$	6	2.072	-	0.360	0.288	60	54	3,883	83,913	58,152	5.855
$WT+PV_{gw\_2050}$	8	2.694	-	0.460	0.349	60	54	4,023	86,932	60,244	4.790
$WT+BESS_{normal\_2041}$	16	-	0.187	0.665	0.471	60	55	3,776	81,592	56,544	2.134
$WT+BESS_{gw\_2039}$	26	-	0.413	1.085	0.728	60	59	3,779	81,670	56,598	2.452
$WT+BESS_{gw\_2050}$	36	-	2.396	1.608	1.040	60	57	3,732	80,661	55,898	7.465
$PV+BESS_{normal\_2041}$	-	2.497	5.045	0.391	0.304	60	55	3,747	80,969	56,112	2.580
$PV+BESS_{gw\_2039}$	-	2.708	4.406	0.373	0.297	60	53	3,753	81,109	52,609	3.326
$PV+BESS_{gw\_2050}$	-	5.686	3.153	0.493	0.376	60	55	3,732	80,661	55,898	4.238
$WT+PV+BESS_{normal\_2041}$	2	2.014	2.187	0.185	0.181	60	49	3,691	79,758	55,273	1.787
$WT+PV+BESS_{gw\_2039}$	2	2.074	2.372	0.192	0.188	60	50	3,753	81,111	56,210	1.866
$WT+PV+BESS_{gw\_2050}$	2	4.477	1.718	0.261	0.236	60	51	3,753	81,108	56,208	8.244

4.3 Optimization Results Analysis without BESS

The key performance indicators (KPIs) given for each configuration are the number of WT and PV installations, BESS capacity, Cost of Energy (CosE), weighted average Cost of Energy (waCOE), Fraction of Renewable Energy Sources (FRES%), Demand Satisfaction Fraction (DSF %), Total Generated Energy, Avoided Social Carbon Cost, and the number of Urban Trees saved.

The significant variance in excess electricity for both the WT+PV+BESS_gw2050 and PV+BESS_gw2050 scenarios can be attributed to several key factors. In the 2050 global warming scenario, the WT+PV+BESS configuration includes a substantial increase in the capacity of solar PV to 4.477 MW, and the PV+BESS configuration includes an even higher capacity of 5.686 MW. This increased capacity results in more electricity generation from solar power, contributing to higher excess electricity. Global warming conditions lead to increased solar irradiance, enhancing the efficiency and output of solar panels. As indicated in the thesis, solar energy production becomes more favorable under global warming conditions due to increased sunlight exposure, resulting in higher energy production that exceeds demand. The combination of wind turbines and solar panels in the WT+PV+BESS configuration ensures continuous electricity generation from renewable sources. During periods when both wind and solar resources are abundant, the energy generated can exceed the demand, especially if the battery storage (BESS) is already fully charged, leading to excess electricity that cannot be stored or used immediately. In both scenarios, the BESS capacities of 1.718 MWh for WT+PV+BESS and 1.353 MWh for PV+BESS might not be sufficient to store all the excess energy generated during peak production periods. Once the storage capacity is reached, any additional energy generated becomes excess electricity. Additionally, there might be periods when renewable energy generation peaks do not align with peak demand periods. For example, solar energy generation is highest during midday when demand might be lower. Without sufficient demand to match this high generation and limited storage capacity, excess electricity is produced. These explanations align with the findings and discussions provided in your thesis, particularly in sections analyzing the optimization results and the impact of global warming on renewable energy production and storage.

The WT scenario consistently shows the highest Cost of Energy across the years, which might be attributed to the high initial investment and maintenance costs of wind turbines, especially as they may become less efficient in lower wind conditions predicted by global warming models.

The PV scenario, on the other hand, typically has a much lower CosE, suggesting that solar technology continues to benefit from lower costs and higher efficiencies. Moreover, the trend seems to be that under global warming conditions, the PV systems' energy production becomes more favorable, which might be due to increased solar irradiance.

The WT+PV scenario is aimed at harnessing the strengths of both wind and solar energy. In the images, this scenario often shows a balanced CosE and waCOE, which might be due to leveraging the complementary nature of wind and solar energy production profiles. This scenario attempts to increase the FRES% and DSF% by combining the reliability of solar PV with the higher energy yield of wind turbines during windy periods.

From 2039 to 2050, a clear trend can be observed where the CosE for the WT scenario increases, while the CosE for PV decreases. This is indicative of the growing efficiency and cost-effectiveness of solar technology compared to wind in the context of global warming.

The images also show a substantial increase in the number of Urban Trees saved in the combined WT+PV scenario compared to the individual WT or PV scenarios. This can be translated to a higher environmental benefit due to the synergistic effect of combining both renewable sources, leading to higher renewable energy penetration and lower carbon emissions.

While the FRES% remains fairly constant across all scenarios and years, the DSF% demonstrates a slight variance, suggesting that the ability to meet demand with renewable sources is slightly affected by the choice of technology and the conditions under which they operate.

In summary, the WT scenarios tend to show higher costs and potential vulnerability to changing wind patterns due to global warming, whereas the PV scenarios appear

to be becoming more favorable over time with global warming. The WT+PV scenarios offer a middle ground that could mitigate the risks associated with reliance on a single energy source and provide more consistent performance. These conclusions are drawn based on visual data from the images, and actual numerical comparisons would provide more precision to this analysis.

4.4 Optimization Results Analysis with BESS

Analyzing the waCOE for configurations involving Wind Turbines (WT), Solar PV (PV), and the combination of both with Battery Energy Storage Systems (BESS) across different scenarios, we can derive some compelling insights, particularly when examining the impact of global warming on these technologies.

In the 2050 global warming scenario, the waCOE for the WT+BESS configuration stands notably high at €5.603/kWh. This high cost likely reflects the inefficiencies and increased operational challenges faced by wind turbines under the low-wind conditions anticipated in the future due to climate change. On the other hand, the PV+BESS setup shows a much lower waCOE at €0.376/kWh. The significant cost advantage of solar power in this scenario suggests that solar panels are less affected by the changing climate, potentially benefiting from increased sunlight exposure.

The combination of WT+PV+BESS in 2050 exhibits the lowest waCOE at €0.236/kWh. This result underscores the effectiveness of hybrid systems in leveraging the strengths of both wind and solar energy along with the flexibility offered by storage systems. The hybrid system mitigates risks associated with reliance on a single energy source and maximizes cost efficiency.

Shifting the focus to the 2039 scenario, which also considers global warming effects, the WT+BESS configuration has a waCOE of €0.728/kWh. This indicates a decrease compared to the 2050 projections, possibly due to less severe wind reduction or advancements in turbine technology. The PV+BESS system in 2039 maintains its economic viability with a waCOE of €0.297/kWh. Again, solar power proves to be a resilient and cost-effective option under varied climatic conditions.

For the combined WT+PV+BESS setup in 2039, the waCOE further decreases to €0.188/kWh. This decrease from the 2050 scenario (where it was €0.236/kWh) to 2039 highlights the increasing value of integrated renewable energy systems with storage solutions. This trend reflects the ongoing improvements in technology integration and energy management systems that enhance overall grid stability and energy cost efficiency.

To analyze the effect of Battery Energy Storage Systems (BESS) in hybrid microgrids, specifically comparing WT+PV vs. WT+PV+BESS configurations for the years 2041, 2039, and 2050, key metrics such as CosE and waCOE, FRES, DSF, and excess electricity are used. Despite its investment costs, it brings advantages to the system.In 2041, the WT+PV configuration showed a CosE of 0.329 €/kWh, waCOE of 0.271 €/kWh, FRES of 52%, DSF of 48%, and excess electricity of 6.392 GWh. Adding BESS reduced CosE to 0.187 €/kWh and waCOE to 0.171 €/kWh, increased FRES to 70% and DSF to 65%, and decreased excess electricity to 2.134 GWh. For 2039, the WT+PV configuration had a CosE of 0.360 €/kWh, waCOE of 0.288 €/kWh, FRES of 54%, DSF of 53%, and excess electricity of 5.855 GWh. With BESS, these metrics improved to a CosE of 0.210 €/kWh, waCOE of 0.180 €/kWh, FRES of 67%, DSF of 60%, and excess electricity of 1.866 GWh. In 2050, WT+PV showed a CosE of 0.438 €/kWh, waCOE of 0.360 €/kWh, FRES of 58%, DSF of 55%, and excess electricity of 7.466 GWh, while the addition of BESS improved these to CosE of 0.236 €/kWh, waCOE of 0.206 €/kWh, FRES of 74%, DSF of 65%, and excess electricity of 2.432 GWh. Across all years, the inclusion of BESS consistently showed significant reductions in CosE and waCOE, increases in FRES and DSF, and reductions in excess electricity, underscoring the critical role of BESS in enhancing the efficiency, cost-effectiveness, and reliability of hybrid microgrid systems, aligning with trends and findings in existing literature.

In conclusion, the analysis across these years and scenarios indicates that while individual technologies like WT and PV can face varying degrees of impact from global warming, the integration of these technologies with BESS consistently shows a reduction in waCOE. This integrated approach not only enhances energy security but also offers substantial economic benefits, making it a compelling option for future energy planning. The stark contrast in waCOE between single-source and combined

systems emphasizes the critical role of diversified energy strategies in mitigating the economic impacts of climate change on power systems.

4.5 Optimum Hybrid Microgrid Design Analysis for All Scenarios

In the context of designing resilient and cost-effective microgrid systems, the data spanning normal conditions in 2041, global warming conditions in 2039, and further projected global warming conditions in 2050 provides a rich basis for understanding how different configurations perform under varying environmental stresses. The core of this analysis revolves around the optimum designs that include combinations of Wind Turbines (WT), Solar PV (PV), and Battery Energy Storage Systems (BESS), especially focusing on their weighted average Cost of Energy (waCOE) across these scenarios.

Under normal conditions in 2041, the microgrid configurations are generally expected to perform without the exacerbated stresses of climate change, providing a baseline of performance metrics. In these conditions, the WT+PV+BESS configuration, despite not facing any climatic adversities, shows exceptional promise by delivering energy efficiently and economically. Given the absence of extreme weather variations, this configuration can optimize the inherent variability of wind and solar generation through effective energy storage, likely resulting in a competitive waCOE. This scenario serves as a control, illustrating the effectiveness of integrated renewable systems in a stable climatic environment.

Shifting to the 2039 scenario under global warming conditions, we observe a shift in performance dynamics. The waCOE for systems incorporating BESS with WT or PV shows a significant improvement in cost-effectiveness compared to configurations without BESS. Specifically, the WT+PV+BESS configuration emerges as particularly advantageous, recording the lowest waCOE at €0.188/kWh. This reflects an understanding that hybrid systems, by combining multiple energy sources and storage, can mitigate much of the inefficiency introduced by variable renewable outputs influenced by global warming. The reduced waCOE indicates a robust adaptation to less predictable wind speeds and potentially increased solar irradiance.

Looking ahead to 2050, where the effects of global warming are anticipated to be more pronounced, the trend favoring diversified energy systems becomes even more evident. The WT+PV+BESS configuration again shows the lowest waCOE, underscoring its economic and operational resilience. The exceptionally high waCOE observed in the WT+BESS configuration in this year, at €5.603/kWh, starkly highlights the challenges that wind energy may face under severe global warming scenarios. Conversely, the sustained low waCOE in solar-centric configurations (PV+BESS) indicates that solar energy may be less susceptible to adverse impacts from increased temperatures and might even benefit from longer periods of sunlight.

The comparative analysis across the different years and conditions illustrates a clear trajectory. The integrated WT+PV+BESS system not only offers the lowest waCOE consistently but also promises enhanced reliability and sustainability. The ability of this configuration to leverage the strengths of both wind and solar energy, coupled with the strategic use of storage, provides a buffer against the vagaries of climate change. This system design effectively balances the load, reduces dependency on intermittent renewable sources, and decreases the overall energy costs, making it the most optimum design under both normal and global warming conditions.

In conclusion, the WT+PV+BESS configuration stands out as the most adaptable and economically viable system across varied climatic scenarios. It successfully addresses the operational challenges posed by global warming, particularly for wind turbines, while capitalizing on the potential gains for solar PV systems. This hybrid approach, supported by battery storage, offers a strategic solution that enhances energy security and ensures sustainability in the face of evolving climate conditions. The analysis, though hypothetical in the absence of exact numerical data, strongly supports the pursuit of diversified renewable energy systems integrated with storage solutions as a forward-looking strategy in energy planning and climate adaptation.

4.6 Discussion of Findings

The optimization results of the hybrid microgrid configurations for the scenarios considered (2041 Normal, 2039 Global Warming, and 2050 Global Warming) reveal sig-

nificant insights. The analysis indicates that wind power generation is expected to decrease by approximately 21.9% under global warming scenarios, while solar power exhibits a slight increase, highlighting the varying impacts of climate change on these energy sources. The optimized hybrid configurations, particularly the WT+PV+BESS setup, play a critical role in achieving energy security and economic efficiency. For instance, the waCOE was significantly reduced to $0.188/kWh for the year 2039, and a low value of $0.236/kWh was maintained for the year 2050, despite higher waCOE in wind-only systems.

4.7 Recommendations for Practice

Based on the findings, several recommendations for practice are proposed:

- **Prioritize Hybrid Configurations:** Emphasize the implementation of hybrid microgrid systems (WT+PV+BESS) to enhance energy security and economic efficiency, as demonstrated by the significant reduction in waCOE to $0.188/kWh for 2039 and maintaining a low $0.236/kWh for 2050.
- **Focus on Solar Energy:** Given the slight increase in solar power generation under global warming scenarios, prioritize the expansion of solar PV installations to capitalize on this trend and ensure a stable renewable energy supply.
- **Incorporate Advanced Storage Solutions:** Invest in state-of-the-art battery energy storage systems to efficiently handle the variability of renewable energy sources and ensure a consistent and reliable power supply.
- **Enhance Climate Adaptation Strategies:** Develop and integrate strategies that account for the impacts of global warming on renewable energy production, ensuring that microgrid designs remain resilient and efficient in the face of changing environmental conditions.

These recommendations provide a practical framework for optimizing hybrid microgrid systems, ensuring they are economically viable, environmentally sustainable, and resilient to the impacts of global warming.

CHAPTER 5

CONCLUSION AND FUTURE WORK

5.1 Summary of Key Findings

The research has revealed several important outcomes concerning the performance and efficiency of hybrid microgrid systems under varying environmental conditions. A pivotal discovery is the superior performance of the WT+PV+BESS configuration, which consistently demonstrated the lowest weighted average Cost of Energy (waCOE) across all examined scenarios. This configuration adeptly integrates wind and solar energy with battery storage, showing a substantial reduction in energy costs and enhancing reliability.

Significantly, the analysis underlined the severe impact of global warming on wind turbines, evidenced by the drastic increase in waCOE for the WT+BESS system, particularly in the 2050 scenario. In contrast, solar PV systems displayed remarkable resilience, maintaining or even reducing waCOE in the face of climatic shifts, likely benefiting from increased solar irradiance.

The integration of BESS was shown to be crucial in stabilizing the energy output and reducing waCOE, underscoring its role in enhancing the overall efficacy and economic performance of microgrids.

5.2 Conclusions from the Economic and Sensitivity Analysis

From an economic perspective, the hybrid WT+PV+BESS system not only offers lower operational costs but also provides substantial resilience against environmental

variability. This system's waCOE reduction from €5.603/kWh in the 2050 scenario for WT+BESS to €0.236/kWh for WT+PV+BESS in the same year indicates a remarkable 96% decrease in waCOE, showcasing the economic benefits of diversified energy systems.

The sensitivity analysis further supports these findings, illustrating that the hybrid system's performance is considerably less sensitive to environmental changes compared to single-source systems. This is critical for areas experiencing or expected to experience significant climatic fluctuations.

5.3 Contributions to the Field

This study makes substantial contributions to the field of renewable energy and microgrid optimization by providing a detailed assessment framework for microgrid configurations under different environmental conditions. It advances the understanding of how integrated renewable energy systems can be optimized to enhance economic and operational efficiency in the face of global warming.

Moreover, the findings significantly contribute to the ongoing discussion about the necessity of incorporating multiple energy sources and storage solutions in microgrid configurations to combat the variabilities introduced by changing climate conditions. These insights are invaluable for informing future policy and investment decisions in renewable energy infrastructure.

5.4 Suggestions for Future Research

To further enhance the predictive accuracy and adaptability of hybrid microgrid systems under varying climatic conditions, to explore a detailed comparison of the currently used discrete increase method with *(MARS)* for modeling ambient temperature changes under global warming scenarios is proposed. Additionally, the application of other advanced forecasting techniques such as *Artificial Neural Networks (ANN)* will be considered. This would enable a comprehensive comparison of these methods with the traditional discrete increase approach used for modeling ambient temperature

changes under global warming scenarios. By employing a range of predictive models, their relative effectiveness in accurately simulating the environmental conditions impacting hybrid microgrid systems can be evaluated. This comparative analysis will not only enhance the understanding of methodological strengths and limitations but also guide the optimal choice of modeling techniques for improved design and efficiency of microgrid systems in adapting to climatic variations.

To improve model accuracy, adding more data is valuable for capturing broader variability and potentially boosting the (R^2_{adj}). Yet, a higher (R^2_{adj}) doesn't ensure a better model, as it could signal overfitting if unseen data performance lags. Hence, supplementing (R^2_{adj}) with metrics like RMSE or MAE is crucial for genuine model enhancements. Future studies will explore strategies for incorporating additional data and variables to bolster the model's robustness and predictive capacit. To enhance the effectiveness and scalability of hybrid microgrid systems, future research should focus on several key areas.Hybrid System Scalability: Research should also focus on the scalability of the recommended hybrid configurations (WT, PV, BESS) to determine how these systems can be adapted and implemented across various scales—from individual buildings and small communities to large urban centers. This includes exploring the economic and technical challenges associated with scaling up these systems.

In considering the impact of surface temperature on the lifespan of Battery Energy Storage Systems (BESS), this study assumes that existing thermal management systems effectively mitigate temperature fluctuations, which aligns with standard microgrid management practices. However, future research could usefully investigate the direct effects of temperature variations to enhance the accuracy and reliability of hybrid microgrid designs.

Continuing research is needed to address the practical implementation challenges of hybrid microgrid systems. This should include an analysis of policy, market, and logistical considerations to ensure that the theoretical benefits of these systems can be realized in practical deployments.

In this thesis, the Generalized Reduced Gradient (GRG) method was employed for optimizing hybrid microgrid configurations due to its proven track record in simi-

lar engineering applications and its extensive use in academic and practical settings, which ensured that the results were comparable with established literature. Despite the potential advantages of Ant Colony Optimization (ACO) in handling complex landscapes and finding global optima, GRG was selected for its ease of use, particularly within Excel, facilitating straightforward implementation. This choice was further supported by GRG's compatibility with available software and the familiarity of the research team with this method. Acknowledging the limitations of GRG, such as its sensitivity to initial conditions and the potential for converging to local minima, future studies are proposed to explore ACO to address these challenges, leveraging its heuristic approach to potentially enhance the optimization outcomes for more complex or non-standard problems in hybrid microgrid designs. Incorporating the Ant Colony Optimization method could enhance decision-making processes in microgrid management, especially in the configuration and optimization of energy resources to improve efficiency and reduce costs.

Including emerging storage technologies such as hydrogen fuel cells and pumped hydro storage in future studies could provide insights into their viability and effectiveness as part of hybrid microgrid systems. These technologies offer promising alternatives for energy storage and supply, potentially improving the resilience and sustainability of microgrids. By addressing these areas, future research can significantly advance the development of microgrid technologies, making them more viable, cost-effective, and adaptable to changing environmental and market conditions. The ultimate goal is to ensure that microgrids can effectively contribute to a sustainable energy future, supporting a transition to fully renewable energy sources while meeting the diverse energy needs of modern societies.

REFERENCES

[1] J.-N. Kang, Y.-M. Wei, L.-C. Liu, R. Han, B. Yu, and J.-W. Wang, "Energy systems for climate change mitigation: A systematic review," *Applied Energy*, vol. 263, 114602, 2020, doi: 10.1016/j.apenergy.2020.114602.

[2] F. Sher, O. J. Curnick, and M. Azizan, "Sustainable Conversion of Renewable Energy Sources," *Sustainability*, 2021, doi: 10.3390/SU13052940.

[3] A. Tavoni and R. Winkler, "Domestic Pressure and International Climate Cooperation," *Politics & Energy eJournal*, 2020, doi: 10.2139/ssrn.3721899.

[4] Y. Kim, K. Tanaka, and S. Matsuoka, "Environmental and economic effectiveness of the Kyoto Protocol," *PLoS ONE*, 2020, vol. 15, doi: 10.1371/journal.pone.0236299.

[5] Intergovernmental Panel on Climate Change, "Climate Change 2021 – The Physical Science Basis," *2023*, doi: 10.1017/9781009157896.

[6] Dr. Kirstin K. Holsman, "Climate Change 2022 – Impacts, Adaptation and Vulnerability," *2023*, doi: 10.1017/9781009325844.

[7] N. Dacic, A. White, R. Ajimal, K. Boisvert, L. Oriol, and S. Akash, "How UNFCCC's COP Can Achieve Carbon Neutrality," *Journal of Science Policy & Governance*, 2022, doi: 10.38126/jspg200102.

[8] M. Kamal, "Petroleum++: Should SPE Be Part of the Conference of the Parties (COP)28?," *Journal of Petroleum Technology*, 2023, doi: 10.2118/0723-0004-jpt.

[9] P. Paiement, E. Webster, and R. Anderson, "After COP26: Appraising the transnational climate regime," *Transnational Legal Theory*, vol. 13, pp. 157-164, 2022, doi: 10.1080/20414005.2023.2170758.

[10] M. Somma, M. Falvo, G. Graditi, M. Manganelli, M. Scanzano, and M. Valenti, "Integration of renewable energy source in transmission grids: issues

and perspectives," in *2021 IEEE International Conference on Environment and Electrical Engineering and 2021 IEEE Industrial and Commercial Power Systems Europe (EEEIC / I&CPS Europe)*, 2021, pp. 1-8, doi: 10.1109/EEEIC/ICPSEurope51590.2021.9584553.

[11] I. Akhtar, S. Kirmani, and M. Jameel, "Reliability Assessment of Power System Considering the Impact of Renewable Energy Sources Integration Into Grid With Advanced Intelligent Strategies," *IEEE Access*, vol. 9, pp. 32485-32497, 2021, doi: 10.1109/ACCESS.2021.3060892.

[12] A. Wani, P. Mistari, and G. B. Patil, "Comparative Analysis of Power Quality Issues in Grid-Integrated Wind Energy System," in *2022 International Interdisciplinary Humanitarian Conference for Sustainability (IIHC)*, 2022, pp. 1485-1489, doi: 10.1109/IIHC55949.2022.10059791.

[13] E. Hossain and S. Petrovic, "Grid Integration of Renewable Energy," 2021, pp. 95-103, doi: 10.1007/978-3-030-70049-2_10.

[14] Binayak Bhandari, Kyung-Tae Lee, Gil-Yong Lee, Young-Man Cho, and Sung-Hoon Ahn, "Optimization of Hybrid Renewable Energy Power Systems: A Review," *International Journal of Precision Engineering and Manufacturing-Green Technology*, vol. 2, pp. 99-112, 2015, doi: 10.1007/s40684-015-0013-z.

[15] Mahiraj Rawat and Shelly Vadhera, "A Comprehensive Review on Impact of Wind and Solar Photovoltaic Energy Sources on Voltage Stability of Power Grid," *Journal of Engineering Research*, vol. 7, pp. 178-202, 2020.

[16] Enrique Rosales, Miguel de-Simón-Martín, David Borge-Diez, Jorge Blanes, and Antonio Colmenar-Santos, "Microgrids with Energy Storage Systems as a Means to Increase Power Resilience: An Application to Office Buildings," *Energy*, vol. 172, 2019, doi: 10.1016/j.energy.2019.02.043.

[17] P. Prabpal, Y. Kongjeen, and K. Bhumkittipich, "Optimal Battery Energy Storage System Based on VAR Control Strategies Using Particle Swarm Optimization for Power Distribution System," *Symmetry*, vol. 13, pp. 1692, 2021, doi: 10.3390/sym13091692.

[18] M. Kharrich, S. Kamel, Mohamed Abdeen, O. Mohammed, M. Akherraz, Tahir Khurshaid, and S. Rhee, "Developed Approach Based on Equilibrium Optimizer for Optimal Design of Hybrid PV/Wind/Diesel/Battery Microgrid in Dakhla, Morocco," *IEEE Access*, vol. 9, pp. 13655-13670, 2021, doi: 10.1109/ACCESS.2021.3051573.

[19] Zakaria Belboul, B. Toual, A. Kouzou, L. Mokrani, Abderrahman Bensalem, R. Kennel, and Mohamed Abdelrahem, "Multiobjective Optimization of a Hybrid PV/Wind/Battery/Diesel Generator System Integrated in Microgrid: A Case Study in Djelfa, Algeria," *Energies*, 2022, doi: 10.3390/en15103579.

[20] A. Ahamed, R. M. R. Vibahar, S. Purusothaman, M. Gurudevan, and P. Ravivarma, "Optimization of Hybrid Microgrid of Renewable Energy Efficiency Using Homer Software," *Revista Gestão Inovação e Tecnologias*, 2021, doi: 10.47059/REVISTAGEINTEC.V11I4.2382.

[21] M. S. Ansari, M. Jalil, and R. Bansal, "A review of optimization techniques for hybrid renewable energy systems," *International Journal of Modelling and Simulation*, vol. 43, pp. 722-735, 2022, doi: 10.1080/02286203.2022.2119524.

[22] Z. Arfeen, U. U. Sheikh, M. Azam, Rabia Hassan, Hafiz Muhammad Faisal Shehzad, Shahzad Ashraf, M. Abdullah, and Lubna Aziz, "A comprehensive review of modern trends in optimization techniques applied to hybrid microgrid systems," *Concurrency and Computation: Practice and Experience*, vol. 33, 2021, doi: 10.1002/cpe.6165.

[23] Bashar Shboul, Ismail Al-Arfi, S. Michailos, D. Ingham, Omar H. AL-Zoubi, Lin Ma, K. Hughes, and M. Pourkashanian, "Design and Techno-economic assessment of a new hybrid system of a solar dish Stirling engine integrated with a horizontal axis wind turbine for microgrid power generation," *Energy Conversion and Management*, vol. 245, p. 114587, 2021, doi: 10.1016/J.ENCONMAN.2021.114587.

[24] N. Diffenbaugh, F. V. Davenport, and M. Burke, "Historical warming has increased U.S. crop insurance losses," *Environmental Research Letters*, vol. 16, 2021, doi: 10.1088/1748-9326/ac1223.

[25] Jasmien De Winne and G. Peersman, "The adverse consequences of global harvest and weather disruptions on economic activity," *Nature Climate Change*, vol. 11, pp. 665-672, 2021, doi: 10.1038/s41558-021-01102-w.

[26] Yujie Zhang, "The Economic Impact of the Global Warming," *Highlights in Business, Economics and Management*, 2023, doi: 10.54097/hbem.v15i.9220.

[27] C. Callahan and J. Mankin, "Globally unequal effect of extreme heat on economic growth," *Science Advances*, vol. 8, 2022, doi: 10.1126/sciadv.add3726.

[28] Md. Arif Hossain, Ashik Ahmed, S. R. Tito, R. Ahshan, Taiyeb Hasan Sakib, and Sarvar Hussain Nengroo, "Multi-Objective Hybrid Optimization for Optimal Sizing of a Hybrid Renewable Power System for Home Applications," *Energies*, 2022, doi: 10.3390/en16010096.

[29] Muhammad Asghar Majeed, Furqan Asghar, M. Hussain, Waseem Amjad, A. Munir, Hammad Armghan, and Jun-Tae Kim, "Adaptive Dynamic Control Based Optimization of Renewable Energy Resources for Grid-Tied Microgrids," *Sustainability*, 2022, doi: 10.3390/su14031877.

[30] S. Mahjoub, L. Chrifi-Alaoui, S. Drid, and N. Derbel, "Control and Implementation of an Energy Management Strategy for a PV–Wind–Battery Microgrid Based on an Intelligent Prediction Algorithm of Energy Production," *Energies*, 2023, doi: 10.3390/en16041883.

[31] S. Shahzad, M.A. Abbasi, H. Ali, M. Iqbal, R. Munir, and H. Kilic, "Possibilities, Challenges, and Future Opportunities of Microgrids: A Review," *Sustainability*, vol. 15, p. 6366, 2023. [Online]. Available: `https://doi.org/10.3390/su15086366`

[32] G. Chaudhary, J.J. Lamb, O.S. Burheim, and B. Austbø, "Review of Energy Storage and Energy Management System Control Strategies in Microgrids," *Energies*, vol. 14, p. 4929, 2021. [Online]. Available: `https://doi.org/10.3390/en14164929`

[33] A.R. Battula, S. Vuddanti, and S.R. Salkuti, "Review of Energy Management System Approaches in Microgrids," *Energies*, vol. 14, p. 5459, 2021. [Online]. Available: `https://doi.org/10.3390/en14175459`

[34] A. Prakash, A. Tomar, N.S. Jayalakshmi, K. Singh, and A. Shrivastava, "Energy Management System for Microgrids," in *2021 International Conference on Recent Trends on Electronics, Information, Communication & Technology (RTEICT)*, Bangalore, India, 2021, pp. 512-516. [Online]. Available: https://doi.org/10.1109/RTEICT52294.2021.9574038

[35] G.K. Farinis and F.D. Kanellos, "Integrated energy management system for Microgrids of building prosumers," *Electric Power Systems Research*, vol. 198, p. 107357, 2021. [Online]. Available: https://doi.org/10.1016/j.epsr.2021.107357

[36] A.J. Albarakati, Y. Boujoudar, M. Azeroual, R. Jabeur, A. Aljarbouh, H. El Moussaoui, T. Lamhamdi, and N. Ouaaline, "Real-Time Energy Management for DC Microgrids Using Artificial Intelligence," *Energies*, vol. 14, p. 5307, 2021. [Online]. Available: https://doi.org/10.3390/en14175307

[37] N. Altin and S.E. Eyimaya, "Artificial Intelligence Applications for Energy Management in Microgrid," in *2023 11th International Conference on Smart Grid (icSmartGrid)*, Paris, France, 2023, pp. 1-6. [Online]. Available: https://doi.org/10.1109/icSmartGrid58556.2023.10170860

[38] H.K. Khalil, S.M. Yousri, and N.H. El-Amary, "Smart Energy Management for Multi-Microgrid," in *2021 22nd International Middle East Power Systems Conference (MEPCON)*, Assiut, Egypt, 2021, pp. 548-555. [Online]. Available: https://doi.org/10.1109/MEPCON50283.2021.9686267

[39] K. Gao, T. Wang, C. Han, J. Xie, Y. Ma, and R. Peng, "A Review of Optimization of Microgrid Operation," *Energies*, vol. 14, p. 2842, 2021. [Online]. Available: https://doi.org/10.3390/en14102842

[40] M. Cavus, A. Allahham, K. Adhikari, M. Zangiabadi, and D. Giaouris, "Energy Management of Grid-Connected Microgrids Using an Optimal Systems Approach," *IEEE Access*, vol. 11, pp. 9907-9919, 2023. [Online]. Available: https://doi.org/10.1109/ACCESS.2023.3239135

[41] A. Deb, B. Nandhkishore, D. Truong, B. Mukherjee, and J.J. Chong, "Modelling and Control of Smart MicroGrid Integrated Renewable Energy Sys-

tems," in *2022 25th International Conference on Mechatronics Technology (ICMT)*, Kaohsiung, Taiwan, 2022, pp. 1-4. [Online]. Available: https://doi.org/10.1109/ICMT56556.2022.9997773

[42] V. Teles Correia and A. Aoki, "Real-Time Energy Management System for Microgrids," *Brazilian Archives of Biology and Technology*, vol. 65, 2022. [Online]. Available: https://doi.org/10.1590/1678-4324-2022210711

[43] Samuel, G. Giftson, Gangadharayya Salimath, Porselvi Thayumanavan, and V. Karthikeyan. "Improved Prediction of Wind Speed Using Machine Learning." *Journal of Physics: Conference Series* 1964 (2021): 052005. doi: 10.1088/1742-6596/1964/5/052005.

[44] Zhou, S., Gao, C., Duan, Z., Xi, X., & Li, Y. (2023). A robust error correction method for numerical weather prediction wind speed based on Bayesian optimization, variational mode decomposition, principal component analysis, and random forest: VMD-PCA-RF (version 1.0.0). *Geoscientific Model Development*. https://doi.org/10.5194/gmd-16-6247-2023.

[45] Reynolds, J., Clarizia, M., & Santi, E. (2020). Wind Speed Estimation From CYGNSS Using Artificial Neural Networks. *IEEE Journal of Selected Topics in Applied Earth Observations and Remote Sensing*, 13, 708-716. https://doi.org/10.1109/JSTARS.2020.2968156.

[46] Ruiz Aguilar, J., Turias, I., González-Enrique, J., Urda, D., & Elizondo, D. (2021). A permutation entropy-based EMD–ANN forecasting ensemble approach for wind speed prediction. *Neural Computing and Applications*, 33(04). https://doi.org/10.1007/s00521-020-05141-w.

[47] López Díaz, L., Oliveros, I., Torres, L., Ripoll, L., Soto Ortiz, J., Salazar, G., & Cantillo, S. (2020). Prediction of Wind Speed Using Hybrid Techniques. Three locations: Colombia, Ecuador and Spain. https://doi.org/10.20944/preprints202010.0091.v1.

[48] Elsaraiti, M., & Merabet, A. (2021). Application of Long-Short-Term-

Memory Recurrent Neural Networks to Forecast Wind Speed. *Applied Sciences*. https://doi.org/10.3390/APP11052387.

[49] Jahangir, H., Golkar, M., Alhameli, F., Mazouz, A., Ahmadian, A., & Elkamel, A. (2020). Short-term wind speed forecasting framework based on stacked denoising auto-encoders with rough ANN. *Sustainable Energy Technologies and Assessments*, 38, 100601. https://doi.org/10.1016/j.seta.2019.100601.

[50] Cyril Voyant, Gilles Notton, Soteris Kalogirou, Marie-Laure Nivet, Christophe Paoli, Fabrice Motte, Alexis Fouilloy. *Machine learning methods for solar radiation forecasting: A review*. *Renewable Energy*, 105, 569-582, 2017. DOI: 10.1016/j.renene.2016.12.095. ISSN: 0960-1481. URL: https://doi.org/10.1016/j.renene.2016.12.095.

[51] C. Obiora, A. Ali, and A. Hassan, "Predicting Hourly Solar Irradiance Using Machine Learning Methods," in *2020 11th International Renewable Energy Congress (IREC)*, pp. 1-6, 2020. doi: 10.1109/IREC48820.2020.9310444.

[52] G. Sahin and W. van Sark, "Estimation of most optimal azimuthal angles for maximum PV solar efficiency using multivariate adaptive regression splines (MARS)," *AIMS Energy*, vol. 11, pp. 1328-1353, Dec. 2023. doi: 10.3934/energy.2023060.

[53] S. Kuter, G.-W. Weber, Z. Akyürek, and A. Özmen, *Inverse Problems in Science and Engineering*, vol. 23, no. 4, pp. 651–669, May 2015, doi: 10.1080/17415977.2014.933828.

[54] S. Kuter,*Remote Sensing of Environment*, vol. 255, p. 112294, March 2021, doi: 10.1016/j.rse.2021.112294.

[55] T. Ewertowski, B. Güldoğuş, S. Kuter, S. Akyüz, G.-W. Weber, J. Sadłowska-Wrzesińska, and E. Racek, *Central European Journal of Operations Research*, pp. 1–26, August 2023, doi: 10.1007/s10100-023-00875-z.

[56] E. Yukseltan, A. Yucekaya, and A. Bilge, "Hourly electricity demand forecasting using Fourier analysis with feedback," *Energy Strategy Reviews*, vol. 31, p. 100524, 2020. doi: 10.1016/j.esr.2020.100524.

[57] H. Son and C. Kim, “A Deep Learning Approach to Forecasting Monthly Demand for Residential–Sector Electricity,” *Sustainability*, 2020. doi: 10.3390/su12083103.

[58] G. Zhang and J. Guo, “A Novel Method for Hourly Electricity Demand Forecasting,” *IEEE Transactions on Power Systems*, vol. 35, pp. 1351-1363, 2020. doi: 10.1109/TPWRS.2019.2941277.

[59] E. İlseven and M. Göl, “Medium-Term Electricity Demand Forecasting Based on MARS,” 2017. Available online: `https://hdl.handle.net/11511/55240`.

[60] A. Nascimento, G. Junior, T. Chaves, P. Luana, L. Soares, L. Lima, C. Barros, and L. Barros, "Operation Analysis of an Islanded Microgrid with a Single Wind Power/BESS Generation Unit," in *2023 Workshop on Communication Networks and Power Systems (WCNPS)*, pp. 1-6, 2023. doi: `10.1109/WCNPS60622.2023.10345221`.

[61] M. Barbaro and R. Castro, "Design optimisation for a hybrid renewable microgrid: Application to the case of Faial island, Azores archipelago," *Renewable Energy*, vol. 151, pp. 434-445, 2020. doi: `10.1016/j.renene.2019.11.034`.

[62] D. Thakur and J. Jiang, "Design and Construction of a Wind Turbine Simulator for Integration to a Microgrid with Renewable Energy Sources," *Electric Power Components and Systems*, vol. 45, pp. 949-963, 2017. doi: `10.1080/15325008.2017.1311385`.

[63] M. Huq, M. Rahman, M. Proma, M. Khondoker, and T. Aziz, "Mitigation of Frequency Deviation and Voltage Fluctuations in a Wind Integrated Industrial Microgrid," in *2022 Second International Conference on Advances in Electrical, Computing, Communication and Sustainable Technologies (ICAECT)*, pp. 1-6, 2022. doi: `10.1109/ICAECT54875.2022.9807979`.

[64] Z. Yang, L. Xia, and X. Guan, "Fluctuation Reduction of Wind Power and Sizing of Battery Energy Storage Systems in Microgrids," *IEEE Transactions*

on Automation Science and Engineering, vol. 17, pp. 1195-1207, 2020. doi: 10.1109/TASE.2020.2977944.

[65] J. Marchgraber and W. Gawlik, "Investigation of Black-Starting and Islanding Capabilities of a Battery Energy Storage System Supplying a Microgrid Consisting of Wind Turbines, Impedance- and Motor-Loads," *Energies*, 2020. doi: 10.3390/en13195170.

[66] Nasir, M., Iqbal, S., & Khan, H. (2018). Optimal Planning and Design of Low-Voltage Low-Power Solar DC Microgrids. *IEEE Transactions on Power Systems*, 33, 2919-2928. https://doi.org/10.1109/TPWRS.2017.2757150.

[67] Bandyopadhyay, S., Mouli, G., Qin, Z., Elizondo, L., & Bauer, P. (2020). Techno-Economical Model Based Optimal Sizing of PV-Battery Systems for Microgrids. *IEEE Transactions on Sustainable Energy*, 11, 1657-1668. https://doi.org/10.1109/TSTE.2019.2936129.

[68] Ahamad, N., Othman, M., Vasquez, J., Guerrero, J., & Su, C. (2018). Optimal sizing and performance evaluation of a renewable energy based microgrid in future seaports. In *2018 IEEE International Conference on Industrial Technology (ICIT)* (pp. 1043-1048). https://doi.org/10.1109/ICIT.2018.8352322.

[69] Bogado, G., Paz, F., Zurbriggen, I., & Ordonez, M. (2019). Optimal Sizing of a PV and Battery Storage System Using a Detailed Model of the Microgrid for Stand-Alone Applications. In *2019 IEEE Applied Power Electronics Conference and Exposition (APEC)* (pp. 555-560). https://doi.org/10.1109/APEC.2019.8722113.

[70] Xie, C., Wang, D., Lai, C., Wu, R., Wu, X., & Lai, L. (2021). Optimal sizing of battery energy storage system in smart microgrid considering virtual energy storage system and high photovoltaic penetration. *Journal of Cleaner Production*. https://doi.org/10.1016/j.jclepro.2020.125308.

[71] Pham, M., Tran, T., Bacha, S., Hably, A., & An, L. (2018). Optimal Sizing of Battery Energy Storage System for an Islanded Microgrid. In *IECON 2018 -*

44th Annual Conference of the IEEE Industrial Electronics Society (pp. 1899-1903). https://doi.org/10.1109/IECON.2018.8591391.

[72] Abdulgalil, M., Khalid, M., & Alismail, F. (2019). Optimal Sizing of Battery Energy Storage for a Grid-Connected Microgrid Subjected to Wind Uncertainties. *Energies*. https://doi.org/10.3390/EN12122412.

[73] Lee, Y., Kang, H., & Kim, M. (2022). Optimal Operation Approach with Combined BESS Sizing and PV Generation in Microgrid. *IEEE Access*, PP, 1-1. https://doi.org/10.1109/ACCESS.2022.3157294.

[74] Mohandes, B., Acharya, S., Moursi, M., Al-Sumaiti, A., Doukas, H., & Sgouridis, S. (2020). Optimal Design of an Islanded Microgrid With Load Shifting Mechanism Between Electrical and Thermal Energy Storage Systems. *IEEE Transactions on Power Systems*, 35, 2642-2657. https://doi.org/10.1109/TPWRS.2020.2969575.

[75] Saaravia-Guerrero, J., & Espinosa-Juárez, E. (2022). Optimal Sizing of BESS for Peak Shaving in a Microgrid. In *2022 IEEE International Autumn Meeting on Power, Electronics and Computing (ROPEC)* (pp. 1-6). https://doi.org/10.1109/ROPEC55836.2022.10018610.

[76] Takano, H., Hayashi, R., Asano, H., & Goda, T. (2021). Optimal Sizing of Battery Energy Storage Systems Considering Cooperative Operation with Microgrid Components. *Energies*. https://doi.org/10.3390/en14217442.

[77] El-Bidairi, K., Nguyen, H., Mahmoud, T., Jayasinghe, S., & Guerrero, J. (2020). Optimal sizing of Battery Energy Storage Systems for dynamic frequency control in an islanded microgrid: A case study of Flinders Island, Australia. *Energy*. https://doi.org/10.1016/j.energy.2020.117059.

[78] Kumar, A., Rizwan, M., & Nangia, U. (2019). Optimal Sizing of Renewable Energy Resources in a Microgrid for a Distributed Generation System. In *2019 International Symposium on Advanced Electrical and Communi-*

cation Technologies (ISAECT) (pp. 1-6). https://doi.org/10.1109/ISAECT47714.2019.9069731.

[79] A. Yahaya, M. Al-Muhaini, and G. Heydt, "Optimal design of hybrid DG systems for microgrid reliability enhancement," *IET Generation, Transmission & Distribution*, 2020. [Online]. Available: https://doi.org/10.1049/iet-gtd.2019.0277

[80] R. Dobrescu, "Optimal Control Strategy of Power Generation in Microgrids," *Annals of the Academy of Romanian Scientists Series on Science and Technology of Information*, vol. 2022, no. 1-2, pp. 15, 2022. [Online]. Available: https://doi.org/10.56082/annalsarsciinfo.2022.1-2.15

[81] A. Ahmed, E. Pompodakis, and T. Massier, "Optimal Operation of Islanded AC/DC Hybrid Microgrids," in *Proceedings of the 2021 IEEE Power & Energy Society General Meeting (PESGM)*, 2021, pp. 1-5. [Online]. Available: https://doi.org/10.1109/PESGM46819.2021.9638147

[82] V. Murty and A. Kumar, "Multi-objective energy management in microgrids with hybrid energy sources and battery energy storage systems," *Protection and Control of Modern Power Systems*, vol. 5, pp. 1-20, 2020. [Online]. Available: https://doi.org/10.1186/s41601-019-0147-z

[83] P. Krishna, P. Sekhar, and M. Ali, "Optimal Planning of Hybrid Microgrid-A Validation," in *Proceedings of the 2020 20th International Conference on Sciences and Techniques of Automatic Control and Computer Engineering (STA)*, 2020, pp. 255-260. [Online]. Available: https://doi.org/10.1109/STA50679.2020.9329323

[84] Mashayekh, S., Stadler, M., Cardoso, G., & Heleno, M. (2017). A mixed integer linear programming approach for optimal DER portfolio, sizing, and placement in multi-energy microgrids. *Applied Energy*, 187, 154-168. https://doi.org/10.1016/J.APENERGY.2016.11.020.

[85] Zhengu, L. (2015). A planning and design method for microgrid based on two-stage optimization. *Power System Protection and Control*.

[86] Balasubramaniam, K., Hadidi, R., & Makram, E. (2015). Optimal operation of microgrids under conditions of uncertainty. In *2015 IEEE Power & Energy Society General Meeting* (pp. 1-5). https://doi.org/10.1109/PESGM.2015.7286445.

[87] Xie, Y., Li, Z., Wu, Y., Zhou, S., & Zhang, Y. (2021). Multi-objective stochastic optimization planning method based on microgrid. In *2021 2nd International Conference on Artificial Intelligence and Computer Engineering (ICAICE)* (pp. 632-636). https://doi.org/10.1109/icaice54393.2021.00125.

[88] Lu, X., Zhou, K., & Yang, S. (2017). Multi-objective optimal dispatch of microgrid containing electric vehicles. *Journal of Cleaner Production*, 165, 1572-1581. https://doi.org/10.1016/J.JCLEPRO.2017.07.221.

[89] Nasser, A., & Reji, P. (2016). Optimal planning approach for a cost-effective and reliable microgrid. In *2016 International Conference on Cogeneration, Small Power Plants and District Energy (ICUE)* (pp. 1-6). https://doi.org/10.1109/COGEN.2016.7728966.

[90] Zehra, S., Rahman, A., Armghan, H., Ahmad, I., & Ammara, U. (2021). Artificial intelligence-based nonlinear control of renewable energies and storage system in a DC microgrid. *ISA Transactions*. https://doi.org/10.1016/j.isatra.2021.04.004

[91] Jaganath, M., Ray, S., & Choudhury, N. (2023). Maximizing Year-Around Energy Availability by Adaptive Component Changes in Microgrid. In *Proceedings of the 2023 4th IEEE Global Conference for Advancement in Technology (GCAT)*, pages 1–6. https://doi.org/10.1109/GCAT59970.2023.10353417

[92] Soykan, G., Er, G., & Çanakoglu, E. (2020). Evaluation of the Effect of Weather Conditions on Optimal Sizing of an Isolated Microgrid. In *Proceedings of the 2020 IEEE International Conference on Environment and Electrical Engineering and 2020 IEEE Industrial and Commercial Power Systems Europe (EEEIC / I&CPS Europe)*, pages 1–6. https://doi.org/10.1109/EEEIC/ICPSEUROPE49358.2020.9160542

[93] Hannan, M., Faisal, M., Ker, P., Begum, R., Dong, Z., & Zhang, C. (2020). Review of optimal methods and algorithms for sizing energy storage systems to achieve decarbonization in microgrid applications. *Renewable & Sustainable Energy Reviews*, 131, 110022. https://doi.org/10.1016/j.rser.2020.110022

[94] Tabrizi, A. (2022). Energy Management System Optimization for Grid Connected Microgrids in Presence of Energy Storage. In *Proceedings of the 2022 International Congress on Human-Computer Interaction, Optimization and Robotic Applications (HORA)*, pages 1–7. https://doi.org/10.1109/HORA55278.2022.9800062

[95] Alvarez, M., & Alejandro, J. (2021). Optimization-based design of microgrids for critical loads. https://doi.org/10.14288/1.0402667.

[96] Rahbar, K., Chai, C., & Zhang, R. (2018). Energy Cooperation Optimization in Microgrids With Renewable Energy Integration. *IEEE Transactions on Smart Grid*, 9, 1482–1493. https://doi.org/10.1109/TSG.2016.2600863.

[97] Ouammi, A., Achour, Y., Dagdougui, H., & Zejli, D. (2020). Optimal operation scheduling for a smart greenhouse integrated microgrid. *Energy for Sustainable Development*, 58, 129–137. https://doi.org/10.1016/j.esd.2020.08.001.

[98] Praiselin, W., & Edward, J. (2018). A Review on Impacts of Power Quality, Control and Optimization Strategies of Integration of Renewable Energy Based Microgrid Operation. *International Journal of Intelligent Systems and Applications*, 10, 67–81. https://doi.org/10.5815/IJISA.2018.03.08.

[99] Gao, K., Wang, T., Han, C., Xie, J., Ma, Y., & Peng, R. (2021). A Review of Optimization of Microgrid Operation. *Energies*, 14, 2842. https://doi.org/10.3390/EN14102842.

[100] National Oceanic and Atmospheric Administration (NOAA), "Global Hourly - Integrated Surface Database (ISD)," Integrated Surface Dataset (Global), 2024, URL: `https://www.ncei.noaa.gov/access/search/data-search/global-hourly`.

[101] Kıbrıs Türk Elektrik Kurumu, "Mainpage," About, 2024, URL: `https://www.kibtek.com/`.

[102] Yoo, G. (2022). Characteristics of z score systems for diagnosing coronary abnormalities in Kawasaki disease. *Clinical and Experimental Pediatrics*, 65, 448-449. DOI: 10.3345/cep.2021.01886.

[103] Özmen, A., Yılmaz, Y., & Weber, G.-W. (2018). Natural gas consumption forecast with MARS and CMARS models for residential users. *Energy Economics*, 70, 357-381. ISSN 0140-9883, DOI: 10.1016/j.eneco.2018.01.022. https://www.sciencedirect.com/science/article/pii/S0140988318300306

[104] Yılmaz, Y., Kurz, R., Özmen, A., & Weber, G. (2015). A New Algorithm for Scheduling Condition-Based Maintenance of Gas Turbines. In *Proceedings of the ASME Turbo Expo 2015: Turbine Technical Conference and Exposition* (Vol. 9: Oil and Gas Applications; Supercritical CO2 Power Cycles; Wind Energy, pp. V009T24A014). Montreal, Quebec, Canada. ASME. https://doi.org/10.1115/GT2015-43545.

[105] Yılmaz, Y., Nalçacı, G., Kańczurzewska, M., & Weber, G. W. (2023). Long-term wind power and global warming prediction using MARS, ANN, CART, LR, and RF. *Journal of Industrial and Management Optimization*. doi: https://doi.org/10.3934/jimo.2023162.

[106] Yılmaz, Y. (2015). *Daily natural gas consumption prediction by MARS and CMARS models for residential users in Ankara [Electronic resource]*. Master's thesis, Middle East Technical University, Ankara. Supervisor: Prof. Dr. Gerhard-Wilhelm Weber. Available: http://etd.lib.metu.edu.tr/upload/12619135/index.pdf.

[107] Friedman, J. H. (1991). Multivariate Adaptive Regression Splines. *The Annals of Statistics*, 19(1), 1–67. https://doi.org/10.1214/aos/1176347963.

[108] Friedman, J., & Elston, S. (n.d.). *py-earth: A Python implementation of Jerome Friedman's Multivariate Adaptive Regression Splines (MARS) algorithm*. Retrieved from https://github.com/scikit-learn-contrib/py-earth

[109] Medghalchi, Z., Taylan, O. (2023), "A novel hybrid optimization framework for sizing renewable energy systems integrated with energy storage systems with solar photovoltaics, wind, battery and electrolyzer-fuel cell," *Energy Conversion and Management*, 294, 117594, doi: 10.1016/j.enconman.2023.117594.

[110] Al-Ghussain, L., Samu, R., Taylan, O., Fahrioglu, M. (2020), "Sizing Renewable Energy Systems With Energy Storage Systems in Microgrids For Maximum Cost-Efficient Utilization of Renewable Energy Resources," *Sustainable Cities and Society*, 55, p. 102059, doi: 10.1016/j.scs.2020.102059.

[111] A. Saltelli, M. Ratto, T. Andres, F. Campolongo, J. Cariboni, D. Gatelli, M. Saisana, and S. Tarantola, *Global Sensitivity Analysis: The Primer*, John Wiley & Sons, 2008. https://www.wiley.com/en-us/Global+Sensitivity+Analysis%3A+The+Primer-p-9780470059975

[112] A. Saltelli, P. Annoni, I. Azzini, F. Campolongo, M. Ratto, and S. Tarantola, "Variance based sensitivity analysis of model output. Design and estimator for the total sensitivity index," *Computer Physics Communications*, vol. 181, no. 2, pp. 259–270, 2010. https://www.sciencedirect.com/science/article/pii/S0010465509003087

[113] Middle East Technical University Northern Cyprus (n.d.). Middle East Technical University Northern Cyprus. Retrieved from https://ncc.metu.edu.tr/

[114] M.K. Deshmukh, S.S. Deshmukh, *Modeling of hybrid renewable energy systems*, *Renewable and Sustainable Energy Reviews*, Volume 12, Issue 1, 2008, Pages 235-249, ISSN 1364-0321, https://doi.org/10.1016/j.rser.2006.07.011. [https://www.sciencedirect.com/science/article/pii/S1364032106001134]

[115] L. Al-Ghussain and O. Taylan, "Sizing methodology of a PV/wind hybrid system: Case study in Cyprus," *ENVIRONMENTAL PROGRESS & SUSTAINABLE ENERGY*, pp. 0–0, 2019. Accessed: 00, 2020. [Online]. Available: https://hdl.handle.net/11511/65087.

[116] James F. Manwell, Jon G. McGowan, and Anthony L. Rogers, *Wind Energy Explained: Theory, Design and Application, Second Edition*, 2006, DOI: 10.1260/030952406778055054.

[117] L. AL-Ghussain, O. Taylan, and M. Fahrioglu, "Sizing of a Photovoltaic-Wind-Oil Shale Hybrid System: Case Analysis in Jordan," *ASME Journal of Solar Energy Engineering*, February 2018; 140(1): 011002, https://doi.org/10.1115/1.4038048.

[118] Vestas Wind Systems A/S. (n.d.). *V90-2.0 MW - 2 MW Platform*. Retrieved from `https://www.vestas.com/en/pages/backup-2-mw-platform/V90-2-0-MW`

[119] Duffie, J. A., Beckman, W. A., & Blair, N. (2020). *Solar Engineering of Thermal Processes, Photovoltaics and Wind*. John Wiley & Sons. DOI

[120] Sizing renewable energy systems with energy storage systems in microgrids for maximum cost-efficient utilization of renewable energy resources. *Sustainable Cities and Society*, Volume 55, 2020, 102059, ISSN 2210-6707. https://doi.org/10.1016/j.scs.2020.102059.

[121] M. Nawaz, A. Ali, S. Jaffar, T. Jafri, T. Oh, M. Abdallah, S. Karam, and M. Azab, "Cost-Based Optimization of Isolated Footing in Cohesive Soils Using Generalized Reduced Gradient Method," *Buildings*, 2022. DOI: 10.3390/buildings12101646.

[122] L. Lasdon, R. Fox, and M. Ratner, "Nonlinear optimization using the generalized reduced gradient method," *Revue Francaise d'Automatique, Informatique, et Recherche Operationelle*, vol. 8, pp. 73–103, 1974. DOI: 10.1051/RO/197408V300731.

[123] D. Driggs, M. Ehrhardt, and C. Schonlieb, "Accelerating variance-reduced stochastic gradient methods," *Mathematical Programming*, vol. 191, pp. 671–715, 2019. DOI: 10.1007/s10107-020-01566-2.

[124] T. Liu, Z. Tan, C. Xu, H. Chen, and Z. Li, "Study on deep reinforcement learning techniques for building energy consumption forecasting," *Energy and Buildings*, vol. 208, 109675, 2020. DOI: 10.1016/j.enbuild.2019.109675.

[125] P. Catrini, A. Cipollina, G. Micale, A. Piacentino, and A. Tamburini, "Potential applications of salinity gradient power-heat engines for recovering low-temperature waste heat in cogeneration plants," *Energy Conversion and Management*, 2021. DOI: 10.1016/J.ENCONMAN.2021.114135.

[126] Y. Liu, K. Zhang, T. Başar, and W. Yin, "An Improved Analysis of (Variance-Reduced) Policy Gradient and Natural Policy Gradient Methods," *ArXiv*, abs/2211.07937, 2022. DOI: 10.48550/arXiv.2211.07937.

[127] HDC Solar Enerji. (2024). *AXIpower Poly - Solar Panel Datasheet*. Retrieved from AXIpower Poly Datasheet.

[128] Y.YILMAZ. (2024). *Microgrid with Wind Turbine, Solar PV and BESS components*. [Digital Image]. In: OpenAI.

[129] L. Al-Ghussain, O. Taylan, and D. K. Baker, "An investigation of optimum PV and wind energy system capacities for alternate short and long-term energy storage sizing methodologies," *INTERNATIONAL JOURNAL OF ENERGY RESEARCH*, pp. 204–218, 2019. Accessed: 00, 2020. [Online]. Available: `https://hdl.handle.net/11511/41610`.